

LIBRARY Michigan State University

This is to certify that the dissertation entitled

SELECTIVE, ULTRATHIN MEMBRANE SKINS PREPARED BY DEPOSITION OF NOVEL POLYMER FILMS ON POROUS ALUMINA SUPPORTS

presented by

Anagi Manjula Balachandra

has been accepted towards fulfillment of the requirements for the

Ph.D.	degree in _	Chemistry
$-\mathcal{H}$	al Ch	re
, ,	Major Profe	ssor's Signature
	8/20/	2003
	,	Date

MSU is an Affirmative Action/Equal Opportunity Institution

PLACE IN RETURN BOX to remove this checkout from your record. TO AVOID FINES return on or before date due. MAY BE RECALLED with earlier due date if requested.

DATE DUE	DATE DUE	DATE DUE
OCT 2 0 2006		

6/01 c:/CIRC/DateDue.p65-p.15

SELECTIVE, ULTRATHIN MEMBRANE SKINS PREPARED BY DEPOSITION OF NOVEL POLYMER FILMS ON POROUS ALUMINA SUPPORTS

Ву

Anagi Manjula Balachandra

A DISSERTATION

Submitted to
Michigan State University
in partial fulfillment of the requirements
for the degree of

DOCTOR OF PHOLOSOPHY

Department of Chemistry

2003

ABSTRACT

SELECTIVE, ULTRATHIN MEMBRANE SKINS PREPARED BY DEPOSITION OF NOVEL POLYMER FILMS ON POROUS ALUMINA SUPPORTS By

Anagi Manjula Balachandra

Membrane-based separations are attractive in industrial processes because of their low energy costs and simple operation. However, low permeabilities often make membrane processes uneconomical. Since flux is inversely proportional to membrane thickness, composite membranes consisting of ultrathin, selective skins on highly permeable supports are required to simultaneously achieve high throughput and high selectivity. However, the synthesis of defect-free skins with thicknesses less than 50 nm is difficult, and thus flux is often limited.

Layer-by-layer deposition of oppositely charged polyelectrolytes on porous supports is an attractive method to synthesize ultrathin ion-separation membranes with high flux and high selectivity. The ion-transport selectivity of multilayer polyelectrolyte membranes (MPMs) is primarily due to Donnan exclusion; therefore increase in fixed charge density should yield high selectivity. However, control over charge density in MPMs is difficult because charges on polycations are electrostatically compensated by charges on polyanions, and the net charge in the bulk of these films is small. To overcome this problem, we introduced a templating method to create ion-exchange sites in the bulk of the membrane. This strategy involves alternating deposition of a Cu²⁺-poly(acrylic acid) complex and poly(allylamine hydrochloride) on a porous alumina support followed by removal of Cu²⁺ and deprotonation to yield free -COO ion-exchange

sites. Difffusion dialysis studies showed that the Cl'/SO₄²⁻ selectivity of Cu²⁺-templated membranes is 4-fold higher than that of membranes prepared in the absence of Cu²⁺. Post-deposition cross-linking of these membranes by heat-induced amide bond formation further increased Cl'/SO₄²⁻ selectivity to values as high as 600.

Room-temperature, surface-initiated atom transfer radical polymerization (ATRP) provides another convenient method for formation of utrathin polymer skins. This process involves attachment of polymerization initiators to a porous alumina support and subsequent polymerization from these initiators. Because ATRP is a controlled polymerization technique, it yields well-defined polymer films with low polydispersity indices (narrow molecular weight distributions). Additionally, this method is attractive because film thickness can be easily controlled by adjusting polymerization time. Gaspermeability data showed that grafted poly(ethylene glycol dimethacrylate) membranes have a CO₂/CH₄ selectivity of 20, whereas poly(2-hydroxyethyl methacrylate) (PHEMA) films grown from a surface have negligible selectivity. However, derivatization of PHEMA with pentadecafluorooctanoyl chloride increases the solubility of CO₂ in the membrane and results in a CO₂/CH₄ selectivity of 9.

Although composite PHEMA membranes have no significant gas-transport selectivity, diffusion dialysis studies with PHEMA membranes showed moderate ion-transport selectivities. Cross-linking of PHEMA membranes by reaction with succinyl chloride greatly enhanced anion-transport selectivities while maintaining reasonable flux. The selectivities of these systems demonstrate that alternating polyelectrolyte deposition and surface-initiated ATRP are indeed capable of forming ultrathin, defect-free membrane skins that can potentially be modified for specific separations.

Copyright by ANAGI MANJULA BALACHANDRA 2003

To my dearest parents, Lalini a endless support and encourager	and Henry Balachandra and ment made this dissertation	my husband, Dhammika. Your and doctoral degree possible.

ACKNOWLEDGMNETS

I would like to extend my deep appreciation and gratitude to my adviser, Prof.

Merlin Bruening, for his excellent guidance, support and encouragement. I was really lucky to be in your group and enjoyed working with you. Thank you for being such a wonderful adviser and a mentor.

I would also thankful to Prof. Gregory Baker for his expertise advices during the polymerization project. I am also thankful for my guidance committee members; Profs, Pinnavaia, Watson and Broderick for their time and suggestions.

I greatly acknowledge the financial support from the NSF Center for Sensor Materials at Michigan State University.

I am very much thankful to Bruening group members past and present; Dan,
Jeremy, Wenxi, Milind, Jinhua, Kangping, Yinda, Skanth, Sandra, Keith, Jacque, Bo
Young, Matt, Brian. Jin, Lei, Sri, Christin and Xiaoyun. Especially, to Dr. Wenxi Huang
for teaching me many of the polymerization techniques. I also want to thank Baker group
members JB, Ying and Bao, it was very nice working with you.

Finally, I like to thank my family, especially, my parents for all their support, encouragement and love. I owe you very much for every single achievement in life.

Biggest thanks go to my husband, Dhammika for his constant support, understanding and love. It want be possible for me to finish my Ph.D. without you.

TABLE OF CONTENTS

List	of Sche	emes	х
List	of Tabl	es	xi
List	of Figu	res	xi
List	of Abb	reviations	xvi
Cha	pter 1:	Introduction	1
1.1	Struct	ure of the Dissertation	1
1.2	Forma	tion and Development of Thin Polymer Films	3
1.3	Multil	ayer Polyelectrolyte Films	6
1.4	Ion Pe	rmeation through MPFs	10
1.5	MPFs	as Ion-separation Membranes	10
1.6	Grafte	d Polymer Brushes	12
1.7	Atom	Transfer Radical Polymerization (ATRP)	16
1.8	Forma	tion of membranes by surface-initiated ATRP	18
		eparation Membranes	22
1.10	Mecha	anism of Gas Transport through Polymer Membranes	24
	Summ		27
1.12	Refere	ences	28
Cha	pter 2:	Enhancing the Anion-Transport Selectivity of Multilayer Polyelectrolyte Membranes by Templating with Cu ²⁺	36
2.1	Introd	uction	36
2.2	-	imental	39
		Chemicals and Solutions	39
		Film Preparation	40
		Film Characterization	41
	2.2.4	Ion-Transport Studies	42
2.3	Result	s and Discussion	44
	2.3.1	Synthesis and Characterization of Cu ²⁺ -Templated PAA/PAH	
		Films	44
	2.3.2	Anion Transport through Cu ²⁺ -Templated PAA/PAH Membranes	47
	2.3.3	Cross-linked Cu ²⁺ -Templated PAA/PAH Membranes	50
	2.3.4	Changing the Surface Charge of Membranes	53
	2.3.5	Anion-Transport through Partially Cross-linked,	
		Cu ²⁺ -Templated Membranes Deposited at Different pH values	54
	2.3.6	Anion-Transport through Partially Cross-linked, Cu ²⁺ -Templated	
	227	Membranes Deposited with Different Cu ²⁺ Concentrations	56
	2.3.7	Modeling of Anion-Transport through Cu ²⁺ -Templated PAA/PAH	50
2.4	Const	Membranes	59
2.4	Conclu		68
2.3	Keiere	nces and Notes	69

Cha	pter 3:	Radical Polymerization Initiated from a Porous Support	73
3.1	Introd	uction	73
3.2	Experi	mental	75
	3.2.1	Chemicals and Solutions	
	3.2.2	Polymerization of EGDMA	76
	3.2.3	Polymerization of HEMA and Subsequent Derivatization	78
	3.2.4	Film Characterization on Gold Wafers	80
	3.2.5	Film Characterization on Alumina Supports	80
	3.2.6	Gas-Permeation Studies	80
3.3	Result	s and Discussion	82
	3.3.1	Synthesis and Characterization of PEGDMA films	82
3.3.2	2 Synthe	esis and Characterization of PHEMA films	87
	3.3.3	Gas Permeation through Polymer Membranes	89
	3.3.4	Gas Permeation through Composite PEGDMA Membranes	94
	3.3.5		98
3.4	Conclu	usions	108
3.5	Refere	ences and Notes	109
Cha	pter 4:	Ion Transport through Grafted Poly (2-hydroxyethyl methacrylate) Membranes and their Derivatives	113
4.1	Introd	uction	113
4.2		mental	115
	•		
	4.2.1 4.2.2	Polymerization of HEMA from Gold-coated wafers and Porous	115
		Alumina	116
		Derivatization of PHEMA with Crown ethers	116
		Chemical Cross-linking of PHEMA	117
		Film Characterization	117
	4.2.6	Ion-Transport Studies with PHEMA Membranes	117
4.3		s and Discussion	118
	4.3.1	Synthesis and Characterization of PHEMA Membranes	118
	4.3.2	Ion-Transport Studies with Composite PHEMA Membranes	119
	4.3.3	Chemically Cross-linked PHEMA Membranes and their	
		Ion-Transport Properties	122
	4.3.4	Crown Ether-Derivatized PHEMA Membranes and their	
		Ion-Transport Properties	129
4.4	Conclu	ısions	134
4.5	Refere	nces	135

Cha	Chapter 5: Conclusions and Future Work	
5.1	Conclusions	136
5.2	Suggestions for Future Work	138
5.3	References	140

LIST OF SCHEMES

Scheme 1.1	Mechanism of ATRP.	17
Scheme 3.1	Growth of cross-linked PEGDMA from an anchored initiator.	86
•	Growth of PHEMA brushes from a gold surface: (1) formation of a monolayer of initiator and (2) polymerization from the initiator-modified gold surface.	91
Scheme 3.3	Derivatization of PHEMA with perfluorooctanoyl chloride.	102
Scheme 4.1	Cross-linking of PHEMA by reaction with succinyl chloride.	124
Scheme 4.2	Functionalization of PHEMA with 2-hydroxy methyl 18-crown-6.	132

LIST OF TABLES

Table 2.1	Anion fluxes (moles cm ⁻² s ⁻¹) through bare porous alumina and alumina coated with PAA/PAH and PAA-Cu/PAH films cross-linked at different temperatures.	51
Table 2.2	Thicknesses, fluxes (moles cm ⁻² s ⁻¹), selectivities and Cu ²⁺ concentrations (M) in partially cross-linked, 10.5-bilayer PAA-Cu/PAH films deposited at different pH values.	55
Table 2.3	Anion Fluxes (moles cm ⁻² s ⁻¹), selectivities, thicknesses, and estimated Cu ²⁺ concentrations (M) of partially cross-linked (130 °C) 10.5-bilayer PAA-Cu/PAH membranes and films deposited using different Cu ²⁺ concentrations.	58
Table 2.4	Diffusion coefficients obtained from modeling ion transport through 10.5-bilayer PAA-Cu/PAH membranes cross-linked at different temperatures.	67
Table 3.1	Gas permeability coefficients, estimated film thicknesses, and idea selectivities for PEGDMA membranes.	96
Table 3.2	Gas Permeability Coefficients, Estimated Film Thicknesses and Idea Selectivities for Underivatized PHEMA Membranes	100
Table 3.3	Estimated film thicknesses, gas permeability coefficients and ideal selectivities for fluorinated PHEMA membranes	107
Table 4.1	Film thicknesses, fluxes and selectivities for composite PHEMA membranes (porous alumina support).	121
Table 4.2	Hydrated radii and hydration energies of various ions.	123
Table 4.3	Film thicknesses, fluxes and selectivities for cross-linked PHEMA membranes in diffusion dialysis with single-salt solutions.	128
Table 4.4	Film thicknesses, normalized fluxes and selectivities for cross-linked PHEMA membranes in diffusion dialysis with mixed salt solutions.	130

LIST OF FIGURES

Figure 1.1	Deposition of a Langmuir-Blodget film from a floating Langmuir monolayer. Figure adapted from.	4
Figure 1.2	Schematic diagram of the "Dip and Rinse" procedure for alternating deposition of oppositely charged polyelectrolytes on a charged substrate. In the actual film structure, polycations and polyanions are interdigitated.	8
Figure 1.3	Synthesis of Cu ²⁺ -templated polyelectolyte films. Step 1: deposition of a polycation (PAH) in the presence of uncomplexed Cu ²⁺ . Step 2: deposition of partially Cu ²⁺ -complexed PAA. Step 3: removal of Cu ²⁺ . Step 4: deprotonation of the free carboxylic acid groups of PAA. Repetition of steps 1 and 2 produes a multilayer film. Inertwining of layers is not shown for figure clarity.	13
Figure 1.4	Two methods for grafting of polymer films onto solid surfaces.	15
Figure 1.5	Cartoon showing the different stages of surface-initiated ATRP.	19
Figure 1.6	Surface initiated atom transfer radical polymerization from (a) polyelectrolyte deposited on alumina and (b) Au-coated alumina.	21
Figure 2.1	Preparation of Cu ²⁺ - templated polyelectrolyte films on porous alumina supports. Step 1-adsorption of partially Cu ²⁺ -complexed PAA on porous alumina. Step 2-adsorption of a polycation (PAH). Step 3- removal of Cu ²⁺ . Step 4-deprotonation of the free carboxylic acid groups of PAA. Repetition of steps 1 and 2 produces multilayer films. Intertwining of layers is not shown for figure clarity.	37
Figure 2.2:	Apparatus for ion-transport measurements.	43
Figure 2.3	Cyclic voltammetry of a MPA-modified gold electrode coated with 10 bilayers of PAH/PAA-Cu before (solid line) and after exposing to pH 3.5 water (dotted line).	46
Figure 2.4	External reflectance FTIR spectra of (a) a 10-bilayer PAH/PAA-Cu film, (b) the same film after exposure to pH 3.5 water, (c) the film after exposure to pH 5-6 water, and (d) a 10-bilayer PAH/PAA film deposited without Cu ²⁺ . All films were deposited on a gold wafer coated with a monolayer of MPA.	48

Figure 2.5	Receiving phase concentration as a function of time for a bare porous alumina membrane (black), an alumina membrane coated with 10.5 bilayers of Cu ²⁺ -templated PAA/PAH (open) and an alumina membrane coated with 10.5 bilayers of PAA/PAH (grey). Different symbols represent different salts: circles-NaCl and squares-Na ₂ SO ₄ . The inset shows SO ₄ ²⁻ concentration vs. time for pure PAA/PAH (grey) and templated PAA/PAH (open). The membrane separates the receiving phase (initially deionized water) from a 0.1 M salt solution.	49
Figure 2.6	External reflectance FTIR spectra of 10-bilayer PAH/PAA-Cu films cross-linked at different temperatures: (a) unheated (b) heated to 160°C. Films were deposited on MPA-coated gold.	52
Figure 2.7	Cyclic voltammetry of 10-bilayer films of PAH/PAA-Cu ²⁺ deposited at different deposition pH values on MPA-modified gold surfaces: pH 5.5-dashed line, pH 6-solid line, and pH 6.6-dotted line. Areas of the reduction peaks were calculated by drawing the base line from the current value at a potential of 0.3V to the current value at -0.5V.	57
Figure 2.8	Cyclic voltammetry of 10-bilayer PAH/PAA-Cu films deposited with different Cu ²⁺ concentrations: 2.5 mM Cu ²⁺ -dotted line, 5.0 mM Cu ²⁺ -solid line and 7.5 mM Cu ²⁺ -dashed line. The area of the reduction peak was calculated after drawing the base line from the current at a potential of 0.3V to that at -0.4V. Films were deposited at pH 6 on MPA-modified gold.	60
Figure 2.9	Schematic representation of the model used to simulate ion transport through templated MPMs. The membrane consists of two charged layers: a surface layer and the membrane bulk. The line represents a hypothetical concentration profile for the excluded ion. C_x^{m1} and C_x^{m2} are the fixed charge concentrations of bulk of the film and surface layer respectively.	61
Figure 3.1	Apparatus for gas-permeation measurements	81
Figure 3.2	Schematic diagram showing polymerization of EGDMA from a polyelectrolyte surface modified with an initiator.	83
Figure 3.3	External reflection FTIR spectra of PAH/PSS/PAH on a MPA-coated Au wafer before (a) and after reaction with an acid bromide initiator (b). Spectrum (c) is from a PEGDMA film grown for 20 hours from PAH/PSS/PAH modified with initiator.	84

Figure 3.4	FESEM images of the filtrate side of porous alumina (0.02 μm surface pore diameter) (a) before depositing polyelectrolytes (b) after depositing one bilayer of PSS/PAH, and (c) after growth of PEGDMA from the surface for 20 hours. Image (d) is a cross-section of the membrane shown in (c).	88
Figure 3.5	Reflectance FTIR spectra of (a) a monolayer of BrC(CH ₃) ₂ COO(CH ₂) ₁₁ S) ₂ and (b) a grafted PHEMA layer.	90
Figure 3.6	Ellipsometric thicknesses of PHEMA films vs polymerization time. Thickness values are the average of three different films, and the error bars represent standard deviations.	92
Figure 3.7	Fluxes of different gases through a PEGDMA membrane (50 nm thick) as a function of transmembrane pressure drop. The outlet pressure was 1 atm and the measurements were performed at room temperature. PEGDMA was deposited on porous alumina.	95
Figure 3.8	Fluxes of different gases through a PHEMA membrane (60 nm thick) as a function of transmembrane pressure drop. The outlet pressure was 1 atm and the measurements were performed at room temperature. PHEMA was deposited on porous alumina.	99
Figure 3.9	Reflectance FTIR spectra of a PHEMA film grown from (BrC(CH ₃) ₂ COO(CH ₂) ₁₁ S) ₂ on gold before (a) and after reaction with pentadecafluorooctanoyl chloride (b).	103
Figure 3.10	Transmission FTIR spectra of a PHEMA film grown from (BrC(CH ₃) ₂ COO(CH ₂) ₁₁ S) ₂ on gold-coated porous alumina (a) before and (b) after reaction with pentadecafluorooctanoyl chloride.	104
Figure 3.11	Fluxes of different gases through a fluorinated-PHEMA membrane (100 nm thick) as a function of transmembrane pressure drop. The outlet pressure was 1 atm and the measurements were performed at room temperature.	106
Figure 4.1	Plot of receiving phase concentration as a function of time in diffusion dialysis when the source phase (0.1 M salt) was separated from the receiving phase (initially deionized water) by a porous alumina substrate capped with 28 nm of PHEMA.	120
Figure 4.2	Reflectance FTIR spectra of a 28-nm thick grafted PHEMA film on a gold-coated wafer before (a) and after reaction with succinvl chloride (b) and subsequent exposure to water (c).	125

	diffusion dialysis when the source phase (0.1 M salt) was separated from the receiving phase (initially deionized water) by a composite membrane of 35 nm cross-linked PHEMA film. The inset expands the concentration scale for SO_4^{2-} and $Fe(CN)_6^{3-}$. PHEMA was cross-linked by succinyl chloride.	127
Figure 4.4	Reflectance FTIR spectra of (a) a grafted PHEMA layer (28 nm) (b) CDI-derivatized PHEMA and (c) CDI-derivatized PHEMA after reaction with 2-hydroxymethyl-18-crown-6 (43 nm).	133

Plot of receiving phase concentration as a function of time in

Figure 4.3

LIST OF ABBREVIATIONS

ATRP atom transfer radical polymerization

bpy bipyridine

CV cyclic voltammogram

DMF N,N-dimethylformamide

EGDMA ethylene glycol dimethacrylate

FESEM field emission scanning electron microscopy

FTIR fourier transform infrared spectroscopy

HEMA 2-hydroxyethyl methacrylate

MPA mercaptopropionic acid

MPF multilayer polyelectrolyte film

MPM multilayer polyelectrolyte membrane

PAA poly(acrylic acid)

PAA-Cu poly(acrylic acid) copper complex

PAH poly(allylamine hydrochloride)

PEGDMA poly(ethylene glycol dimethacrylate)

PHEMA poly(2-hydroxyethyl methacrylate)

PSS poly(styrene sulfonate)

CHAPTER 1

Introduction

1.1 Structure of the Dissertation

Membrane-based separations are attractive because of low energy costs and simple operation. However, low flux through selective membranes often limits their utility.^{1,2} The most common strategy for increasing flux is the use of asymmetric or composite membranes that consist of an ultrathin, selective skin on a highly porous support. The minimal thickness of the skin allows high flux, while the support provides mechanical strength.³ The selective skin should be as thin as possible to achieve the highest flux, but synthesis of defect-free skins with thicknesses less than 50 nm is an ongoing challenge.⁴ My research focused on the development of methods for formation of defect-free, ultrathin polymer skins and the use of these skins for separations. Specifically, this dissertation discusses the fabrication of ultrathin skins on porous alumina supports using two techniques: alternating polyelectrolyte deposition and grafting of polymers from a surface using atom transfer radical polymerization (ATRP). These techniques afford composite membranes that allow selective ion and/or gas transport.

Chapter 1 of this dissertation describes previous research on thin film formation with special emphasis on alternating polyelectrolyte deposition and polymerization from a surface using atom transfer radical polymerization (ATRP). This chapter also contains background information about membranes for gas and ion separations and sets forth the motivation behind my research.

Chapter 2 concerns templating of multilayer polyelectrolyte films (MPFs) to enhance their ion-transport selectivities. I first discuss some of the limitation of MPFs as ion-separation membranes and then show how these challenges can be overcome by using Cu²⁺ as a placeholder during polyelectrolyte deposition. Specifically, I utilized Cu²⁺-chelated poly(acrylic acid) (PAA) and post-deposition removal of Cu²⁺ to introduce ion-exchange sites into the bulk of PAA/poly(allylamine hydrochloride) films. Diffusion dialysis studies showed 5-fold higher Cl⁷/SO₄²⁻ selectivities with Cu²⁺-templated membranes than with similar membranes deposited without Cu²⁺. Post-deposition cross-linking of Cu²⁺-templated membranes by heat-induced amide bond formation from carboxylate and ammonium groups further increased Cl⁷/SO₄²⁻ selectivity to values as high as 600. Ion-transport simulations suggest that both analyte size and analyte charge are important in effecting selective transport.

The third chapter of the dissertation discusses formation of composite membranes by polymerization from porous alumina and examines gas transport through these systems. We synthesized cross-linked poly(ethylene glycol dimethacrylate) (PEGDMA) and non cross-linked poly(2-hydroxyethyl methacrylate) (PHEMA) films by ATRP from initiators immobilized on porous alumina. Gas-permeation studies with PEGDMA films showed a CO₂/CH₄ selectivity of 20, whereas PHEMA films exhibited a selectivity of 0.7. However, fluorination of PHEMA through reaction of hydroxyl groups with pentadecafluorooctanoyl chloride increased the CO₂/CH₄ selectivity to 9.

Chapter 4 describes the performance of PHEMA and derivatized-PHEMA films as ion-separation membranes. Diffusion dialysis studies indicate that PHEMA membranes have a Cl⁻/SO₄²⁻ selectivity of 15, a K⁺/Mg²⁺ selectivity of 47 and a Fe(CN)₆³⁻

/Cl⁻ selectivity of 160. Unlike polyelectrolyte membranes, PHEMA is a neutral polymer, and the observed selectivities are probably due to differences in size or hydration energies among the various ions. Although PHEMA has moderate selectivities, Cl⁻ fluxes through these membranes were quite low. To achieve high selectivity while maintaining reasonable flux, we cross-linked very thin (28 nm) PHEMA films by reaction with a di-acid chloride. Diffusion-dialysis studies with these cross-linked PHEMA membranes showed a Cl⁻/SO₄²⁻ selectivity of 300 and only a 50% decrease in Cl⁻ flux compared to that of bare alumina.

Finally, chapter 5 contains conclusions and suggestions for future work.

1.2 Formation and Development of Thin Polymer Films

Development of thin organic films has been a highly active area of research for nearly 100 years.⁵⁻⁷ Coating a solid substrate with a thin film plays a vital role in controlling surface properties for applications in optics,⁸ sensing,^{9,10} corrosion protection,¹¹ and separations,¹²⁻¹⁴ and many of these applications require well-defined films with uniform morphologies.^{7 5}

Langmuir-Blodgett (LB) films were the first examples of multilayer coatings prepared in a controlled layer-by-layer fashion. The deposition of LB films begins by mechanically assembling an array of amphiphilic molecules on a water surface. Once the molecules are compressed to the desired organization, the film can then be transferred to a solid support as shown in Figure 1.1. This results in deposition of a single layer of

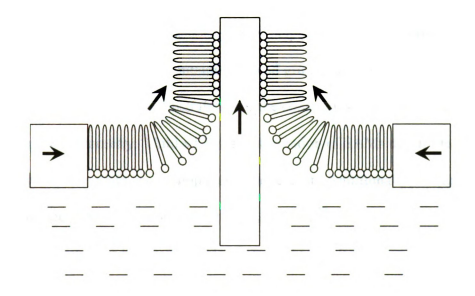


Figure 1.1: Deposition of a Langmuir-Blodgett film from a floating Langmuir monolayer. Figure adapted from http://www.nes.coventry.ac.uk/research/cmbe/filmbal.htm.

molecules, and subsequent immersions in the trough result in the deposition of more layers. LB films have been used to investigate phenomena ranging from optical properties of chromophores to ordered polymerizations on a substrate. However, these coatings have two limitations which greatly restrict their applications. First, LB films are fragile because the layers are linked by weak van der Waals forces. Second, fabrication of these materials requires pre-assembly at the air-water interface, so only ampiphillic molecules form films.

A more recent step in the development of ultrathin films was the discovery of self-assembled monolayers (SAMs).^{5,18-21} The principle behind formation of these monolayers is simple; a molecule containing a head group that adsorbs to a surface, e.g. thiols on gold, assembles on the substrate under the constraints of intermolecular forces and adsorption site geometry. Unlike LB films, formation of SAMs doesn't require any pre-assembly, so their synthesis is simple and convenient. Additionally, because they are bound to a surface, SAMs are more robust than LB films.²²

The most common family of SAMs is organothiols adsorbed on gold, and the first systematic study of these materials was done by Nuzzo and Allara in 1985. Since then, organothiol monolayers have been the subject of thousands of investigations. By employing thiols with different tail groups, SAMs can be easily used to modify surface properties. In addition to Au, other substrates such as Al/Al₂O₃, Si/SiO₂ and Cu have also been used to support SAMs. Also been used to support SAMs.

The main drawback to SAMs is the limited film thickness available from monolayer formation. Additionally, although self-assembled coatings are more

convenient and stable than LB films, the stability of Au-thiol films is still an issue at high temperatures.²⁵

More recently a number of techniques were developed to prepare multilayer films.

26-30 The most convenient of these methods is probably alternating deposition of anionic and cationic polyelectrolytes on charged supports. This strategy overcomes many of the limitations imposed by LB films and SAMs, although multilayered polyelectrolyte films are not well-ordered structures. Polyelectrolyte films are very stable because of the multiple electrostatic interactions between layers, and synthesis of these coatings requires only a simple dip and rinse procedure. The versatility and simplicity of alternating polyelectrolyte deposition are evident from the variety of charged substrates used for deposition 33-36 and the wide range of polyelectrolytes that can form these films. 33,37-44

Because polyelectrolyte films form the basis of much of my work, I describe them in more detail below.

1.3 Multilayer Polyelectrolyte Films

Using colloidal alumina and colloidal silica, Iler⁴⁵ first demonstrated the fabrication of multilayers by sequential adsorption of oppositely charged materials.

Later, Decher and Hong extended this idea and employed alternating deposition of oppositely charged polyelectrolytes (e.g. poly(allylamine hydrochloride) and sodium poly(styrenesulfonate)) on charged supports to form multilayer polyelectrolyte films (MPFs). Their technique allowed rapid formation of multilayer films with control over film thickness on the nm scale. More recently, alternating polyelectrolyte deposition

has been demonstrated on a variety of charged substrates with polyelectrolytes ranging from poly(styrenesulfonate)^{37,46,47} to DNA⁴⁷ and charged viruses.³⁸

Deposition of MPFs occurs as shown in Figure 1.2.⁴⁸ The procedure begins with immersion of a charged substrate into a solution containing an oppositely charged (with respect to the substrate) polyelectrolyte. A film forms due to electrostatic attraction between the substrate and the polyelectrolyte, but the thickness of this film is limited by electrostatic repulsion of incoming chains by adsorbed polymer. (This picture is oversimplified because the main driving force behind film formation is actually the increase in entropy that results when adsorption of a polyelectrolyte chain displaces many counterions from the substrate surface).⁴⁹ Rinsing of the substrate with water and immersion in a second solution containing an oppositely charged polyelectrolyte then yields another layer on the surface, and repetition of this adsorption sequence results in a multilayer film. Charge overcompensation at each deposition step is the key to subsequent adsorption of an oppositely charged polyelectrolyte. Typically, film thickness increases linearly with the number of polyelectrolyte layers after deposition of the first 3 or 4 layers.⁵⁰⁻⁵²

Several features of alternating polyelectrolyte deposition make it a unique technique for thin film formation. First, this procedure is environmentally friendly because in most cases, the solvent is water. Second, the only stipulation on the substrate for film formation is that it should contain sufficient charge. Thus, substrates with a wide range of topologies can support film growth. The electrostatic interactions between polyelectrolytes and surface charge also allow good adhesion between the polymer and the substrate. Finally, the thickness of films can be easily controlled by varying

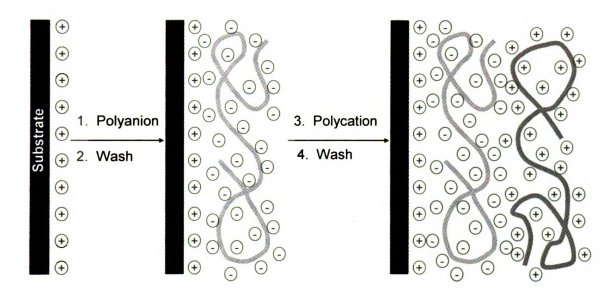


Figure 1.2: Schematic diagram of the "Dip and Rinse" procedure for alternating deposition of oppositely charged polyelectrolytes on a charged substrate. In the actual film structure, polycations and polyanions are interdigitated. Figure adapted from reference 46.

deposition parameters such as the number of adsorption steps, ^{50,53} the pH of deposition solutions, ^{54,55} deposition time, ³⁷ and the supporting electrolyte concentration in deposition solutions. ^{50,56-58}

Since the introduction of MPFs, these materials have been subjected to numerous studies to understand their structure and the mechanism of film formation. Small-angle X-ray scattering³⁸ and UV/visible spectroscopy^{33,35,40} provided evidence for layer-by-layer growth, but neutron reflectometry showed that multilayer films are not highly stratified. Strong interdigitation of polycations and polyanions occurs over several neighboring layers.^{59,60} A variety of other methods were also used to characterize these multilayers, including: electrochemical techniques,⁵⁸ surface plasmon resonance,^{36,56,61} ellipsometry,⁵⁸ quartz-crystal-microbalance gravimetry,^{36,62} X-ray photoelectron spectroscopy.^{57,63} atomic force microscopy,³⁴ and scanning electron microscopy.^{14,34}

Many recent studies showed that MPFs have potential applications in areas such as light-emitting devices, ^{64,65} non-linear optics, ^{43,66-70} sensors, ^{56,71,72} conductive coatings, ^{73,74} surface patterning, ⁷⁵ protective coatings, ^{76,77} separation membranes ^{13,14,78-85} and nano-particle formation. ⁸⁶ Some of these applications require impermeable films (e.g., protective coatings), while others necessitate films with high or selective permeabilities (e.g., separation membranes). In the specific area of separation membranes, efficient separation requires an understanding of the factors that affect transport of molecules or ions through MPFs. Below, I discuss literature that relates specifically to ion transport through MPFs.

1.4 Ion Permeation through MPFs

Several recent papers reported studies of ion permeation through MPFs.

Schlenoff and co-workers used electrochemical methods to examine the transport of redox-active ions thorough a thin MPF on an electrode. Transport rates of redox-active ions decreased with increasing charge, suggesting that diffusion through MPFs occurs via hopping between ion-exchange sites. The need for more ion-exchange sites to compensate the charge on multivalent ions should result in fewer hopping sites for these species, and hence slower transport. Möhwald and von Klitzing studied the transport of neutral quenchers through polyelectrolyte films by total internal reflection fluorescence spectroscopy. They showed that the diffusion of molecules through the bulk of the film is much slower than through the outer layers. This probably occurs because layers in the bulk of the film pack more tightly than outer layers.

In situ ellipsometric and cyclic voltammetric studies done by our group showed that the permeability of MPFs depends on the pH and ionic strength of polyelectrolyte deposition solutions, the number of layers in the film, and the nature of constituent polymers. More recently, Möhwald and co-workers investigated the release of fluorescein from multilayered polyelectrolyte capsules and showed that the rate of release is a function of the number of assembled polyelectrolyte layers. These studies provide important background for designing separation membranes containing MPFs.

1.5 MPFs as Ion-separation Membranes

Several recent studies exploited the simplicity and versatility of layer-by-layer adsorption of polyanions and polycations to form ion-separation membranes. Krasemann

and Tieke examined ion permeation through 60 bilayers of poly(sodium styrene sulfonate) (PSS)/poly(allylamine hydrochloride) (PAH) deposited on a polymeric support. These membranes exhibited a Na⁺/Mg²⁺ selectivity of 112 and a CI⁻/SO₄²⁻ selectivity of 45.⁷⁹ Selectivity increased with both the number of bilayers and the ionic strength of deposition solutions. Krasemann and Tieke suggested that the increase in selectivity with the number of layers is due to the multi-bipolar nature of the polyelectrolyte film. They thought that electrostatic repulsion would occur at each bilayer, resulting in higher monovalent/divalent ion selectivities for films with many layers. However, several studies suggest that polyelectrolyte bilayers are completely intertwined and that the bulk of these films have a net neutral charge.⁹¹ Thus, repulsion of ions should occur only at the film-solution interface. Perhaps large numbers of bilayers resulted in membranes with fewer defects.

Our group showed that membranes composed of 5 PSS/PAH bilayers on porous alumina have a Cl⁻/SO₄²⁻ selectivity of 6 and that Cl⁻/SO₄²⁻ selectivity does not increase after deposition of an additional 5 bilayers. ¹⁴ Selectivity is largely due to the electrostatic exclusion of multiply charged ions by surface charge, as selectivity depends on whether the membrane is terminated with a polycation or a polyanion. Stair *et.al*⁸⁰ found that upon changing the surface of PAA/PAH-capped films from PAA to PAH, Cl⁻/SO₄²⁻ selectivity decreased from 360 to 2. This observation further confirmed that outer layer charge plays a dominant role in determining selectivity.

All of these previous studies suggest that electrostatic exclusion is a major factor behind ion-transport selectivity in multilayer polyelectrolyte membranes. Therefore, increasing the charge density in the bulk or at the surface of these membranes should

enhance monovalent/divalent ion-transport selectivity. However, as mentioned, control over charge density in the bulk of MPFs is difficult because polycation charge is essentially completely compensated by polyanion charge, giving little net fixed charge density in interior of the film. ^{42,91} Insertion of net charge into MPF interiors likely requires a post-deposition reaction.

We utilized Cu²⁺ as a template to create ion-exchange sites (fixed charge) in the bulk of poly(acrylic acid) (PAA)/PAH membranes. This strategy involves alternating deposition of PAA-Cu (1 Cu²⁺ per 8 COO groups) and PAH on porous alumina supports followed by removal of Cu²⁺ and deprotonation to yield free -COO ion-exchange sites (Figure 1.3). Diffusion dialysis studies showed that the selectivity of Cu²⁺-templated membranes is dramatically higher than that of membranes prepared in the absence of Cu²⁺, presumably due to the higher concentration of fixed charge in the bulk of the film. Post-deposition cross-linking of these membranes by heat-induced amide bond formation further increased Cl⁷/SO₄²⁻ selectivity to values as high as 600. These remarkable selectivities are achieved with no significant decrease in flux relative to pure PAA/PAH membranes.

1.6 Grafted Polymer Brushes

Attachment of polymer chains to substrates provides another attractive way of controlling surface properties. 92-94 Assemblies of polymers that are linked to a surface and yet highly extended into solution are often termed polymer brushes. 95 These tethered polymer chains have potential applications in chemical separations, sensing, stabilization of colloidal suspensions, control of wetting and adhesion, corrosion resistance,

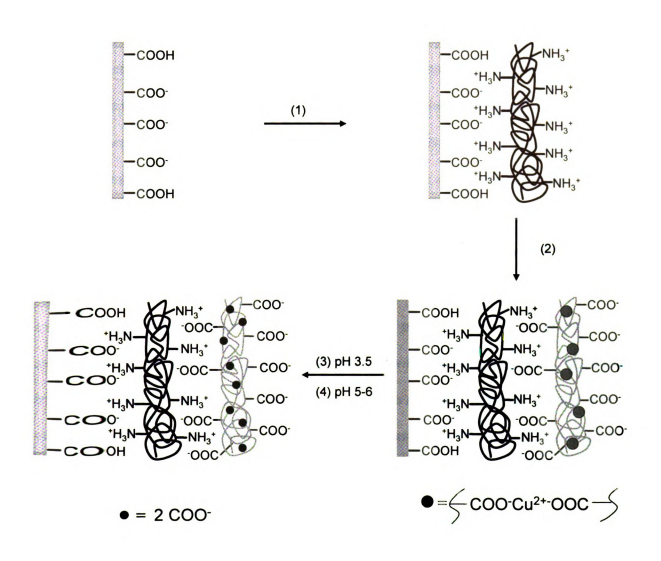


Figure 1.3: Synthesis of Cu^{2^+} -templated polyelectolyte films. Step 1: deposition of a polycation (PAH) in the presence of uncomplexed Cu^{2^+} . Step 2: deposition of partially Cu^{2^+} -complexed PAA. Step 3: removal of Cu^{2^+} . Step 4: deprotonation of the free carboxylic acid groups of PAA. Repetition of steps 1 and 2 produces a multilayer film. Intertwining of layers is not shown for figure clarity.

microfluidics, fouling resistance and "chemical gating". Methods for formation of polymer brushes include covalent attachment and physisorption of chains to a substrate.

The latter method generally utilizes block copolymers containing one block that strongly interacts with the surface and a second block that forms the brush layer. In this case, attachment to the surface occurs via van der Waals forces or hydrogen bonding, and thus these brushes can be desorbed by good solvents or displaced by other polymers.

Covalent tethering of polymer brushes to a surface greatly enhances film stability.

Covalent attachment of polymer brushes to a substrate can occur by either the "grafting to" or the "grafting from" method (Figure 1.4). ¹⁰¹ In the case of "grafting to" a surface, functional groups on a pre-synthesized polymer react with groups on the substrate to anchor the polymer. ¹⁰² Although this technique provides strong adhesion between the surface and the polymer, thicknesses of films prepared in this way are generally limited to less than 5 nm. After formation of a relatively thin film, a diffusion barrier prohibits more polymer molecules from reaching reactive surface sites, resulting in thir films with low grafting densities.

The "grafting from" technique is attractive because of the potential for formation of long polymer brushes with a high grafting density. In this technique, initiators are first immobilized on the surface, and polymer growth subsequently proceeds from these sites. Growth occurs as small monomers diffuse to the surface and reach growing chain ends, and thus, in contrast to the "grafting to" technique, there is no large diffusion barrier to polymer growth.

Among the numerous polymerization techniques, free radical polymerization is

"Grafting to" a surface

"Grafting from" a surface

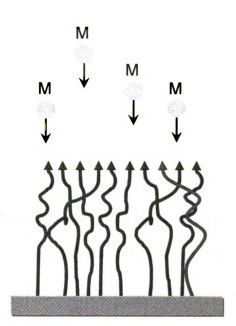


Figure 1.4: Two methods for grafting of polymer films onto solid surfaces. **Figure** adapted from reference 101.

the most widely used process because it is relatively easy to perform, and a wide range of monomers can be used. However, free radical polymerization provides limited control over molecular weight and molecular weight distribution because of rapid radical-radical termination reactions. This limitation inspired the emergence of new controlled/"living" radical polymerization techniques.

The key feature of any "living" process is that chain growth proceeds without the occurrence of irreversible termination steps, i.e., chain transfer, radical coupling, and disproportionation, and molecular weight is a linear function of conversion. The first reported "living" procedure was the sequential anionic polymerization of two non-polar monomers to produce block copolymers. Since then, numerous studies demonstrated controlled/"living" polymerization techniques. In the mid 1990s, two research groups reported the discovery of a controlled/"living" radical polymerization method that employs transfer of a halide atom between a transition metal salt and a growing radical. This process was termed atom transfer radical polymerization (ATRP). Today, of the many different "living" polymerization techniques (cationic, anionic, ring-opening, and nitroxide-mediated polymerization; and reversible addition fragmentation chain transfer 109,110), ATRP is probably the most powerful, versatile and attractive technique.

1.7 Atom Transfer Radical Polymerization (ATRP)

ATRP, as the name implies, is the reversible formation of a radical by transfer of the lateral definition and alkyl halide to a transition metal of low oxidation state (Scheme 1). 111 Upon transfer of the halide atom, the transition metal undergoes a one-electron

oxidation. After formation, radicals can either propagate via reaction with monomer or reform the dormant species by abstraction of a halide atom from a metal-ion complex.

Cu(I) complexes are the most common ATRP catalysts, but other transition metal ions

have also been used (Ru(II), 107 Fe(II), 112,113 Ni(II), 114,115 Pd(II) and Rh(II) 115). Monomers

Polymerized using ATRP include styrenes, (meth)acrylates, acrylonitriles,

(meth)acrylamides, methacrylic acids and vinylpyridine. 116 Compounds containing weak

carbon-halogen or hetero-halogen bonds, e.g., α-bromocarbonyl groups or sulfonyl

halides, serve as initiators.

R-X + Cu^IX/Ligand
$$\frac{k_a}{k_d}$$
 R• + Cu^{II}X₂/Ligand Initiator Catalyst k_d k_p R -R

Initiator – Alkyl halide M = Monomer

Catalyst – Transition metal (Cu, Fe, Ru, Ni, Pd) X = Halogen atom complexed by one or more ligands

Scheme 1.1: Mechanism of ATRP (adapted from reference 111).

ATRP is a controlled or "living" process when the atom-transfer equilibrium strongly favors the dormant species to give low radical concentrations. Because radical coupling and disproportionation kinetics are second order with respect to radical concentration, termination in ATRP can be minimal compared to propagation, leading to the formation of well-defined polymers with low polydispersity. To control polymerization, the transition metal/ligand ATRP catalyst is generally selected so that the

activation rate constant (k_a) is much lower than the deactivation rate constant (k_d).

Advantages of ATRP over conventional radical polymerizations include: compatibility with a variety of functional monomers, tolerance to trace impurities (water, oxygen, and inhibitor), control over molecular weights and molecular weight distributions, and possible block-copolymer formation by sequential activation of the dormant chain end in the presence of different monomers.

ATRP initiated from surfaces provides an attractive and convenient way to synthesize dense, uniform polymer brushes with controllable thickness (Figure 1.5).

When initiators are covalently attached to a surface, atom-transfer results in the formation of radicals on the substrate but not in solution, limiting unwanted polymerization in solution. The ability to perform ATRP at room temperature 117-121 also helps to avoid autopolymerization in solution, and thus extensive extraction of adsorbed polymer after growth of a polymer brush is not necessary. Miminal solution polymerization is especially important when synthesizing cross-linked polymer films because cross-linked, physisorbed polymer is difficult to remove from a surface. Recently, numerous reports described the use of ATRP to grow polymer brushes from a variety of substrates in a well-defined manner. The lateral properties and composition of polymer brushes.

1-8 Formation of membranes by surface-initiated ATRP

Like alternating polyelectrolyte deposition, surface-initiated ATRP provides a for formation of ultrathin membrane skins on porous alumina supports. This ess involves immobilization of an initiator on porous alumina and subsequent

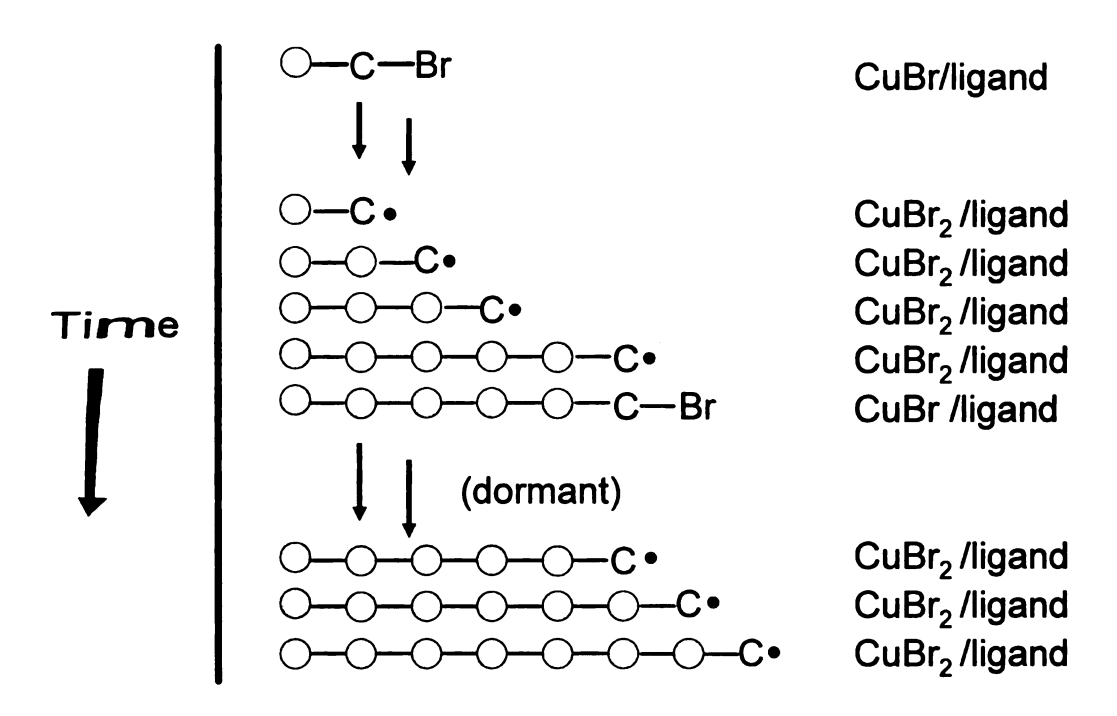


Figure 1.5: Cartoon showing the different stages of surface-initiated ATRP.

polymerization from the anchored initiator sites (Figure 1.6). We used two strategies to anchor the initiator to alumina. The first method employed adsorption of a few layers of charged polyelectrolytes and subsequent attachment of the initiator to the MPF surface. while the second procedure involved gold sputtering followed by formation of a selfassembled monolayer of a disulfide initiator. Polymerization from these immobilized initiators occurred using room-temperature ATRP. Using these procedures, we grew two kinds of polymer films, cross-linked poly(ethylene glycol dimethacrylate) (PEGDMA) and non cross-linked poly(2-hydroxyethyl methacrylate) (PHEMA). Cross-linked mer films are very attractive in separations because of their mechanical stability and low free volume. 126,127 PHEMA films are also attractive membrane materials because their hydroxyl groups can be easily derivatized in high yields to tailor films for specific separations. 118 The polymer growth from alumina was monitored by transmission-FTIR spectroscopy and scanning electron microscopy (SEM). Both top-down and crosssectional SEM images of these polymer films showed that they effectively covered the surface pores of the alumina.

Gas permeation studies with cross-linked PEGDMA membranes showed a gastransport selectivity of 20 for CO₂ over CH₄. In contrast, non cross-linked PHEMA membranes exhibited minimal gas transport selectivities that depended primarily on the molar masses of the permeating gases. However, after derivatization of the hydroxyl groups of PHEMA with pentadecafluorooctanoyl chloride, CO₂/CH₄ selectivity increased to ~ 9. A detailed description of gas-separation membranes prepared by ATRP from Porous alumina supports will form chapter 3 of the dissertation. Below I give some

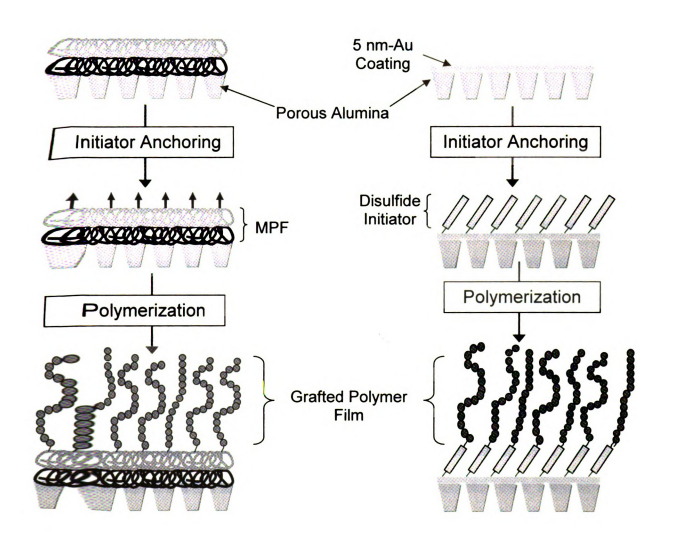


Figure 1.6: Surface-initiated atom transfer radical polymerization from (a) a **pol** yelectrolyte film deposited on alumina and (b) a self-assembled initiator **mon**olayer on Au-coated alumina.

1.9 Gas-Separation Membranes

Gas separation with polymer membranes was initially described over a century ago. Mitchell first reported that different gases permeate through natural rubber at different rates. ¹⁰⁸ In 1866, Graham demonstrated the enrichment of air with O₂ by permeation through a natural rubber membrane. 128 He showed that a mixture of gases could be separated according to their molecular weights by permeation through a microporous membrane, and the proportionality of gas flux to the reciprocal of the square root of molecular weight later became the well-known Graham's Law of Diffusion. Subsequently, there was little development of gas-separation membranes until the 1960's when Loeb and Souirajan¹²⁹ invented the first asymmetric membrane of industrial interest. This membrane, which was prepared from cellulose acetate by phase inversion, was originally made for desalination of water and later modified for gas separation. The asymmetric membrane contained a thin, dense, selective skin at the surface of a highly porous material, and this structure allowed much greater fluxes than thick, homogeneous membranes. The dense skin also exhibited higher selectivities than the porous structures that behaved according to Graham's law, while the underlying porous material provided mechanical strength.

The era of commercial gas separations began in the 1970's. Monsanto initiated the first large-scale separation of gases in 1977 for the recovery of H₂ from industrial gas streams using membranes made of polysulfone. In the 1980s, Permea introduced the prism membrane for separation and recovery of hydrogen from purge gas streams of ammonia plants. This was a polysulfone membrane coated with silicone rubber. In the

mid 1980s, Cyanara, Separex and GMS used dried cellulose acetate membranes for removal of CO_2 from natural gas, and in 1982, Generon produced the first N_2 /Air separation membrane using poly(4-methyl-1-pentene). This system had an O_2/N_2 selectivity of \sim 4. In the mid 1990s, Generon, Praxair and Medal produced a polyimide membrane for O_2/N_2 separation with a selectivity of 6-8. Other recent developments in gas-separation membranes include the commercialization of composite membranes. Composite membranes are made by depositing a thin layer of polymer on a highly porous substrate. The thin selective layer acts as a discriminating film to give selectivity, and the porous layer provides mechanical stability to the system. Composite membranes have the advantage that only a small amount of expensive skin material is needed, while the porous support can be made from an inexpensive polymer.

Membrane geometry is also critical for practical separations, as surface area must be maximized. Asymmetric membranes can be packed as hollow fibers or in a spiral-wound configuration. A spiral-wound module consists of series of membrane envelopes, and each envelope consists of two membrane sheets, which are separated by a feed spacer. In a hollow fiber module, asymmetric hollow fibers are bundled together to achieve a very high surface area. Some commercial hollow fiber modules contain more than a million hollow fibers. ^{130,131}

Current membrane-based gas separations include a wide range of applications such as recovery of H₂ from synthesis gases and petrochemical process streams, removal of CO₂ from mixtures of hydrocarbons and natural gases, N₂ or O₂ enrichment from air, SO₂ removal from smelter gas streams, H₂S and water removal from natural gas and air streams, and NH₃ removal from recycle streams in ammonia synthesis.¹⁰⁷ These

processes use both composite and asymmetric membranes as well as several different membrane geometries including hollow fiber and spiral wound systems.^{3,132}

Of special relevance to this thesis, several studies demonstrated the possibility of using various poly(alkyl methacrylates) in gas separation membranes, e.g., poly(ethyl methacrylate), poly(tert-butyl methacrylate), and a styrene/methacrylate copolymer. Yoshikawa and co-workers showed that the presence of amine moieties in poly(methacrylate) films greatly enhances CO₂/N₂ separation. The use of fluorinated poly(methacrylates) provides another way to enhance CO₂/N₂ or CO₂/CH₄ selectivity. Most previous studies with poly(alkyl methacrylates) employed cast membranes with large thicknesses, and decreasing the thickness of these films would greatly enhance flux. Although many successes have been achieved in gas separation membrane research, fabrication of utrathin (<50 nm) polymer skins is still a challenge, so the focus of this work was to develop methods for deposition of selective, ultrathin polymer skins.

To develop either thin or thick membrane materials, one needs to understand the factors affecting gas separation and the mechanism of separation. Below I discuss the mechanism of gas transport through polymer membranes and the factors that determine selectivity for one gas over another.

1.10 Mechanism of Gas Transport through Polymer Membranes

Gas-transport selectivity is usually based on one of three mechanisms: Knudsen diffusion, molecular sieving or solution/diffusion. Knudsen diffusion dominates when membrane pores are larger than the gas molecules being separated but smaller than the mean free path of these gases. Permeation rates are inversely proportional to the square

root of the gas molecular weight of the gas so selectivity is the reciprocal of the square root of the ratio of the molecular weights of the gases being separated.¹³⁸ Because most gases of interest have similar molecular weights, separations based on Knudsen-diffusion are not highly selective.

Molecular sieving of common gases occurs when pore diameters in a membrane are smaller than 7 Å. Selectivities between gases of different sizes can be nearly infinite when one gas is incapable of entering a pore. This method, however, is limited by relatively low fluxes and the difficulty of preparing defect-free membranes with uniform pore sizes.

Solution-diffusion is the most common mechanism that operates in practical gas separations. In this mechanism, transport of gases occurs in three steps: sorption of the penetrant into the polymer film at the high-pressure interface, diffusion of the penetrant through the polymer film, and finally, desorption at the permeate side (low-pressure interface). Thus, gas flux depends on the diffusivity and solubility of the gas in the polymer as well as the transmembrane partial pressure gradient. Fick's first law (equation 1.1) describes the transport of a species within a nonporous membrane. Flux, *J*, is proportional to the concentration gradient, dc/dx, and the diffusion coefficient, *D*, for the molecule in the membrane.

$$J = -D\frac{dc}{dx}$$

According to Henry's law, the concentration, C, of a specific gas in the membrane at the high- or low-pressure interface is proportional to partial pressure, p, and the solubility coefficient, S (equation 1.2).

$$C = S p 1.2$$

Using Henry's law to determine concentrations at the two gas-membrane interfaces, and assuming steady-state flux and constant values of D and S allows transformation of equation 1.1 to equation 1.3.

$$J = D S \Delta p / \delta$$
 1.3

In this equation, Δp is the partial pressure difference between the feed and permeate, and δ is the membrane thickness. The permeability coefficient, P, of a particular membrane for a specific gas is then defined by equation 1.4.

$$P = D S = J \delta/\Delta p$$
 1.4

Selectivity for one gas over another, α_{AB} , is given by the ratio of the permeability coefficients of two gases (equation 1.5). This ratio is a measure of the relative fluxes of the two gases at the same driving force. Since permeability coefficients depend on both solubility and diffusion coefficients, selectivity also contains diffusivity (D_A/D_B) and solubility (S_A/S_B) components. Diffusion selectivity generally favors small molecules, while solubility selectivity favors more condensable gases.

$$\alpha_{AB} = \frac{P_A}{P_B} = \frac{D_A}{D_B} \frac{S_A}{S_B}$$
 1.5

Both selectivity and permeability determine membrane performance, and thus the careful selection of polymer materials is vital for efficient separations.

1.11 Summary

As discussed earlier, the main objective of this work is the fabrication of defectfree, ultrathin polymer skins on porous supports and the use of these composite
membranes in ion and gas separation to achieve high selectivity along with high flux. In
this chapter, I tried to show the need for ultrathin polymer skins in separation membranes
and the challenges in forming these polymer skins with controllable thicknesses. I also
discussed background on the development of polyelectrolyte films and polymerization
from a surface, the theory behind gas transport through polymer membranes and some
relevant past research done on the development of gas and ion separation membranes.

1.11 References

- (1) Spillman, R. W. Chem. Eng. Prog. 1989, 85, 41-62.
- (2) Henis, J. M. S.; Tripodi, M. K. Science 1983, 220, 11-17.
- (3) Baker, R. W. Ind. Eng. Chem. Res. 2002, 41, 1393-1411.
- (4) Chiou, J. S.; Paul, D. R. J. Membr. Sci. 1989, 45, 167-189.
- (5) Ulman, A. Chem. Rev. 1996, 96, 1533-1554.
- (6) Swalen, J. D.; Allara, D. L.; Andrade, J. D.; Chandross, E. A.; Garoff, S.; Israelachvili, J.; McCarthy, T. J.; Murray, R.; Pease, R. F.; et al. *Langmuir* 1987, 3, 932-950.
- (7) Ulman, A. Introduction to Ultrathin organic films: from Langmuir-Blodgett to self-assembly; Academic Press: Boston, 1991.
- (8) Bubeck, C.; Neher, D.; Kaltbeitzel, A. Makromol. Chem., Macromol. Symp. 1990, 37, 239-245.
- (9) Miller, L. S.; McRoberts, A. M.; Walton, D. J.; Peterson, I. R.; Parry, D. A.; Sykesud, C. G. D.; Newton, A. L.; Powell, B. D.; Jasper, C. A. *Thin Solid Films* 1996, 284-285, 927-931.
- (10) Petty, M. C. Biosensors Bioelectron. 1995, 10, 129-134.
- (11) Whitesides, G. M.; Laibinis, P. E. Langmuir 1990, 6, 87-96.
- (12) Stroeve, P.; Vasquez, V.; Coelho, M. A. N.; Rabolt, J. F. *Thin Solid Films* **1996**, 284-285, 708-712.
- (13) van Ackern, F.; Krasemann, L.; Tieke, B. *Thin Solid Films* **1998**, *327-329*, 762-766.
- (14) Harris, J. J.; Stair, J. L.; Bruening, M. L. Chem. Mater. 2000, 12, 1941-1946.
- (15) Langmuir, I. J. Am. Chem. Soc. 1917, 39, 1848-1906.
- (16) Blodgett, K. B. J. Am. Chem. Soc. 1935, 57, 1007-1022.
- (17) Embs, F.; Funhoff, D.; Laschewsky, A.; Licht, U.; Ohst, H.; Prass, W.; Ringsdorf, H.; Wegner, G.; Wehrmann, R. Adv. Mater. 1991, 3, 25-31.
- (18) Allara, D. L.; Nuzzo, R. G. Langmuir 1985, 1, 45-52.

- (19) Allara, D. L.; Fowkes, F. M.; Noolandi, J.; Rubloff, G. W.; Tirrell, M. V. *Mater. Sci. Eng.* **1986**, *83*, 213-226.
- (20) Bishop, A. R.; Nuzzo, R. G. Curr. Opin. Coll. Int. Sci. 1996, 1, 127-136.
- (21) Nuzzo, R. G.; Fusco, F. A.; Allara, D. L. J. Am. Chem. Soc. 1987, 109, 2358-2368.
- (22) Knoll, W.; Matsuzawa, M.; Offenhausser, A.; Rühe, J. Isr. J. Chem. 1997, 36, 357-369.
- (23) Allara, D. L.; Nuzzo, R. G. Langmuir 1985, 1, 52-66.
- Bain, C. D.; Troughton, E. B.; Tao, Y. T.; Evall, J.; Whitesides, G. M.; Nuzzo, R. G. J. Am. Chem. Soc. 1989, 111, 321-335.
- (25) Bain, C. D.; Evall, J.; Whitesides, G. M. J. Am. Chem. Soc. 1989, 111, 7155-7164.
- (26) Cao, G.; Hong, H. G.; Mallouk, T. E. Acc. Chem. Res. 1992, 25, 420-427.
- (27) Fang, M.; Kaschak, D. M.; Sutorik, A. C.; Mallouk, T. E. J. Am. Chem. Soc. 1997, 119, 12184-12191.
- (28) Kim, H.-N.; Keller, S. W.; Mallouk, T. E.; Schmitt, J.; Decher, G. Chem. Mater. 1997, 9, 1414-1421.
- (29) Kohli, P.; Blanchard, G. J. Langmuir 1999, 15, 1418-1422.
- (30) Huc, V.; Bourgoin, J.-P.; Bureau, C.; Valin, F.; Zalczer, G.; Palacin, S. J. Phys. Chem. B 1999, 103, 10489-10495.
- (31) Decher, G.; Hong, J. D. Makromol. Chem., Macromol. Symp. 1991, 46, 321-327.
- (32) Decher, G.; Hong, J. D. Ber. Bunsenges. Phys. Chem. 1991, 95, 1430-1434.
- (33) Lvov, Y.; Ariga, K.; Ichinose, I.; Kunitake, T. J. Am. Chem. Soc. 1995, 117, 6117-6123.
- (34) Caruso, F.; Furlong, D. N.; Ariga, K.; Ichinose, I.; Kunitake, T. *Langmuir* 1998, 14, 4559-4565.
- (35) Ferreira, M.; Rubner, M. F. *Macromolecules* **1995**, 28, 7107-7114.
- (36) Caruso, F.; Niikura, K.; Furlong, D. N.; Okahata, Y. *Langmuir* **1997**, *13*, 3427-3433.

- (37) Lvov, Y.; Decher, G.; Möehwald, H. Langmuir 1993, 9, 481-486.
- (38) Lvov, Y.; Haas, H.; Decher, G.; Möehwald, H.; Mikhailov, A.; Mtchedlishvily, B.; Morgunova, E.; Vainshtein, B. *Langmuir* 1994, 10, 4232-4236.
- (39) Lvov, Y. M.; Lu, Z.; Schenkman, J. B.; Zu, X.; Rusling, J. F. J. Am. Chem. Soc. 1998, 120, 4073-4080.
- (40) Sukhorukov, G. B.; Möehwald, H.; Decher, G.; Lvov, Y. M. *Thin Solid Films* 1996, 284-285, 220-223.
- (41) Schlenoff, J. B.; Laurent, D.; Ly, H.; Stepp, J. Adv. Mater. 1998, 10, 347-349.
- (42) Laurent, D.; Schlenoff, J. B. *Langmuir* **1997**, *13*, 1552-1557.
- (43) Lindsay, G. A.; Roberts, M. J.; Chafin, A. P.; Hollins, R. A.; Merwin, L. H.; Stenger-Smith, J. D.; Yee, R. Y.; Zarras, P.; Wynne, K. J. *Chem. Mater.* 1999, 11, 924-929.
- (44) Lvov, Y.; Munge, B.; Giraldo, O.; Ichinose, I.; Suib, S. L.; Rusling, J. F. *Langmuir* **2000**, *16*, 8850-8857.
- (45) Iler, R. K. J. Coll. Int. Sci 1966, 21, 569-594.
- (46) Decher, G.; Hong, J. D.; Schmitt, J. *Thin Solid Films* **1992**, 210/211, 831-835.
- (47) Lvov, Y.; Decher, G.; Sukhorukov, G. *Macromolecules* 1993, 26, 5396-5399.
- (48) Decher, G. Science 1997, 277, 1232-1237.
- (49) Bertrand, P.; Jonas, A.; Laschewsky, A.; Legras, R. Macromol. Rapid. Commun. 2000, 21, 319-348.
- (50) Dubas, S. T.; Schlenoff, J. B. *Macromolecules* **1999**, *32*, 8153-8160.
- (51) Laschewsky, A.; Mayer, B.; Wischerhoff, E.; Arys, X.; Jonas, A. *Ber. Bunsenges. Phys. Chem.* **1996**, *100*, 1033-1038.
- (52) Arys, X.; Jonas, A. M.; Laguitton, B.; Laschewsky, A.; Legras, R.; Wischerhoff, E. *Thin Solid Films* 1998, 327-329, 734-738.
- (53) Hoogeveen, N. G.; Stuart, M. A. C.; Fleer, G. J.; Boehmer, M. R. *Langmuir* 1996, 12, 3675-3681.
- (54) Yoo, D.; Shiratori, S. S.; Rubner, M. F. *Macromolecules* **1998**, *31*, 4309-4318.

- (55) Shiratori, S. S.; Rubner, M. F. *Macromolecules* **2000**, *33*, 4213-4219.
- (56) Caruso, F.; Niikura, K.; Furlong, D. N.; Okahata, Y. *Langmuir* **1997**, *13*, 3422-3426.
- (57) Sukhorukov, G. B.; Schmitt, J.; Decher, G. Ber. Bunsenges. Phys. Chem. 1996, 100, 948-953.
- (58) Harris, J. J.; Bruening, M. L. Langmuir 2000, 16, 2006-2013.
- (59) Schmitt, J.; Grüenewald, T.; Decher, G.; Pershan, P. S.; Kjaer, K.; Löesche, M. *Macromolecules* 1993, 26, 7058-7063.
- (60) Löesche, M.; Schmitt, J.; Decher, G.; Bouwman, W. G.; Kjaer, K. *Macromolecules* **1998**, *31*, 8893-8906.
- (61) Kurth, D. G.; Osterhout, R. Langmuir 1999, 15, 4842-4846.
- (62) Lvov, Y.; Ariga, K.; Onda, M.; Ichinose, I.; Kunitake, T. *Collid Surf. A* **1999**, 146, 337-346.
- (63) Chen, W.; McCarthy, T. J. *Macromolecules* **1997**, *30*, 78-86.
- (64) Liu, Y.; Ma, H.; Jen, A. K. Y. Chem Commun. 1998, 2747-2748.
- (65) Wu, A.; Yoo, D.; Lee, J. K.; Rubner, M. F. J. Am. Chem. Soc. 1999, 121, 4883-4891.
- (66) Koetse, M.; Laschewsky, A.; Mayer, B.; Rolland, O.; Wischerhoff, E. *Macromolecules* **1998**, *31*, 9316-9327.
- (67) Laschewsky, A.; Wischerhoff, E.; Kauranen, M.; Persoons, A. *Macromolecules* **1997**, *30*, 8304-8309.
- (68) Roberts, M. J.; Lindsay, G. A.; Herman, W. N.; Wynne, K. J. J. Am. Chem. Soc. 1998, 120, 11202-11203.
- (69) Wang, X.; Balasubramanian, S.; Kumar, J.; Tripathy, S. K.; Li, L. Chem. Mater. 1998, 10, 1546-1553.
- (70) Balasubramanian, S.; Wang, X.; Wang, H. C.; Yang, K.; Kumar, J.; Tripathy, S. K.; Li, L. *Chem. Mater.* **1998**, *10*, 1554-1560.
- (71) Yang, X.; Johnson, S.; Shi, J.; Holesinger, T.; Swanson, B. Sens. Actuators, B 1997, B45, 87-92.

- (72) Lowy, D. A.; Finklea, H. O. *Electrochim. Acta* 1997, 42, 1325-1335.
- (73) Fou, A. C.; Rubner, M. F. *Macromolecules* **1995**, *28*, 7115-7120.
- (74) Lukkari, J.; Vinikanoja, A.; Salomaki, M.; Aaritalo, T.; Kankare, J. Synth. Met. **2001**, 121, 1403-1404.
- (75) Zheng, H.; Rubner, M. F.; Hammond, P. T. Langmuir **2002**, 18, 4505-4510.
- (76) Dai, J.; Sullivan, D. M.; Bruening, M. L. Ind. Eng. Chem. Res. 2000, 39, 3528-3535.
- (77) Farhat, T. R.; Schlenoff, J. B. Electrochem. Solid-State Lett. 2002, 5, B13-B15.
- (78) Krasemann, L.; Tieke, B. Mater. Sci. Eng. C 1999, C8-C9, 513-518.
- (79) Krasemann, L.; Tieke, B. *Langmuir* **2000**, *16*, 287-290.
- (80) Stair, J. L.; Harris, J. J.; Bruening, M. L. Chem. Mater. 2001, 13, 2641-2648.
- (81) Stroeve, P.; van Os, M.; Kunz, R.; Rabolt, J. F. *Thin Solid Films* **1996**, *284-285*, 200-203.
- (82) Krasemann, L.; Tieke, B. Chem. Eng. Tech. 2000, 23, 211-213.
- (83) Krasemann, L.; Tieke, B. J. Membr. Sci. 1998, 150, 23-30.
- (84) Meier-Haack, J.; Lenk, W.; Lehmann, D.; Lunkwitz, K. J. Membr. Sci. 2001, 184, 233-243.
- (85) Levaesalmi, J.-M.; McCarthy, T. J. Macromolecules 1997, 30, 1752-1757.
- (86) Dai, J.; Bruening, M. L. *Nano Letters* **2002**, *2*, 497-501.
- (87) Farhat, T. R.; Schlenoff, J. B. Langmuir **2001**, 17, 1184-1192.
- (88) Von Klitzing, R.; Möhwald, H. Thin Solid Films 1996, 284-285, 352-356.
- (89) Qiu, X.; Donath, E.; Möhwald, H. Macromolecular Materials and Engineering **2001**, 286, 591-597.
- (90) Antipov, A. A.; Sukhorukov, G. B.; Donath, E.; Möhwald, H. J. Phys. Chem. B **2001**, 105, 2281-2284.
- (91) Schlenoff, J. B.; Ly, H.; Li, M. J. Am. Chem. Soc. 1998, 120, 7626-7634.

- (92) Rühe, J.; Knoll, W. Supramolecular Polymers 2000, 565-613.
- (93) Zhao, B.; Brittain, W. J. Prog. Polym, Sci. 2000, 25, 677-710.
- (94) Uyama, Y.; Kato, K.; Ikada, Y. Adv. Polym. Sci. 1998, 137, 1-39.
- (95) Milner, S. T. Science 1991, 251, 905-914.
- (96) Ito, Y.; Nishi, S.; Park, Y. S.; Iminishi, Y. Macromolecules 1997, 30, 8096.
- (97) Mayes, A. M.; Kumar, S. K. MRS Bull. 1997, 22, 43-47.
- (98) Halperin, A.; Tirrell, M.; Lodge, T. P. Adv. Poly. Sci., 1991, 100, 31-71.
- (99) Nagale, M.; Kim, B. Y.; Bruening, M. L. J. Am. Chem. Soc. 2000, 122, 11670-11678.
- (100) Belder, G. F.; ten Brinke, G.; Hadziioannou, G. Langmuir 1997, 13, 4102-4105.
- (101) Jordan, R.; Ulman, A.; Kang, J. F.; Rafailovich, M. H.; Sokolov, J. J. Am. Chem. Soc. 1999, 121, 1016-1022.
- (102) Mansky, P.; Liu, Y.; Huang, E.; Russell, T. P.; Hawker, C. Science 1997, 275, 1458-1460.
- (103) Matyjaszewski, K. In ACS Symposium Series; Matyjaszewski, K., Ed.; American Chemical Society: Washington DC, 1998; Vol. 685, pp 2-30.
- (104) Szwarc, M. Nature 1956, 178, 1168-1169.
- (105) Van Beylen, M.; Bywater, S.; Smets, G.; Szwarc, M.; Worsfold, D. J. Adv. Polym. Sci. 1988, 86, 87-143.
- (106) Wang, J.-S.; Matyjaszewski, K. Macromolecules 1995, 28, 7901-7910.
- (107) Kato, M.; Kamigaito, M.; Sawamoto, M.; Higashimura, T. *Macromolecules* 1995, 28, 1721-1723.
- (108) Husseman, M.; Malmström, E. E.; McNamara, M.; Mate, M.; Mecerreyes, D.; Benoit, D. G.; Hedrick, J. L.; Mansky, P.; Huang, E.; Russell, T. P.; Hawker, C. J. *Macromolecules* 1999, 32, 1424-1431.
- (109) Baum, M.; Brittain, W. J. Macromolecules 2002, 35, 610-615.
- (110) Tsujii, Y.; Ejaz, M.; Sato, K.; Goto, A.; Fukuda, T. Macromolecules 2001, 34, 8872-8878.

- (111) Matyjaszewski, K.; Xia, J. Chem. Rev. 2001, 101, 2921-2990.
- (112) Wei, M.; Xia, J.; Matyjaszewski, K. Polym. Prepr. (Am. Chem. Soc., Div. Polym. Chem.) 1997, 38, 233-234.
- (113) Wei, M.; Xia, J.; McDermott, N. E.; Matyjaszewski, K. Polym. Prepr. (Am. Chem. Soc., Div. Polym. Chem.) 1997, 38, 231-232.
- (114) Granel, C.; Dubois, P.; Jerome, R.; Teyssie, P. *Macromolecules* 1996, 29, 8576-8582.
- (115) Uegaki, H.; Kotani, Y.; Kamigaito, M.; Sawamoto, M. Macromolecules 1997, 30, 2249-2253.
- (116) Matyjaszewski, K.; Xia, J. Chem. Rev., 101, 2921-2990.
- (117) Kim, J.-B.; Bruening, M. L.; Baker, G. L. J. Am. Chem. Soc. 2000, 122, 7616-7617.
- (118) Huang, W.; Kim, J.-B.; Bruening, M. L.; Baker, G. L. *Macromolecules* 2002, 35, 1175-1179.
- (119) Huang, W.; Baker, G. L.; Bruening, M. L. Angew. Chem. Int. Ed. 2001, 40, 1510-1512.
- (120) Matyjaszewski, K.; Miller, P. J.; Shukla, N.; Immaraporn, B.; Gelman, A.; Luokala, B. B.; Siclovan, T. M.; Kickelbick, G.; Vallant, T.; Hoffmann, H.; Pakula, T. *Macromolecules* 1999, 32, 8716-8724.
- (121) Jones, D. M.; Huck, W. T. S. Adv. Mater. 2001, 13, 1256-1259.
- (122) Shah, R. R.; Merreceyes, D.; Husemann, M.; Rees, I.; Abbott, N. L.; Hawker, C. J.; Hedrick, J. L. Macromolecules 2000, 33, 597-605.
- (123) Huang, X.; Wirth, M. J. *Macromolecules* 1999, 32, 1694-1696.
- (124) Huang, X.; Doneski, L. J.; Wirth, M. J. Anal. Chem. 1998, 70, 4023-4029.
- (125) Huang, X.; Doneski, L. J.; Wirth, M. J. Chemtech 1998, 28, 19-25.
- (126) Jia, J.; Baker, G. L. J. Polym. Sci., Part B: Polym. Phys. 1998, 36, 959-968.
- (127) Eisenbach, C. D. Polymer 1980, 21, 1175-1179.
- (128) Graham, T. *Philos. Mag.* **1866**, *32*, 401-420.

- (129) Loeb, S.; Sourirajan, S. Adv. Chem. Ser. 1963, 38, 117-132.
- (130) Henis, J. M. S.; Tripodi, M. K. J. Membr. Sci. 1981, 8, 233-246.
- (131) Fritzsche, A. K. Polymer News 1988, 13, 266-274.
- (132) Meyer, H. S.; Gamez, J. P. In *Proceedings of the Laurance Reid Gas Conditioning Conference*, 1995; Vol. 45th, pp 284-307.
- (133) Wright, C. T.; Paul, D. R. Polymer 1997, 38, 1871-1878.
- (134) Raymond, P. C.; Paul, D. R. J. Polym. Sci., Part B: Polym. Phys. 1990, 28, 2079-2102.
- (135) Yoshikawa, M.; Fujimoto, K.; Kinugawa, H.; Kitao, T.; Ogata, N. Chem. Lett. 1994, 243-246.
- (136) Arnold, M. E.; Nagai, K.; Freeman, B. D.; Spontak, R. J.; Betts, D. E.; DeSimone, J. M.; Pinnau, I. *Macromolecules* **2001**, *34*, 5611-5619.
- (137) Koros, W. J.; Fleming, G. K. J. Membr. Sci. 1993, 83, 1-80.
- (138) Uhlhorn, R. J. R.; Keizer, K.; Burggraaf, A. J. J. Membr. Sci. 1989, 46, 225-241.
- (139) Koresh, J. E.; Soffer, A. Sep. Sci. Technol. 1987, 22, 973-982.
- (140) Way, J. D.; Roberts, D. L. Sep. Sci. Technol. 1992, 27, 29-41.

CHAPTER 2

Enhancing the Anion-Transport Selectivity of Multilayer Polyelectrolyte Membranes by Templating with Cu²⁺

2.1 Introduction

Alternating adsorption of polyanions and polycations is an attractive method for forming ultrathin separation membranes because of its versatility and simplicity. 1,2 Previous studies of multilayer polyelectrolyte membranes (MPMs) deposited on porous supports showed selective separation of monovalent and divalent ions, ³⁻⁵ modest gas separations^{3,6-9} and highly selective pervaporation.^{3,8,10,11} This study focuses on enhancing the anion-transport selectivities of MPMs by increasing their fixed negative charge density through templating with Cu²⁺. Introduction of ion-exchange sites occurs due to partial Cu²⁺ complexation by the carboxylate groups of poly(acrylic acid) (PAA) during the deposition of PAA/poly(allylamine hydrochloride) (PAH) membranes. Removal of Cu²⁺ in acidic solution and subsequent deprotonation of -COOH groups yields fixed -COO ion-exchange sites as shown in Figure 2.1. Studies of ion transport through Cu²⁺-templated PAA (PAA-Cu)/PAH membranes show a 4-fold increase in Cl⁻ /SO₄² selectivities compared to pure PAA/PAH membranes deposited under similar conditions. Cross-linking 12,13 of templated films through heat-induced amidation can yield Cl⁻/SO₄² selectivities as high as 610, and these selectivities can be achieved without a diminution in flux relative to PAA/PAH membranes that are not templated or crosslinked.

Such separations of ions of different valence are important in applications such as removal of harmful ions from water, ¹⁴⁻¹⁶ water softening, ^{17,18} production of edible

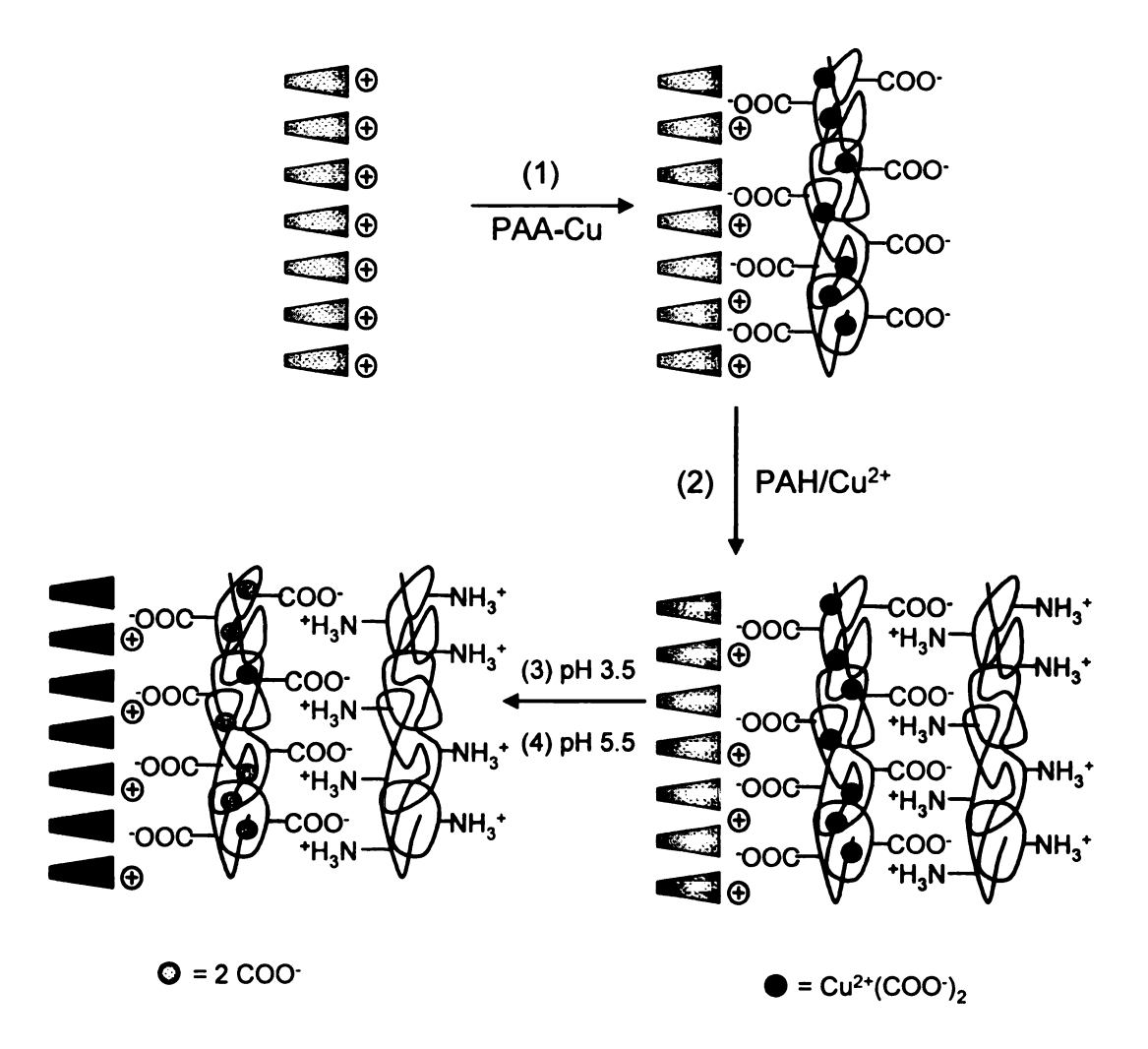


Figure 2.1: Preparation of Cu²⁺- templated polyelectrolyte films on porous alumina supports. Step 1-adsorption of partially Cu²⁺-complexed PAA on porous alumina. Step 2-adsorption of a polycation (PAH). Step 3-removal of Cu²⁺. Step 4-deprotonation of the free carboxylic acid groups of PAA. Repetition of steps 1 and 2 produces multilayer films. Intertwining of layers is not shown for figure clarity.

salt from sea water, ¹⁹ and prevention of fouling by cooling water. ²⁰ Most of these applications require high permselectivity among different ions as well as high flux. Previous research on ion-exchange membranes showed that permselectivity can be controlled by alteration of hydrophilicity/hydrophobicity, ^{21,22} cross-linking ^{23,24} or surface charge density. ²⁵ To achieve maximum efficiency in ion-separation processes, a minimal membrane thickness is also vital for achieving high flux. Multilayer polyelectrolyte films (MPFs) are attractive for ion separation membranes in part because of their minimal thickness.

Several studies on ion-exchange membranes already showed an increase in monovalent/ divalent ion selectivities after adsorption of one layer of polyelectrolyte to the surface of the membrane. However, even better permselectivities might be obtained when membranes are exclusively composed of multilayer polyelectrolyte films (MPFs). MPFs are attractive as separation membranes because both their thickness and surface charge density can, in principle, be controlled by varying deposition conditions such as pH, 28,29 salt concentration, 30-34 and the number of adsorbed layers. Recent studies show that MPMs exhibit monovalent/divalent ion-transport selectivities are at least in part due to Donnan exclusion at the charged surface layer of the polyelectrolyte films. Control over the charge density either at the surface or in the bulk of MPMs should thus yield control over membrane selectivity. Previous characterization of MPFs showed, however, that the bulk of the film is intrinsically charge compensated (i.e., polycations exactly neutralize the charge on polyanions), and total exchangeable charge resides only at the surface of the film. Enhancement of ion-

transport selectivity by introduction of charge into the bulk of MPFs will likely require post-deposition film modification.

In this study, we use Cu²⁺-complexed PAA³⁸⁻⁴⁰ to control the charge density within PAA/PAH films. Several groups recently integrated metallosupramolecular polyelectrolytes into polyelectrolyte assemblies.⁴¹⁻⁴⁵ For example, Kurth and coworkers used iron-coordinated terpyridine as a polycation to form MPFs with poly(styrene sulfonate).⁴⁵ However, in the present case, we only partially complex PAA with Cu²⁺, so that PAA is still deposited as a polyanion. This allows the introduction of cation-exchange sites after removal of Cu²⁺, and formation of highly selective membranes. Diffusion-dialysis studies and simple modeling of transport through these membranes suggest that selectivity is due to both Donnan exclusion and diffusional selectivity.

2.2 Experimental

2.2.1 Chemicals and Solutions

Poly(allylamine hydrochloride) (PAH) (M_w = 70,000), poly(acrylic acid) (PAA) (M_w = 2,000) and 3-mercaptopropionic acid (MPA) were used as received from Aldrich. We used a relatively low molecular weight PAA to increase its solubility when complexed with Cu²⁺. NaCl, CuCl₂·5H₂0, and Na₂SO₄ were used as received from Spectrum. AnodiscTM porous alumina membranes with 0.02 μm-diameter surface pores (Whatman Anodisc) were used as supports for deposition of polyelectrolyte films. ^{46,47} For cross-linked PAA/PAH membranes, the outer polypropylene support ring of the alumina membrane was burned off prior to film deposition by heating at 400 °C for 18-20 hours. This was done in order to prevent melting of the polymer ring into the pores of the

membrane during heat-induced cross-linking. Gold slides (200 nm of sputtered Au on 20 nm Cr on Si (100) wafers) were used as substrates for ellipsometry, external reflection FTIR spectroscopy and cyclic voltammetry.

2.2.2 Film Preparation

Prior to film deposition, porous alumina substrates were cleaned in a UV/ozone cleaner (Boekel UV-Clean model 135500) for 15 min. Deposition of polyelectrolyte films began by dipping the substrate into a solution of PAA (0.04 M with respect to the repeating unit) containing CuCl₂ (2.5mM to 7.5 mM) for 5 min followed by rinsing for 1 min with water (Milli-O, 18 M Ω -cm). The substrate was then immersed in a solution of PAH (0.04 M with respect to the repeating unit and containing the same CuCl₂ concentration as PAA) for 5 min and rinsed with water for 1 min. The above procedure was repeated until the desired number of bilayers was deposited. The pH values of the deposition solutions were adjusted to 5.5, 6, or 6.6 using dilute HCl and NaOH solutions. Both PAH and PAA solutions contained 0.5 M NaCl as a supporting electrolyte to increase film thickness, and PAH and PAA depositions were always done at the same pH. The porous alumina membrane is asymmetric such that the permeate side contains 0.2 μm-diameter pores, while pores on the filtrate side are 0.02 μm in diameter. Deposition of polyelectrolytes was limited to the filtrate side by using an o-ring holder. After deposition of the desired number of layers, membranes were rinsed well with water and dried with N₂. For cross-linking, membranes were placed in a flask that was subsequently purged with N_2 for 30 min and then slowly heated to the desired temperature (~45 min ramping time). Heating continued at the desired temperature (100-160 °C) for an additional 2 hours under N₂ purging.

Similar to porous alumina supports, gold slides were UV/ozone cleaned prior to deposition. However, before polyelectrolyte adsorption, slides were immersed in an ethanolic solution of 2 mM MPA for 30 min and rinsed well with ethanol followed by deionized water (Milli-Q, 18 M Ω -cm). This produces a carboxylic acid-containing monolayer on the surface that will be charged upon deprotonation. The polyelectrolyte deposition on gold was the same as for porous alumina except that depositions started with PAH rather than PAA. We used MPA rather than a long-chain alkanoic acid to avoid possible blocking of electron transfer at the gold surface. 48,49

2.2.3 Film Characterization

Film thickness was determined with a rotating analyzer ellipsometer (J.A. Wollam model M-44), assuming a film refractive index of 1.5. The refractive index and absorption coefficient of the substrates were determined after deposition of the MPA layer. For each sample, thicknesses at three different spots were taken. External reflectance FTIR spectra were obtained with a Nicolet Magna-560 FTIR spectrometer using a Pike grazing angle attachment (80° angle of incidence). The spectrometer employs a MCT detector. Electrochemical measurements were performed with a CH-Instrument Electrochemical Analyzer (model 605) employing a standard three-electrode cell containing a Ag/AgCl (3M KCl) reference electrode and a Pt wire counter electrode. The working electrode was a gold slide in a plastic holder that exposed an area of 0.1 cm². The supporting electrolyte in all electrochemical experiments was 0.1M Na₂SO₄. Before measuring cyclic voltammograms (scan rate of 0.1 V/s), solutions were purged with N₂ for 20-30 min.

2.2.4 Ion-Transport Studies.

Diffusion dialysis was performed using two glass half cells as shown in Figure 2.2. The membrane was clamped between the two half cells, with the film side of the membrane facing towards the feed cell, so as to expose 2 cm² of membrane to the feed solution. The permeate cell contained deionized water (90 mL), and the feed cell contained 0.1 M solutions (90 mL) of NaCl or Na₂SO₄. After dialysis with a particular salt, the apparatus was washed well with water, and both cells were equilibrated with deionized water for 30 min before examining the next salt. Alternating NaCl (pH 5.3) and Na₂SO₄ (pH 5.6) transport experiments were performed until two successive chloride fluxes matched within 15%. Once the membrane achieved a steady Cl⁻ flux value (this usually occurs after 4 to 5 NaCl and Na₂SO₄ runs), it was removed from the permeability apparatus and dipped in pH 3.5 water (dilute HCl solution) for one hour to ensure that all the copper was removed from the membrane. Then the membrane was immersed in deionized water (adjusted to pH 5-6 with a dilute NaOH solution) for 1-2 hours to deprotonate the -COOH groups that were created upon removal of Cu²⁺. Permeability experiments were then repeated, and Cl⁻ fluxes differed by less than 5% when performed before and after a Na₂SO₄ permeability experiment. The Cl⁻/SO₄²⁻ selectivities and flux values reported here are calculated exclusively from permeability studies performed directly after immersing in pH 3.5 water followed by pH 5-6 water. (In fact, the initial conditioning runs are probably not necessary).

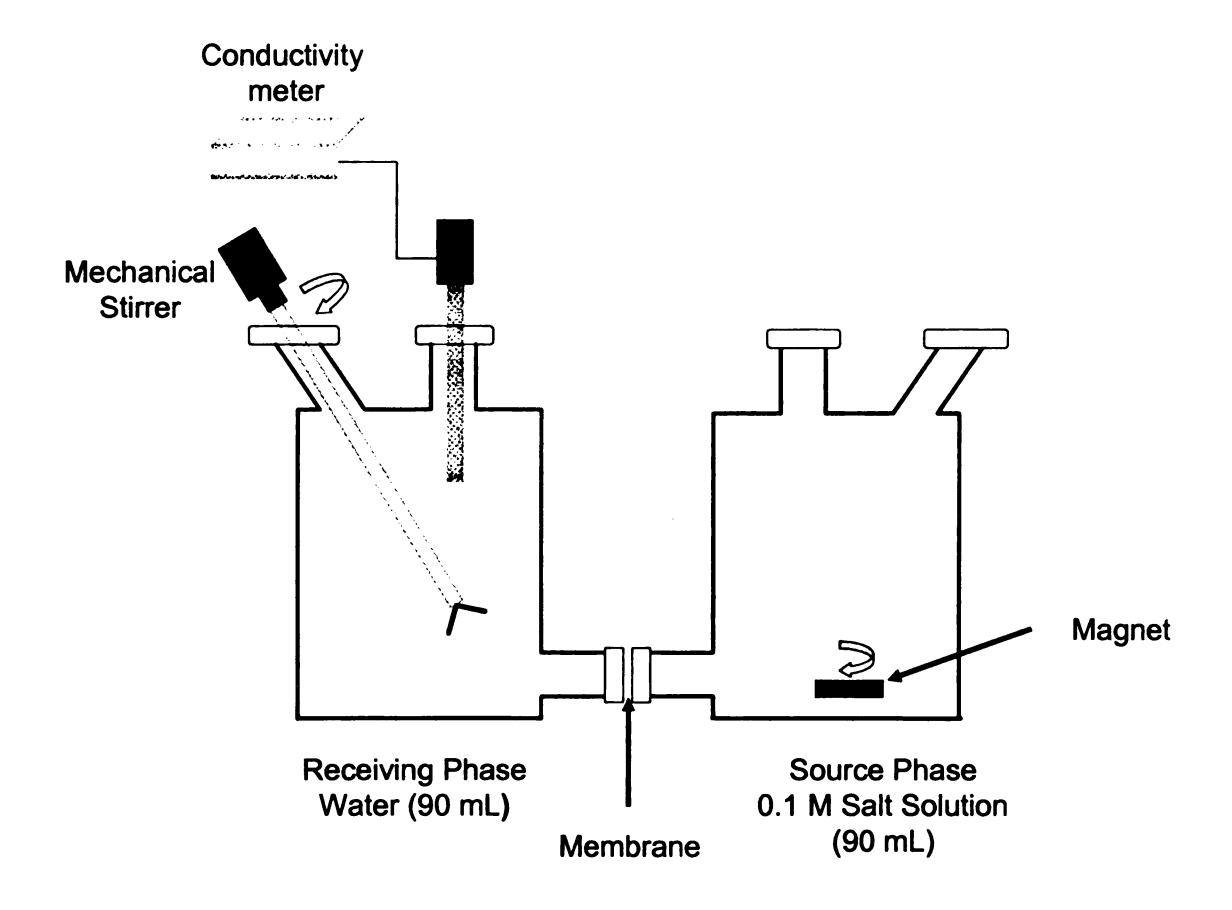


Figure 2.2: Apparatus for ion-transport measurements.

The permeate-cell conductivity values were converted to concentration using a calibration plot of conductivity versus concentration for a particular salt. The flux (J) for each permeating ion was calculated using equation 2.1, and the selectivity (α) of one ion over the other was obtained from equation 2.2.

$$J = \frac{\Delta C}{\Delta t} \frac{V}{A}$$
 2.1

$$\alpha = \frac{J_I}{J_I}$$
 2.2

In these equations, $\Delta C/\Delta t$ is the concentration change in the receiving cell with time obtained from the slope of a plot of concentration versus time; V is the volume of the solution in the receiving cell after 90 min, A is the exposed surface area of the membrane; and subscripts 1 and 2 refers to the two different permeating ions.

2.3 Results and Discussion

2.3.1 Synthesis and Characterization of Cu²⁺-Templated PAA/PAH Films.

Figure 2.1 shows schematically the preparation of Cu²⁺-templated PAA/PAH films on porous alumina supports. The procedure begins by preparing PAA complexed with Cu²⁺. To do this, we employ a PAA repeating unit to Cu²⁺ ratio of 8:1 so that ~25% of the -COO⁻ groups of PAA will be complexed with Cu²⁺ (two -COO⁻ groups should bind with one Cu²⁺ ion). The pH of the solution must be around 5.5 so that –COO⁻ groups are mostly deprotonated and Cu(OH)₂ does not precipitate. Alternating adsorption of the Cu²⁺-complexed PAA (uncomplexed -COO⁻ groups allow PAA to act as a polyanion) and PAH (polycation) results in a MPF. Although UV/visible spectroscopy

suggests that PAH does not form a complex with Cu²⁺ at pH 5.5,⁵⁰ we use the same Cu²⁺ concentration in PAH deposition as for PAA to prevent leaching of Cu²⁺ from the deposited PAA-Cu layer during immersion in the PAH solution. After deposition of the desired number of layers, we expose films to an HCl solution (pH 3.5) to exchange protons for Cu²⁺ and create free -COOH groups on PAA chains. Subsequent immersion in a pH 5.5 solution deprotonates these -COOH groups (exchange of protons for Na⁺) and increases the fixed negative charge density in the bulk of the film. The Cu²⁺-templated PAA/PAH films differ from pure PAA/PAH films in that they contain -COO⁻ groups that are electrically compensated by mobile cations (Na⁺) rather than neighboring ammonium groups of PAH. For cross-linked films, we use the same deposition procedure (Figure 2.1), except the removal of Cu²⁺ and the deprotonation of COOH groups (Steps 3 and 4 in Figure 2.1) occur after heating the films for two hours. Heating results in the formation of amide cross-links from -COO⁻-NH₃⁺ pairs. ^{12,51,52}

Cyclic voltammetry (Figure 2.3) of PAH/PAA-Cu films deposited on gold wafers confirms the presence of Cu²⁺ in these films as well as its removal at low pH. The peaks due to Cu²⁺/Cu completely disappear after immersion of the electrode in water at pH 3.5 (pH adjusted with 0.1 M HCl). Integration of the reduction or oxidation peak allows estimation of the amount of Cu²⁺ in the film, and this proves useful in modeling of ion transport (vide infra). As a comparison, we also tried to put Cu²⁺ into a 10-bilayer PAH/PAA film (deposited under similar conditions) by immersing the film in a 0.1 M CuCl₂ solution for 20 hours.⁵³ Cyclic voltammetry of this film showed that the amount of adsorbed /absorbed Cu²⁺ is about 1/6 of that in a Cu²⁺-templated film.

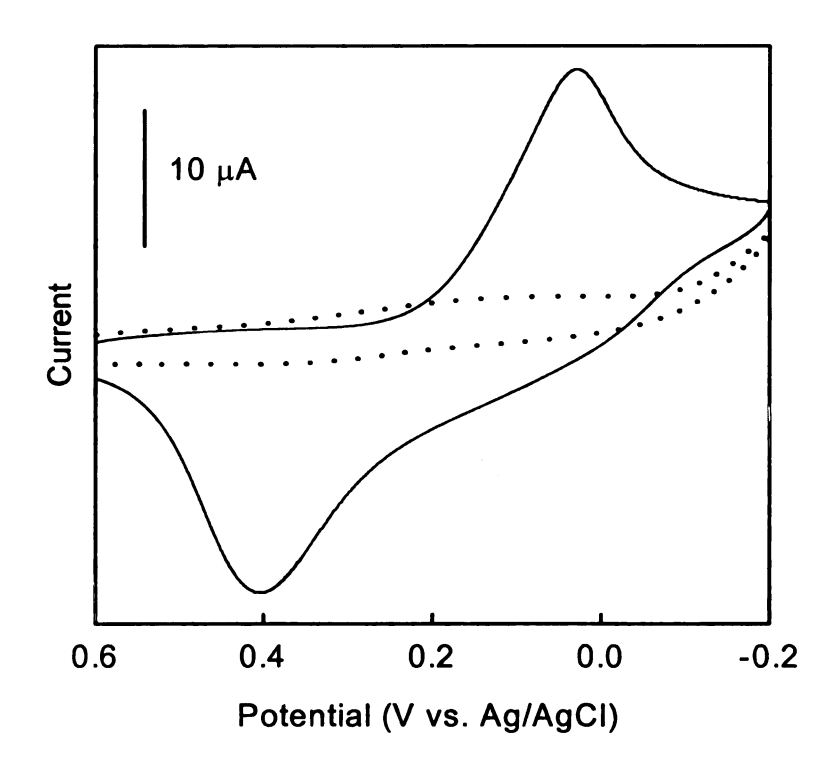


Figure 2.3: Cyclic voltammetry of a MPA-modified gold electrode coated with 10 bilayers of PAH/PAA-Cu before (solid line) and after exposure to pH 3.5 water (dotted line).

Reflectance FTIR spectra also confirm templating of PAH/PAA-Cu films with Cu²⁺. The spectrum of a PAH/PAA-Cu film (spectrum a, Figure 2.4) shows a broadening of the -COO symmetric stretch compared with the spectrum of a pure PAH/PAA film (spectrum d, Figure 2.4). This broadening results from counter-ion-induced changes in the energy of the -COO stretch. Upon exposure to pH 3.5 water and removal of Cu²⁺ (spectrum b, Figure 2.4), the -COO symmetric stretch looks like that of a pure PAH/PAA film. Further, a 50% increase in the acid carbonyl peak (1715 cm⁻¹) after immersion in pH 3.5 water suggests that lowering of pH creates free -COOH groups from the Cu²⁺ complexes, as would be expected. Immersing the film in pH 5-6 water deprotonates -COOH groups and results in a decrease in the acid carbonyl peak (spectrum c, Figure 2.4).

2.3.2 Anion Transport through Cu²⁺-Templated PAA/PAH Membranes.

Ion-transport studies show that PAA-Cu/PAH membranes on porous alumina supports are significantly more selective than similar pure PAA/PAH membranes. Figure 2.5 shows a plot of receiving-phase concentration as a function of time for membranes sandwiched between deionized water (receiving phase) and 0.1 M NaCl or Na₂SO₄ (source phase). These plots show that the Cl⁻ flux through both Cu²⁺-templated and pure PAA/PAH membranes is about 40 % of that through bare porous alumina. However, 10.5-bilayer PAA-Cu/PAH membranes (the top layer in the film is PAA-Cu) show a 4-fold decrease in SO₄²⁻ flux relative to pure 10.5-bilayer PAA/PAH membranes as shown in the inset of Figure 2.5. Overall, Cl⁻/SO₄²⁻ selectivity increases 4-fold due to templating of 10.5-bilayer films (Table 2.1).

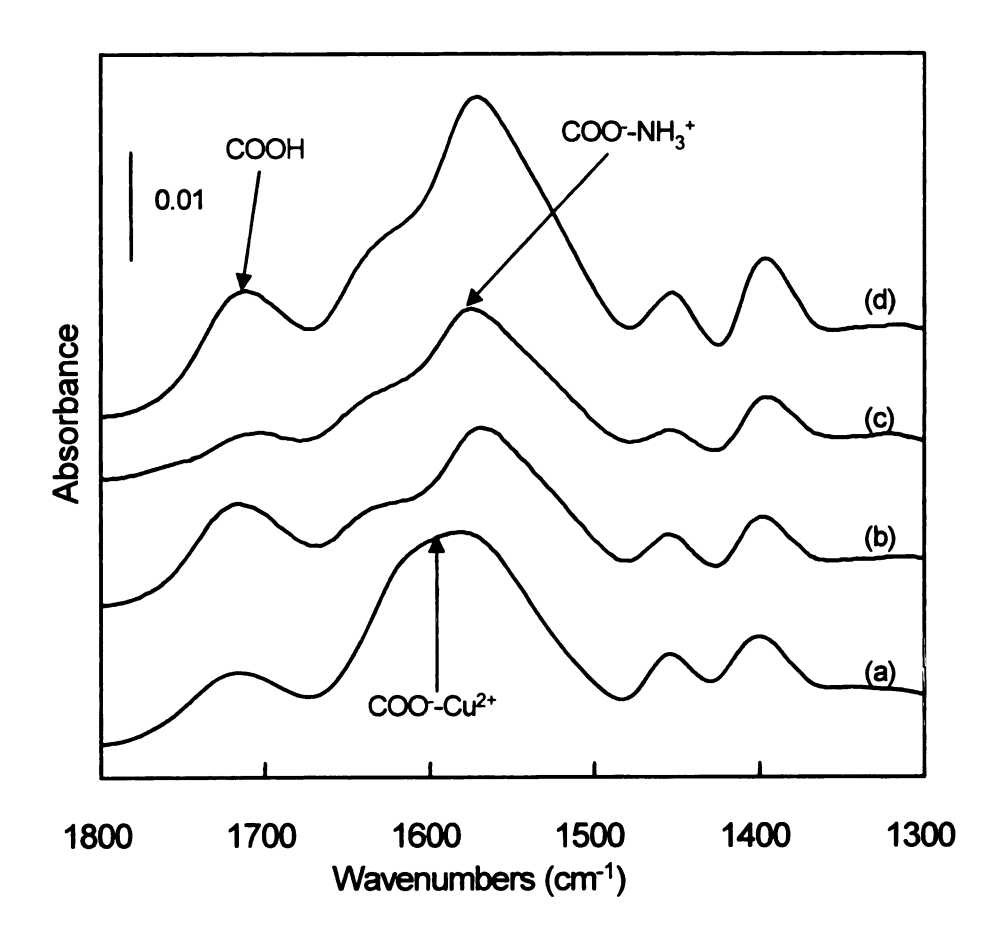


Figure 2.4: External reflectance FTIR spectra of (a) a 10-bilayer PAH/PAA-Cu film, (b) the same film after exposure to pH 3.5 water, (c) the film after subsequent exposure to pH 5.5 water, and (d) a 10-bilayer PAH/PAA film deposited without Cu²⁺. All films were deposited on a gold wafer coated with a monolayer of MPA.

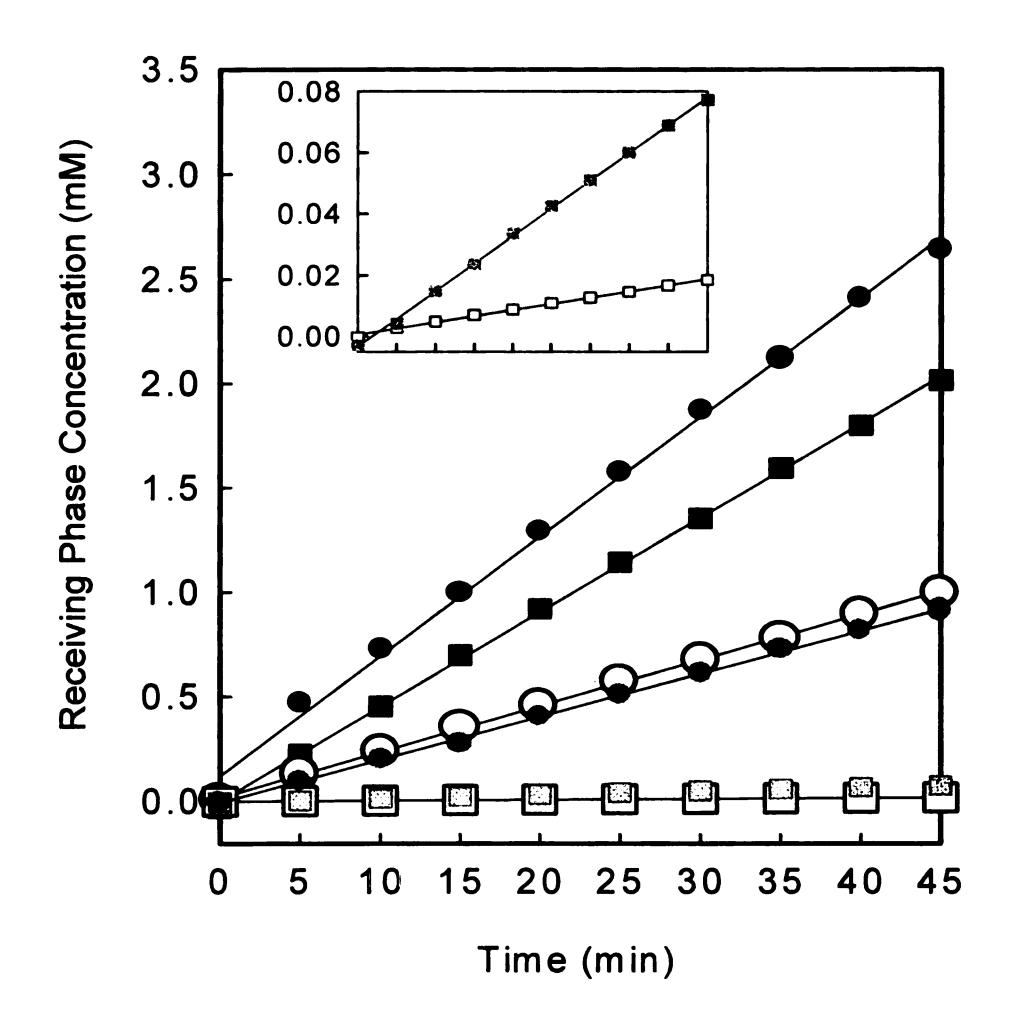


Figure 2.5: Receiving phase concentration as a function of time for a bare porous alumina membrane (black), an alumina membrane coated with 10.5 bilayers of Cu²⁺-templated PAA/PAH (open) and an alumina membrane coated with 10.5 bilayers of PAA/PAH (grey). Different symbols represent different salts: circles-NaCl and squares-Na₂SO₄. The inset shows SO₄²⁻ concentration vs. time for pure PAA/PAH (grey) and templated PAA/PAH (open). The membrane separates the receiving phase (initially deionized water) from a 0.1 M salt solution.

2.3.3 Cross-linked Cu²⁺-Templated PAA/PAH Membranes.

One possible limitation to CI/SO₄²⁻ selectivity is that swelling in water may decrease charge density and reduce Donnan exclusion of SO₄²⁻. In an effort to limit film swelling, we cross-linked PAA-Cu/PAH films by heating under N₂ to form amide bonds through reaction of the ammonium groups of PAH and the carboxylate groups of PAA that are not complexed with Cu²⁺. Reflectance FTIR spectroscopy confirms that the cross-linking reaction occurs.¹² After heating at 160 °C, external reflectance FTIR spectra of 10-bilayer PAH/PAA-Cu films show a large reduction in the intensity of – COO peaks at 1570 cm⁻¹ and 1400 cm⁻¹ and the appearance of amide peaks at 1660 cm⁻¹ and 1550 cm⁻¹ (Figure 2.6). With lower heating temperatures, the amide peaks are more clearly visible after exposing the cross-linked films to low-pH solutions because peaks due to Cu²⁺-COO complexes also appear in this region of the spectrum. The degree of cross-linking depends greatly on heating temperature as indicated by amide peaks that increase with cross-linking temperature.¹²

Diffusion dialysis studies show that as heating temperature (and hence the degree of cross-linking) increases, Cl⁻/SO₄²⁻ selectivity increases and then peaks at a heating temperature of 130 °C (Table 2.1, 10.5-bilayer PAA-Cu/PAH films). Partially cross-linked 10.5-bilayer PAA-Cu/PAH membranes (130 °C) show a 10-fold increase in Cl⁻/SO₄²⁻ selectivity relative to unheated, templated membranes, and this increase is achieved with only a 20% decrease in Cl⁻ flux. At higher cross-linking temperatures,

Table 2.1: Anion fluxes^a (moles cm⁻²s⁻¹) through bare porous alumina and alumina coated with PAA/PAH and PAA-Cu/PAH films cross-linked at different temperatures.

Film Composition	Cross-linking T (°C)	10 ⁸ × Cl ⁻ Flux ^a	$10^8 \times SO_4^{2}$ Flux ^a	Cl ⁻ /SO ₄ ²⁻ Selectivity ^c
Bare	-	4.2±1	3.3±0.2	1.3±0.09
10 PAA/PAH	-	1.0±0.2	1.5±0.2	0.7±0.03
10 PAA-Cա/PAH ^b	-	2.3±0.3	0.27±0.01	9±1
10.5 PAA/PAH	-	1.3±0.4	0.11±0.05	13±3
10.5 PAA-Cu/PAH ^b	-	1.6±0.2	0.03±0.001	55±3
10.5 PAA-Cu/PAH ^b	100	1.6±0.5	0.02±0.004	80±15
10.5 PAA-Cu/PAH ^b	120	1.4±0.2	0.006±0.002	2 40±80
10 PAA/PAH	130	0.09±0.03	0.027±0.005	3±0.4
10 PAA-Cu/PAH ^b	130	2.0±0.06	0.032±0.005	62±11
10.5 PAA/PAH	130	0.07±0.01	0.0028±0.0009	26±7
10.5 PAA-Cu/PAHb	130	1.3±0.05	0.0021±0.0001	610±20
10.5 PAA-Cu/PAH ^b	140	0.51±0.2	0.0016±0.0005	330±70
10.5 PAA-Cu/PAH ^b	160	0.087±0.04	0.0003±0.0001	29±1.3

^a Flux values were calculated from the slopes of plots of concentration in the receiving phase vs. time. Errors represent standard deviations of at least three measurements.

^b Flux was measured after removal of Cu²⁺ from the membrane and deprotonation of newly formed —COOH groups.

^c Calculated as the average of selectivity values for each membrane and not from average flux values.

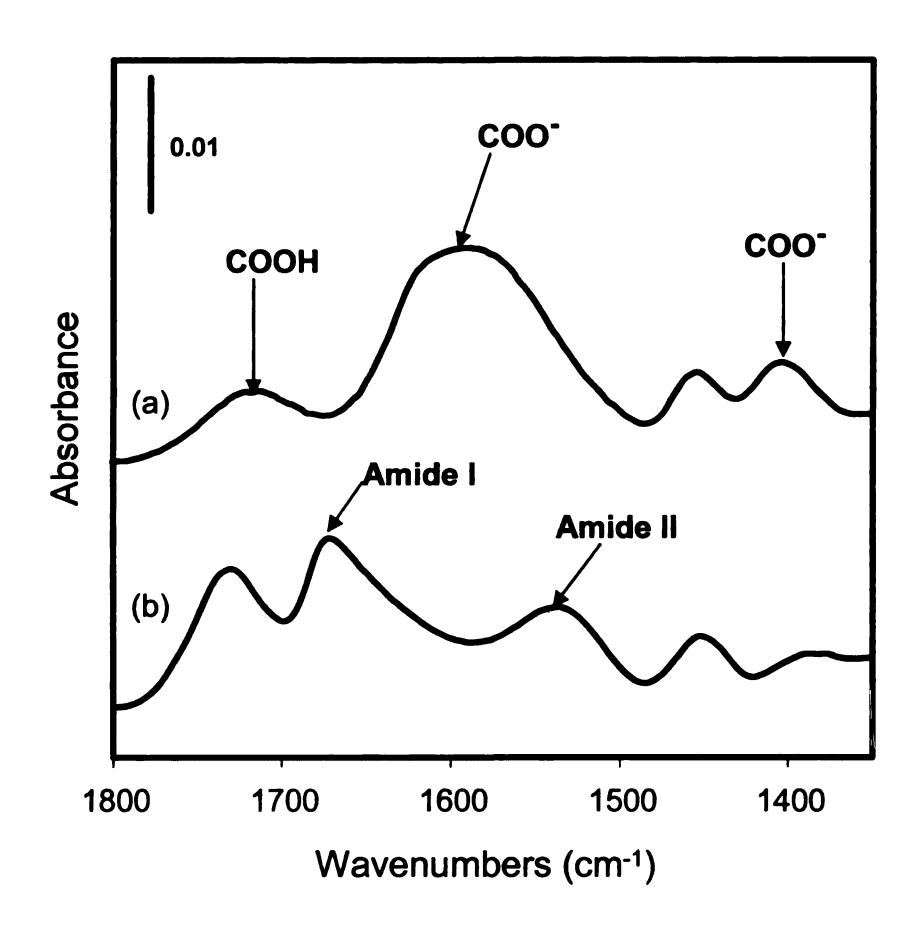


Figure 2.6: External reflectance FTIR spectra of 10-bilayer PAH/PAA-Cu films (a) before and (b) after heating at 160°C. Films were deposited on MPA-coated gold.

Cl⁻ flux drops rapidly, presumably due to a tighter membrane structure. Sulfate flux does not continue to drop significantly at higher cross-linking temperatures, and thus Cl⁻/SO₄²⁻ selectivity eventually decreases. Compared with pure PAA/PAH membranes, the selectivities and fluxes through partially cross-linked PAA-Cu/PAH membranes are remarkable. Table 2.1 shows that partially cross-linked (130 °C) 10.5-bilayer PAA-Cu/PAH membranes show a 20-fold increase in Cl⁻/SO₄²⁻ selectivity relative to similar cross-linked pure PAA/PAH membranes. Additionally, the Cl⁻ flux through these cross-linked Cu²⁺-templated membranes is 20-fold higher than the Cl⁻ flux through pure PAA/PAH membranes cross-linked at the same temperature. This may be due to the formation of new transport pathways upon removal of Cu²⁺ or a lower degree of cross-linking in the templated film.

2.3.4 Changing the Surface Charge of Membranes.

Our previous studies^{5,13} of MPMs showed that much of the ion-transport selectivity in these systems is due to a high charge density at the membrane surface. However, Cu²⁺-templated membranes differ from previous MPMs in that they contain fixed charge throughout the membrane. In an effort to understand more about selectivities in PAA-Cu/PAH membranes, we changed the terminating layer of these films from PAA to positively charged PAH. If selectivity in these systems is largely due to charge at their surface, changing the outer layer from a polyanion to a polycation should have a dramatic effect on ion transport.

Changing the surface from PAA-Cu (10.5-bilayer films) to PAH (10-bilayer films) in cross-linked (130 °C), templated films resulted in a 15-fold increase in SO₄²-flux and a 50% increase in Cl⁻ flux (Table 2.1). Thus Cl⁻/SO₄²- selectivity decreased from

610 to 60 on going from a 10.5-bilayer to a 10-bilayer cross-linked PAA-Cu/PAH film. In the case of unheated Cu²⁺-templated membranes, terminating with PAH rather than PAA-Cu yielded a decrease in Cl⁻/SO₄²⁻ selectivity from 55 to 9. These data clearly indicate that Donnan exclusion at the film surface plays a large role in determining selectivity. For unheated, pure PAA/PAH membranes, selectivity actually reverses (from 13 to 0.7) upon changing the top layer from PAA to PAH. However, with Cu²⁺-templated films, we still see a significant Cl⁻/SO₄²⁻ selectivity when the surface of the membrane is positively charged because of fixed negative charge density in the bulk of the membrane.

2.3.5 Anion-Transport through Partially Cross-linked, Cu²⁺-Templated Membranes Deposited at Different pH values.

Variation of the pH at which PAA-Cu/PAH films are deposited allows some control over the amount of Cu²⁺ in these films and may provide a means for controlling transport selectivity. Table 2.2 gives the Cl⁻/SO₄²⁻ selectivity values for partially crosslinked 10.5-bilayer PAA-Cu/PAH membranes deposited from solutions at three different pH values (5.5, 6, and 6.6). We also tried to deposit membranes at pH values <5.5, but under these conditions, polymer precipitates from deposition solutions. Selectivity is highest for films deposited at pH 5.5 and decreases at higher deposition pH values. The ellipsometric thicknesses (Table 2.2) of similar films on gold wafers are independent of pH over this range of values, ⁵⁵ so selectivity differences are likely due to changes in charge density. The UV/visible spectra of the PAH/Cu²⁺ solutions showed a shift in the

Table 2.2: Thicknesses, fluxes (moles cm⁻²s⁻¹), selectivities and Cu²⁺ concentrations (M) in partially cross-linked, 10.5-bilayer PAA-Cu/PAH films deposited at different pH values.

Deposition pH ^a	Thickness ^b (Å)	Cl ⁻ Flux ^c ×10 ⁸	SO ₄ ²⁻ Flux ^c ×10 ¹¹	Cl ⁻ /SO ₄ ²⁻ Selectivity ^d	Cu ²⁺ Concentration ^e
5.5	170±3	1.3±0.05	2.1±0.1	610±20	1.0±0.06
6	170±6	1.1±0.2	2.6±0.4	430±90	0.9±0.04
6.6	170±10	1.6±0.3	170±42	11±4	0.3±0.1

^aBoth PAA-Cu and PAH were deposited at this pH.

^bThicknesses are for 10-bilayer PAH/PAA-Cu films deposited on gold wafers as described in the experimental section.

^cError values represents standard deviations.

^dCalculated as the average of selectivity values for each membrane and not from average flux values.

^eCu²⁺ concentration in the membrane was estimated from the area of the reduction peak in a cyclic voltammagram of a film on gold. This area was converted to number of moles of Cu²⁺/cm², and this value was divided by the ellipsometric film thickness to obtain the concentration.

Cu²⁺ absorption peak from 820 nm at pH 5.5 to 780 nm at pH 6 and to 710 nm at pH 6.6, suggesting that the amine groups of PAH begin to form complexes with Cu²⁺ at the higher pH values. In addition, at higher pH values Cu²⁺ can form hydroxide complexes. These competing reactions probably reduce the amount of Cu²⁺ deposited in the membrane as -COO⁻-Cu²⁺ complexes.

To quantitatively investigate fixed-charge density in PAH/PAA-Cu membranes, we employed cyclic voltammetry to estimate Cu²⁺ concentrations in analogous films deposited on gold (Figure 2.7). By integrating the area of the reduction peak, Cu²⁺ concentrations could be estimated. In agreement with transport studies, Table 2.2 shows that the maximum amount of copper is deposited at pH 5.5. Hence, after removal of Cu²⁺ from the film, higher charge densities should enhance Cl⁻/SO₄²⁻ selectivity for films deposited at the lower pH values.

2.3.6 Anion Transport through Partially Cross-linked, Cu²⁺-Templated Membranes Deposited with Different Cu²⁺ Concentrations.

Altering the amount of Cu²⁺ present during deposition should provide another means for controlling fixed charge and selectivity in membranes. To examine this possibility, we prepared cross-linked PAH/PAA-Cu membranes using Cu²⁺ concentrations of 2.5 mM, 5 mM or 7.5 mM in both PAA and PAH deposition solutions. Table 2.3 gives the Cl⁷/SO₄²⁻ selectivities and flux values for these membranes. (We deposited PAA and PAH at pH 6 because at pH 5.5, higher Cu²⁺ concentrations resulted in precipitation).

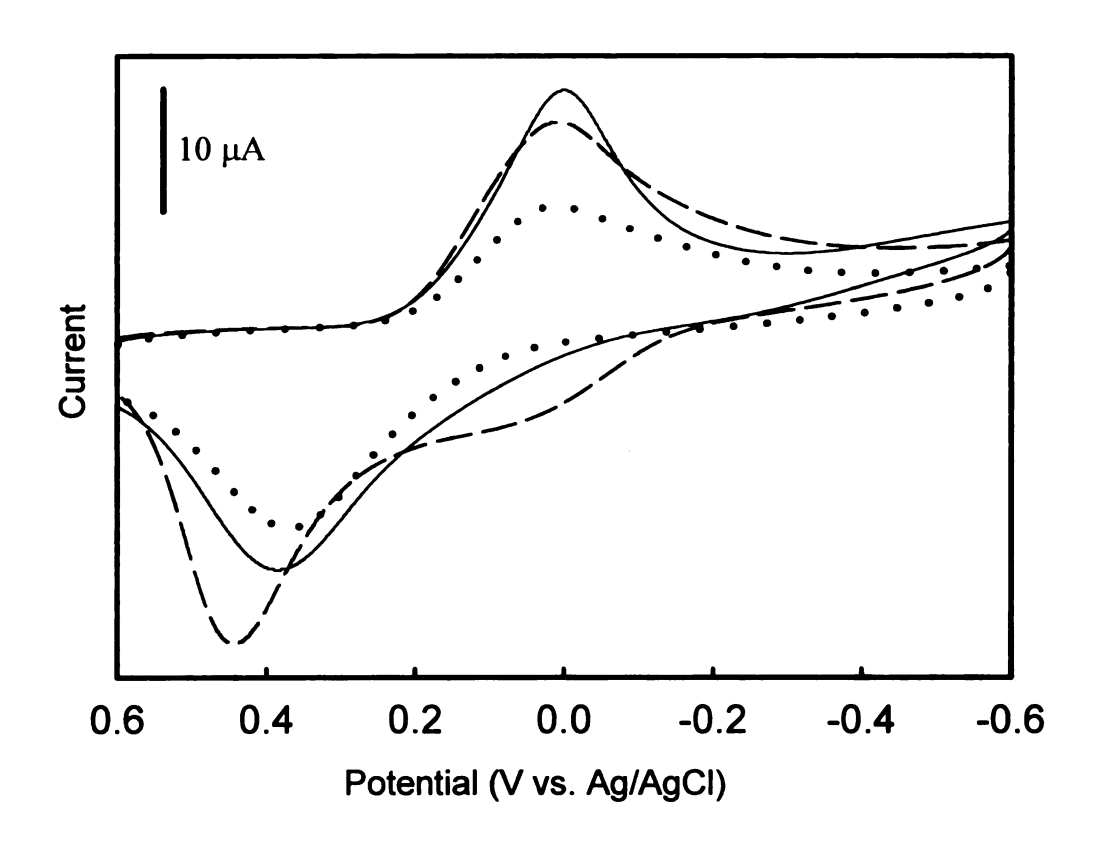


Figure 2.7: Cyclic voltammetry of 10-bilayer PAH/PAA-Cu films deposited at different deposition pH values on MPA-modified gold surfaces: pH 5.5-dashed line, pH 6-solid line, and pH 6.6-dotted line. Areas of the reduction peaks were calculated by drawing the baseline from the value of current at a potential of 0.3 V to the value of current at -0.5 V.

Table 2.3: Anion Fluxes (moles cm⁻²s⁻¹), selectivities, thicknesses, and estimated Cu²⁺ concentrations (M) of partially cross-linked (130 °C) 10.5-bilayer PAA-Cu/PAH membranes and films deposited using different Cu²⁺ concentrations.

Cu ²⁺ Concentration used in deposition ^a (mM)	Cl ⁻ Flu x ×10 ⁸	SO ₄ ² · Flux ×10 ¹¹	CI ⁻ /SO ₄ ²⁻ Selectivity ^b	Thickness° (Å)	Estimated Cu ²⁺ Concentration ^d
0	0.056±0.01	5±2	11±2	177±26	0
2.5	1.5±0.1	19±2	81±3	204±9	0.3±0.01
5.0	1.1±0.2	2.6±0.4	430±90	170±6	1.0±0.06
7.5	2.5±0.3	71±15	41±11	316±14	0.6±0.04

^aBoth PAA and PAH deposition solutions contained the same concentration of Cu²⁺ and had a pH of 6.

°Thicknesses reported are those for 10-bilayer PAH/PAA-Cu films on gold wafers after cross-linking at 130 °C for 2 ^bCalculated as the average of selectivity values for each membrane and not from average flux values.

hours as described in the experimental section.

^dCu²⁺ concentration was determined using cyclic voltammetry before cross-linking and ellipsometric thicknesses measured after cross-linking. Cl⁷/SO₄²⁻ selectivity was highest when the concentration of Cu²⁺ present during deposition was 5 mM. Cyclic voltammetry (Figure 2.8) and ellipsometric data (Table 2.3) for analogous films deposited on gold wafers indicate that the highest Cu²⁺ concentration occurs in films deposited with 5 mM Cu²⁺. This happens because film thickness increases greatly when the Cu²⁺ concentration during deposition is 7.5 mM. Hence, the highest selectivity is observed for the MPMs deposited in the presence of 5 mM Cu²⁺. The structure of films probably depends on the Cu²⁺ concentration present during deposition,^{56,57} and this might explain why films deposited with 7.5 mM Cu²⁺ are less selective than films deposited with 2.5 mM Cu²⁺, even though the former films have a higher concentration of Cu²⁺.

2.3.7 Modeling of Anion Transport through Cu²⁺-Templated PAA/PAH Membranes

To better understand the observed selectivities and fluxes through templated membranes, we began developing a simple model for ion transport based on previous models of ion-exchange membranes^{58,59} and MPMs.⁶⁰ We employed a two-layer model of the MPF, assuming the bulk of the membrane as one layer and the surface as another (Figure 2.9). The charge density in these two regions should be different, as several recent studies^{36,61} show that net charge in MPFs resides primarily at the film surface. However, in templated films, removal of Cu²⁺ yields cation-exchange sites in the bulk of the membrane as well as on the surface. We estimated the fixed negative charge density in the bulk of templated films from the amount of deposited Cu²⁺ determined from cyclic

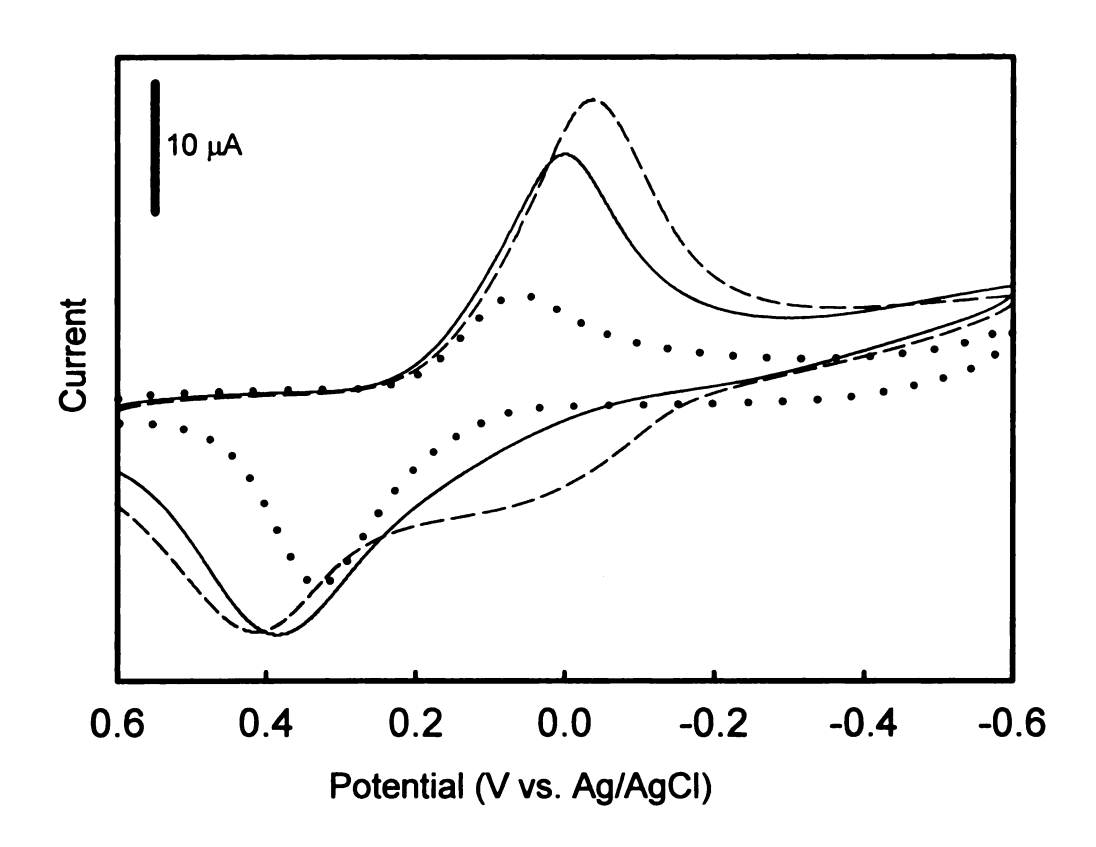


Figure 2.8: Cyclic voltammetry of 10-bilayer PAH/PAA-Cu films deposited with different Cu²⁺ concentrations: 2.5 mM Cu²⁺ -dotted line, 5.0 mM Cu²⁺ solid line and 7.5 mM Cu²⁺-dashed line. The area of the reduction peak was calculated after drawing the baseline from the current at a potential of 0.3 V to that at -0.4 V. Films were deposited at pH 6 on MPA-modified gold.

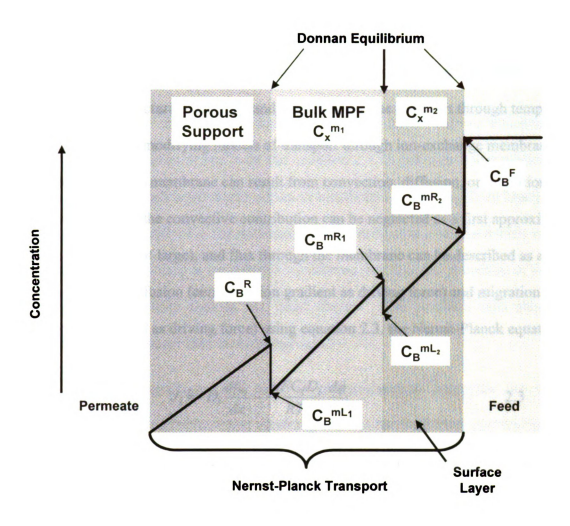


Figure 2.9: Schematic representation of the model used to simulate ion transport through templated MPMs. The membrane consists of two charged layers: a surface layer and the membrane bulk. The line represents a hypothetical concentration profile for the excluded ion. C_x^{m-n} are the fixed charge concentrations of bulk of the film and surface layer respectively.

voltammetry (noting that every Cu²⁺ binds with two COO groups) and from the ellipsometric thicknesses of corresponding films deposited on gold. To estimate surface charge density, we assumed that the surface layer was composed of pure PAA.⁶²

With a structural model in hand, one can examine transport through templated polelectrolytes by modifying models of transport through ion-exchange membranes. Ion transport through a membrane can result from convection, diffusion, or migration. In diffusion dialysis, the convective contribution can be neglected as a first approximation (osmotic flow is not large), and flux through the membrane can be described as a combination of diffusion (concentration gradient as driving force) and migration (electrical potential as driving force) using equation 2.3, the Nernst-Planck equation. 63

$$J_i = -D_i \frac{dC_i}{dx} - \frac{z_i F C_i D_i}{RT} \frac{d\phi}{dx}$$
 2.3

In this equation, J_i is the flux of ion i, C_i is the ion concentration, D_i is the diffusion coefficient, z_i is the ion charge, F is the Faraday constant, R is the gas constant, T is the absolute temperature and ϕ is the electrical potential. In this study, the presence of fixed charge in the membrane results in a very low concentration of excluded ion in the membrane, and the migration term for this ion is negligible. Thus, one can simply use Fick's law for steady-state diffusion to calculate flux for the excluded ion (equation 2.4).

$$J_B = -D_B \left(\frac{C_B^{mR} - C_B^{mL}}{d} \right)$$
 2.4

In equation 2.4, d is the thickness of the polyelectrolyte region (surface or bulk), and C_B^{mR} and C_B^{mL} are the excluded ion concentrations at the right and left side of the region.

To calculate mobile ion concentrations in the membrane, we assumed Donnan equilibria at the interfaces and used the equation 2.4 to calculate concentration profiles within layers. Donnan equilibrium occurs in membranes containing fixed charge because *mobile* anions and cations in the membrane are not present in a stoichiometric ratio. This results in a potential drop at the solution-membrane interface and exclusion of ions whose charge is of the same sign as the fixed charge. The potential also enhances the concentration of counter ions in the membrane.

Equating membrane and solution electrochemical potentials for each ion, neglecting activity coefficients and assuming that the standard state chemical potential is the same in the membrane and in the solution results in equation 2.5, which describes the distribution of excluded ion B between the membrane and the solution.⁶⁴

$$\frac{C_B^m}{C_B} = \left(\frac{\left|z_B\right| C_B^m + \left|z_X\right| C_X^m}{\left|z_B\right| C_B}\right)^{\left(z_B\right] / \left|z_A\right|}$$
2.5

In this equation, C_B^m , C_x , z_B and z_x are the concentrations (in the membrane) and charges of the excluded ion and the fixed charge respectively. The charge of the co-ion is z_A , and C_B is the concentration of the excluded ion in solution.

The procedure for calculating a concentration profile through the membrane involves several steps. First, we calculate the excluded ion concentration (C_B^R) in the porous alumina at the alumina/polyelectrolyte film interface using equation 2.6 and the experimental flux values through bare porous alumina (J_{bare}) and porous alumina coated with a polyelectrolyte membrane (J_{coated}). This equation assumes a negligible receiving-phase ion concentration so flux is simply proportional to the concentration in the alumina at the alumina-polyelectrolyte or alumina-feed interface. The linear relationship between receiving-phase concentration and time suggests that receiving-phase concentration is indeed negligible. In the case of a bare membrane, the concentration at the alumina/feed interface is simply the source-phase concentration, C_B^F .

$$C_B^R = \frac{J_{coated}}{J_{bare}} \times C_B^F$$
 2.6

The next step in determining the concentration profile is calculation of the concentration of excluded ion $(C_B^{mL_i})$ in the polyelectrolyte film at the alumina/bulk film interface using equation 2.7.

$$\frac{C_{B}^{mL_{1}}}{C_{B}^{R}} = \left(\frac{|z_{B}|C_{B}^{mL_{1}} + |z_{X}|C_{X}^{m_{1}}}{|z_{B}|C_{B}^{R}}\right)^{\left(|z_{B}|/|z_{A}|\right)}$$
2.7

Here, $C_X^{m_1}$ is the concentration of the fixed charge in the bulk of MPF and C_B^R is the excluded ion concentration in the porous alumina at the alumina/polyelectrolyte film interface. Subsequently, we solve equation 2.4 to calculate the concentration of excluded

ion $(C_B^{mR_I})$ in the bulk film at the bulk film/surface layer interface. Donnan equilibrium at the bulk film/surface layer interface is slightly different than at the alumina/bulk film interface because both films contain fixed charge, albeit in different amounts. The Donnan equilibrium assumptions for this interface give equation 2.8, which allows for calculation of the concentration of excluded ion $(C_B^{mL_2})$ in the surface layer at the surface layer/bulk film interface.

$$\frac{C_B^{mL_2}}{C_B^{mR_1}} = \left(\frac{|z_X| C_X^{m_2} + |z_B| C_B^{mL_2}}{|z_X| C_X^{m_1} + |z_B| C_B^{mR_1}} \right)^{|z_B|/|z_A|}$$
2.8

In this equation, $C_x^{m_2}$ and $C_x^{m_I}$ are the concentrations of fixed charge in the surface layer and in the bulk respectively and $C_B^{mR_I}$ is the concentration of excluded ion in the bulk at the bulk film/ surface layer interface. Finally, using equation 2.4, we calculate the concentration of excluded ion in the surface layer at the surface layer/feed interface using Fick's law and subsequently solve equation 2.9 for the concentration of the excluded ion in the source phase (C_B^F) .

$$\frac{C_B^F}{C_B^{mR_2}} = \left(\frac{|z_B|C_B^F}{|z_B|C_B^{mR_2} + |z_X|C_X^{m_2}}\right)^{|z_B|/|z_A|}$$
 2.9

In this equation $C_x^{m_2}$ is the concentration of the fixed charge in the surface layer and $C_B^{mR_2}$ is the concentration of excluded ion in the surface layer at the surface layer/feed

interface. z_B , z_A and z_x are the charges of excluded ion, co-ion and the fixed charge respectively.

We performed this entire calculation iteratively using the experimental flux values and varying the diffusion coefficient of the excluded ion in the polyelectrolyte film until the calculated source-phase excluded ion concentration matched the experimental value (0.1 M). Table 2.4 lists the diffusion coefficients determined for Cl⁻ and SO₄²⁻ in this way. (We assumed that the diffusion coefficient was the same in the bulk and surface film layers). These calculations on unheated, templated membranes yielded Cl⁻ diffusion coefficients on the order of 10⁻⁸ cm²/s, and the Cl⁻ diffusion coefficient was a factor of 6 higher than that of SO₄²⁻. Miyoshi reported⁵⁸ that diffusion coefficients through ion exchange membranes are ~10⁻⁸ cm²/s for Na⁺ and Mg²⁺, reasonably close to the Cl⁻ values we calculate. The calculated diffusion coefficients suggest that selectivity is about equally due to Donnan exclusion and diffusivity differences.

Modeling studies on cross-linked, templated membranes show that as the cross-linking temperature increases, diffusion coefficients generally decrease (Table 2.4). This is reasonable because cross-linking reduces swelling, and hence free volume. At low cross-linking temperatures, decreases in the SO_4^{2-} diffusion coefficient are more dramatic than those for Cl⁻, and this may be due to size exclusion and/or hydrophobicity effects.

21,65,66 On going from a cross-linking temperature of 140 to 160 °C, the diffusion coefficient of SO_4^{2-} actually increased, probably because fixed charge decreased at this temperature, and we couldn't take this into account. At a cross-linking temperature of 130 °C, the calculated Cl⁻ diffusion coefficient was 25-fold higher than that of SO_4^{2-} .

Table 2.4: Diffusion coefficients obtained from modeling ion transport through 10.5bilayer PAA-Cu/PAH membranes cross-linked at different temperatures.

Cross- linking Temperature (°C)	Cl ⁻ Diffusion Coefficient (cm ² s ⁻¹)	SO ₄ ²⁻ Diffusion Coefficient (cm ² s ⁻¹)	Bulk Fixed Charge Density ^a (mol/cm ³)	Estimated Surface Fixed Charge Density ⁶² (mol/cm ³)	Diffusional Selectivity ^b	Electrostatic Exclusion Selectivity ^c
Unheated	8.8×10 ⁻⁹	1.4×10 ⁻⁹	1.4×10 ⁻³	1.1×10 ⁻²	6	9
100	8.8×10 ⁻⁹	1.1×10 ⁻⁹	1.5×10 ⁻³	1.2×10 ⁻²	8	10
120	7.4×10 ⁻⁹	3.6×10 ⁻¹⁰	1.6×10 ⁻³	1.3×10 ⁻²	20.5	11.7
130	6.8×10 ⁻⁹	1.5×10 ⁻¹⁰	2.0×10 ⁻³	1.6×10 ⁻²	45	13.6
140	2.4×10 ⁻⁹	1.1×10 ⁻¹⁰	1.9×10 ⁻³	1.5×10 ⁻²	22	15
160	4.1×10 ⁻¹⁰	2.2×10 ⁻¹⁰	2.1×10 ⁻³	1.7×10 ⁻²	1.7	17

^a Determined using cyclic voltammetry and ellipsometry.

^b The diffusional selectivity is the ratio of diffusion coefficients obtained from the model.

^c Total Cl⁻/SO₄²⁻ selectivity divided by diffusional selectivity.

These simple calculations suggest that the highest selectivities in cross-linked films are about equally due to diffusion and Donnan selectivities. We should note, however, that this model does not take into account activity coefficients or the effect of hydrophobicity on partitioning.

Several previous studies showed that diffusion through charged membranes can be complicated due to electrostatic interactions between the membrane and the diffusing ions. Additionally, charge distributions in our simulations are oversimplified and only approximate. However, the modeling studies do strongly indicate that selectivity is only partly due to Donnan exclusion. A full understanding of transport through MPMs will likely require measurement of diffusion and partition coefficients.

2.4 Conclusions

Partial complexation of the -COO groups of PAA with Cu²⁺ provides a convenient method to enhance fixed negative charge density in MPMs. Removal of Cu²⁺ leaves behind -COOH groups that behaves as ion-exchange sites. Diffusion-dialysis studies with Cu²⁺-templated membranes show that templating increases anion-transport selectivities, and post deposition cross-linking of these membranes further enhances Cl⁻/SO₄²⁻ selectivities to values high as 610. Changing the surface layer from negatively charged PAA to positively charged PAH greatly reduces Cl⁻/SO₄²⁻ selectivity, showing that selectivity is highly dependent on surface charge. Simulation of ion-transport data using a simple two-layer model of MPFs suggests that the observed Cl⁻/SO₄²⁻ selectivities are due to both Donnan exclusion and differences in diffusivities of ions.

2.5 References and Notes

- (1) Decher, G.; Hong, J. D. Ber. Bunsenges. Phys. Chem. 1991, 95, 1430-1434.
- (2) Decher, G. Science 1997, 277, 1232-1237.
- (3) Krasemann, L.; Tieke, B. *Mater. Sci. Eng.*, C 1999, 8-9, 513-518.
- (4) Krasemann, L.; Tieke, B. Langmuir 2000, 16, 287-290.
- (5) Harris, J. J.; Stair, J. L.; Bruening, M. L. Chem. Mater. 2000, 12, 1941-1947.
- (6) Leväsalmi, J.-M.; McCarthy, T. J. *Macromolecules* **1997**, *30*, 1752-1757.
- (7) Stroeve, P.; Vasquez, V.; Coelho, M. A. N.; Rabolt, J. F. *Thin Solid Films* **1996**, 285, 708-712.
- (8) van Ackern, F.; Krasemann, L.; Tieke, B. *Thin Solid Films* **1998**, *329*, 762-766.
- (9) Kotov, N. A.; Magonov, S.; Tropsha, E. Chem. Mater. 1998, 10, 886-895.
- (10) Krasemann, L.; Tieke, B. Chem. Eng. Technol. 2000, 23, 211-213.
- (11) Krasemann, L.; Tieke, B. J. Membr. Sci. 1998, 150, 23-30.
- (12) Harris, J. J.; DeRose, P. M.; Bruening, M. L. J. Am. Chem. Soc. 1999, 121, 1978-1979.
- (13) Stair, J. L.; Harris, J. J.; Bruening, M. L. Chem. Mater. 2001, 13, 2641-2648.
- (14) Hell, F.; Lahnsteiner, J.; Frischherz, H.; Baumgartner, G. Desalination 1998, 117, 173-180.
- (15) Amor, Z.; Bariou, B.; Mameri, N.; Taky, M.; Nicolas, S.; Elmidaoui, A. *Desalination* **2001**, *133*, 215-223.
- (16) Sata, T.; Yamaguchi, T.; Matsusaki, K. J. Chem. Soc., Chem. Commun. 1995, 11, 1153-1154.
- (17) Mika, A. M.; Childs, R. F.; Dickson, J. M. Desalination 1999, 121, 149-158.
- (18) Brett, S. W.; Gaterell, M. R.; Morse, G. K.; Lester, J. N. *Environ. Technol.* **1999**, 20, 1009-1018.
- (19) Takata, K.; Yamamoto, Y.; Sata, T. Bull. Chem. Soc. Jpn. 1996, 69, 797-804.

- (20) Bader, M. S. H. J. Hazard. Mater. 2000, B73, 269-283.
- (21) Sata, T.; Mine, K.; Higa, M. J. Membr. Sci. 1998, 141, 137-144.
- (22) Sata, T.; Mine, K.; Tagami, Y.; Higa, M.; Matsusaki, K. J. Chem. Soc., Faraday Trans. 1998, 94, 147-153.
- (23) Sata, T.; Nojima, S. J. Polym. Sci. Polym. Phys. Ed. 1999, 37, 1773-1785.
- (24) Sata, T.; Emori, S. I.; Matsusaki, K. J. Polym. Sci. Polym. Phys. Ed. 1999, 37, 793-804.
- (25) Matsusaki, K.; Hashimoto, N.; Kuroki, M.; Sata, T. Anal. Sci. 1997, 13, 345-349.
- (26) Tsuru, T.; Nakao, S.-I.; Kimura, S. J. Membr. Sci. 1995, 108, 269-278.
- (27) Urairi, M.; Tsuru, T.; Nakao, S.; Kimura, S. J. Membr. Sci. 1992, 70, 153-162.
- (28) Yoo, D.; Shiratori, S. S.; Rubner, M. F. *Macromolecules* **1998**, *31*, 4309-4318.
- (29) Shiratori, S. S.; Rubner, M. F. *Macromolecules* **2000**, *33*, 4213-4219.
- (30) Sukhorukov, G. B.; Schmitt, J.; Decher, G. Ber. Bunsenges. Phys. Chem. 1996, 100, 948-953.
- (31) Sukhishvili, S. A.; Granick, S. J. Chem. Phys. 1998, 109, 6861-6868.
- (32) Dubas, S. T.; Schlenoff, J. B. *Macromolecules* **1999**, *32*, 8153-8160.
- (33) Lösche, M.; Schmitt, J.; Decher, G.; Bouwman, W. G.; Kjaer, K. *Macromolecules* 1998, 31, 8893-8906.
- (34) Lvov, Y.; Decher, G.; Möhwald, H. Langmuir 1993, 9, 481-486.
- (35) Decher, G.; Hong, J. D.; Schmitt, J. *Thin Solid Films* **1992**, *210/211*, 831-835.
- (36) Schlenoff, J. B.; Ly, H.; Li, M. J. Am. Chem. Soc. 1998, 120, 7626-7634.
- (37) Laurent, D.; Schlenoff, J. B. Langmuir 1997, 13, 1552-1557.
- (38) Gotoh, Y.; Igarashi, R.; Ohkoshi, Y.; Nagura, M.; Akamatsu, K.; Deki, S. J. *Mater. Chem.* **2000**, *10*, 2548-2552.
- (39) Rivas, B. L.; Schiappacasse, N.; Basaez, L. A. *Polym. Bull.* **2000**, *45*, 259-265.
- (40) Porasso, R. D.; Benegas, J. C.; Hoop, M. A. G. T. v. d. *J. Phys. Chem. B* 1999,

- 103, 2361-2365.
- (41) Kurth, D. G.; Osterhout, R. Langmuir 1999, 15, 4842-4846.
- (42) Caruso, F.; Schuler, C.; Kurth, D. G. Chem. Mater. 1999, 11, 3394-3399.
- (43) Xiong, H.; Cheng, M.; Zhou, Z.; Zhang, X.; Shen, J. Adv. Mater. 1998, 10, 529-532.
- (44) Zhang, X.; Shen, J. C. Adv. Mater. 1999, 11, 1139-1143.
- (45) Schutte, M.; Kurth, D. G.; Linford, M. R.; Colfen, H.; Möhwald, H. *Angew. Chem. Int. Ed.* **1998**, *37*, 2891-2893.
- (46) Chen, W.-J.; Aranda, P.; Martin, C. R. J. Membr. Sci. 1995, 107, 199-207.
- (47) Chen, W.-J.; Martin, C. R. J. Membr. Sci. 1995, 104, 101-108.
- (48) Dai, Z.; Ju, H. Phys. Chem. Chem. Phys. 2001, 3, 3769-3773.
- (49) Bain, C. D.; Troughton, E. B.; Tao, Y. T.; Evall, J.; Whitesides, G. M.; Nuzzo, R. G. J. Am. Chem. Soc. 1989, 111, 321-335.
- (50) At ph 5.5, the UV/vis spectrum of PAH/Cu²⁺ solution is identical to that of a CuCl₂ solution containing the same Cu²⁺ concentration.
- (51) Dai, J.; Sullivan, D. M.; Bruening, M. L. Ind. Eng. Chem. Res. 2000, 39, 3528-3535.
- (52) Dai, J.; Jensen, A. W.; Mohanty, D. K.; Erndt, J.; Bruening, M. L. *Langmuir* **2001**, *17*, 931-937.
- (53) Joly, S.; Kane, R.; Radzilowski, L.; Wang, T.; Wu, A.; Cohen, R. E.; Thomas, E. L.; Rubner, M. F. *Langmuir* **2000**, *16*, 1354-1359.
- (54) Deacon, G. B.; Phillips, R. J. Coord. Chem. Rev. 1980, 33, 227-250.
- (55) Rubner and coworkers reported that thickness of similar MPF's are dependent on deposition pH (reference 29). However, in our case we use a supporting electrolyte (NaCl) and Cu²⁺ in the deposition solution.
- (56) Mendelsohn, J. D.; Barrett, C. J.; Chan, V. V.; Pal, A. J.; Mayes, A. M.; Rubner, M. F. Langmuir 2000, 16, 5017-5023.
- (57) Fery, A.; Schoeler, B.; Cassagneau, T.; Caruso, F. *Langmuir* **2001**, *17*, 3779-3783.

- (58) Miyoshi, H. J. Membr. Sci. 1998, 141, 101-110.
- (59) Manzanares, J. A.; Mafé, S.; Pellicer, J. J. Phys. Chem 1991, 95, 5620-5624.
- (60) Lebedev, K.; Ramirez, P.; Mafe, S.; Pellicer, J. *Langmuir* **2000**, *16*, 9941-9943.
- (61) Lowack, K.; Helm, C. A. Macromolecules 1998, 31, 823-833.
- (62) To estimate the charge density in the surface layer, we first determined the concentration of Cu²⁺ in a 10-bilayer film using cyclic voltammetry and ellipsometry and then multiplied this value by a factor of 8 to get the -COO⁻/
 -COOH concentration in the film. Then we multiplied this value by a factor of 2 because the surface of the film is mostly PAA rather than PAH/PAA. We assumed that -COOH groups were completely deprotonated.
- (63) Higa, M.; Kira, A. J. Phys. Chem. B 1995, 99, 5089-5093.
- (64) Peeters, J. M. M.; Boom, J. P.; Mulder, M. H. V.; Strathmann, H. J. Membr. Sci. 1998, 145, 199-209.
- (65) Sata, T. J. Membr. Sci. 1994, 93, 117-135.
- (66) Sata, T.; Yamaguchi, T.; Matsusaki, K. J. Phys. Chem 1995, 99, 12875-12882.
- (67) Beerlage, M. A. M.; Peeters, J. M. M.; Nolten, J. A. M.; Mulder, M. H. V.; Strathmann, H. J. Appl. Polym. Sci. 2000, 75, 1180-1193.
- (68) Robertson, B. C.; Zydney, A. L. J. Membr. Sci. 1990, 49, 287-303.

CHAPTER 3

Preparation of Composite Membranes by Atom Transfer Radical Polymerization Initiated from a Porous Support

3.1 Introduction

Synthesis of practical separation membranes requires methods for creating thin, selective skins at the surface of highly permeable supports. Composite membranes prepared by depositing an expensive skin on a relatively inexpensive support are especially attractive in this regard because only a small amount of the selective skin material is needed. The most common methods for formation of composite membranes include interfacial polymerization, casting, plasma polymerization, and solution coating. Even with the successes of these methods, synthesis of selective membrane skins with minimal (<50 nm) thicknesses is still difficult. This chapter describes our initial investigations into the possibility of using polymerization from a surface to create ultrathin membrane skins with unique structures.

Many recent studies demonstrate the use of controlled polymerization techniques to grow polymer chains from surfaces in a well-defined way.¹⁴⁻²³ These procedures generally involve attachment of polymerization initiators to a surface and subsequent polymerization from these initiators. Of the many types of possible polymerization strategies (e.g., radical,²⁴ cationic,²¹ anionic,¹⁵ ring-opening,²⁵ and ring-opening metathesis²⁶), atom transfer radical polymerization (ATRP) is especially attractive because it yields polymers of low polydispersity and is compatible with a variety of functional monomers. Since the initial discovery of ATRP,^{27,28} we and others have

adapted this technique for surface-initiated polymerization. The recent discovery of transition metal complexes that catalyze ATRP from a surface at room temperature is particularly important because low-temperature polymerization from a substrate can occur with minimal simultaneous polymerization in solution. This helps to avoid physisorption of unbound polymer chains and allows synthesis of cross-linked polymer films. Additionally, the controlled nature of ATRP affords control over skin thickness by variation of polymerization time.

This work demonstrates the versatility of surface-initiated ATRP for forming ultrathin membrane skins on a porous support and examines gas permeation through these membranes. We utilized ATRP to synthesize two kinds of membrane skins: cross-linked poly(ethylene glycol dimethacrylate) (PEGDMA)³¹ and poly(2-hydroxyethyl methacrylate) (PHEMA).¹⁹ The synthesis involves covalent attachment of an ATRP initiator³² to a modified porous alumina support followed by room-temperature polymerization with a suitable monomer.

Cross-linked polymer membranes such as PEGDMA are potentially attractive for gas separations because they should be able to function in high levels of plasticizing and condensable vapors that often degrade membrane performance.³⁴⁻³⁸ Recent methods for forming cross-linked membranes include UV-irradiation of benzophenone-containing polymers, heating of polyimides that contain diacetylene groups, ^{37,40} and chemical cross-linking of polyimides with diamino compounds.⁴¹ Koros and coworkers demonstrated that chemical cross-linking of carboxylic acid-containing polyimides with ethylene glycol greatly increases the CO₂ plasticization pressure and also increases CO₂/CH₄ selectivity.¹⁰ Preparation of cross-linked membranes can also occur by casting

a solution containing cross-linkable monomer and subsequently polymerizing the film. Although this method does not result in ultrathin skins, Hirayama and co-workers showed that cross-linked polymer films containing polyethylene oxide chains have a CO_2/N_2 selectivity of $65.^{42,43}$

This work demonstrates that ATRP from a surface allows controlled synthesis of ultrathin, cross-linked and derivatizable membrane skins. Gas-permeation studies with PEGDMA films grown on porous alumina supports show that these membranes are free of defects and have a CO₂/CH₄ selectivity of ~20. In comparison, PHEMA brushes show selectivity values typical of Knudsen diffusion. One advantage of the PHEMA membranes, however, is that they can be readily derivatized with a variety of functional groups. Esterification of PHEMA with pentadecafluorooctanoyl chloride increases the CO₂ permeability of these membranes, but still yields a CO₂/CH₄ selectivity of only 8. Future work aims at exploiting the versatility of ATRP for creating membranes for specialty applications.

3.2 Experimental

3.2.1 Chemicals and Solutions

Poly(allylamine hydrochloride) (PAH) (M_w = 70,000), sodium poly(styrenesulfonate) (PSS) (M_w = 70,000), 3-mercaptopropionic acid (MPA), pentadecafluorooctanoyl chloride (97%), pyridine, dimethylformamide (DMF, anhydrous, 99.8%), tetrahydrofuran (THF, anhydrous, inhibitor free, 99.8 %), methanol (anhydrous, 99.8%), 2-bromopropionylbromide (2-BPB), CuCl (99.999%), CuBr (99.999%), CuBr₂ (99%) and 2,2'-bipyridine (bpy, 99%) were used as received from

Aldrich. MnCl₂ (Acros) and NaBr (Spectrum) were also used as received. Triethylamine (Spectrum, 98%) was vacuum distilled over CaH₂. 2-Hydroxyethyl methacrylate (HEMA, Aldrich, 98%, inhibited with 300 ppm hydroquinone monomethyl ether (MEHQ)) and ethylene glycol dimethacrylate (EGDMA, Aldrich, 98%, inhibited with 100 ppm MEHQ) were purified by passing them through a column of activated basic alumina (Spectrum). Deionized water (Milli-Q, 18.2 MΩ cm) was used for preparation of solutions and rinsing. The disulfide initiator, (BrC(CH₃)₂COO(CH₂)₁₁S)₂, was synthesized according to a literature procedure. AnodiscTM porous alumina membranes (Fisher) with 0.02 μm-diameter surface pores were used as supports for membrane formation. Gold slides (200 nm of sputtered Au on 20 nm Cr on a Si (100) wafer) were used as substrates for ellipsometry and Fourier transform infrared (FTIR) external reflection spectroscopy.

3.2.2 Polymerization of EGDMA

The initial step in the polymerization procedure is the attachment of initiating groups to the substrate. In some cases, we first deposited a multilayer polyelectrolyte film on the substrate and subsequently anchored initiators to these modified surfaces. The deposition of polyelectrolytes occurred as follows. Au-coated wafers were cleaned in a UV/ozone chamber (Boekel UV-Clean model 135500) for 15 minutes and subsequently immersed in a 1 mM ethanolic solution of MPA for 30 minutes, rinsed with ethanol and deionized H₂O, and dried with N₂. This procedure yields a carboxylic acid-terminated surface. Substrates were then immersed in a polycation solution (0.02 M PAH, 0.5 M NaBr, pH 2.3) for 5 minutes and rinsed with deionized water. (Molarities of polymers are given with respect to the repeating unit.) Subsequent immersion in a

polyanion solution (0.02 M PSS, 0.5 M MnCl₂, pH 2.1) for 2 minutes and rinsing with deionized water yielded a polyelectrolyte bilayer on the surface. A second layer of PAH was then adsorbed on top of the PAH/PSS layer to provide amine functional groups for initiator anchoring.

Initiator was attached to PAH/PSS films via reaction with 2-BPB in the presence of triethylamine.³² The gold slide was first immersed in a solution of triethylamine (0.242 g in 10 mL THF), and then the initiator solution (0.432 g of 2-BPB in 10 mL THF) was added drop-wise while stirring. Because the reaction is exothermic, both solutions were cooled to 0 °C prior to the reaction. The reaction was stopped after 2 minutes by transferring the slide to a THF solution. Initiator attachment was performed in a glove box because the acid bromide is moisture sensitive. Further rinsing with ethyl acetate, ethanol, and deionized water followed by drying with N₂ was done outside the glove box.

Polymerization of EGDMA occurred by immersing the initiator-modified surfaces in a solution containing EGDMA (monomer), DMF, deionized H₂O and the Cu catalyst system.³¹ In this procedure, the monomer mixture, 42 mL of solution containing EGDMA, H₂O and DMF (3:3:8, v:v:v) was first degassed in a three necked flask by three freeze-pump-thaw cycles. Then, CuCl (180 mg, 1.8 mmol), CuBr₂ (120 mg, 0.54 mmol), and bpy (731 mg, 4.68 mmol) were quickly added to the degassed mixture under a nitrogen atmosphere. This mixture was immediately degassed using another two freeze-pump-thaw cycles and then warmed to room temperature with continuous stirring until the solution became a homogeneous dark brown color. The sealed vessel containing the monomer/catalyst solution was next transferred into a glove bag that was subsequently

purged with nitrogen for at least an hour. The polymerization solution was then transferred to vials containing polyelectrolyte-coated gold wafers modified with initiators, and polymerizations were carried out in the glove bag at room temperature for different times. After polymerization, substrates were removed from the vessels, rinsed with DMF, sonicated (1 minute) in DMF, rinsed with THF followed by ethanol, and dried under a flow of N_2 .

To grow PEGDMA on porous alumina, one bilayer of PSS/PAH was deposited directly on UV/ozone-cleaned alumina, and the initiator attachment and polymerization occurred as described above. Polyelectrolyte depositions were limited to the filtrate side of the alumina membrane by using a holder, and the initiator attachment and polymerization were done without the holder.

3.2.3 Polymerization of HEMA and Subsequent Derivatization

For the polymerization of HEMA from gold wafers, substrates were first cleaned in a UV/ozone chamber for 15 minutes, immersed in an ethanol/water (50:50, v:v) solution for 10 minutes, rinsed with water, and dried with nitrogen. These Au-coated supports were then immersed in a 1 mM ethanolic solution of the disulfide initiator, (BrC(CH₃)₂COO(CH₂)₁₁S)₂, for 12 hours to form a monolayer of initiator. After monolayer formation, the substrates were rinsed with ethanol and dried with N₂.

Polymerization of HEMA occurred by immersion of the initiator monolayer-coated substrates in a methanolic solution containing HEMA and the Cu catalyst system. To prepare this solution, 42 mL of HEMA and methanol (1:1, v:v) were first degassed in a three-necked flask by three freeze-pump-thaw cycles. Then, 552 mg (3.84 mmol) of CuBr, 86 mg (0.39 mmol) of CuBr₂, and 1329 mg (8.52 mmol) of bpy were quickly

added to the HEMA/methanol while flowing N_2 over the solution. This mixture was immediately subjected to another two freeze-pump-thaw cycles and subsequently stirred until a homogeneous dark brown solution formed. The sealed vessel containing the polymerization solution was then transferred to a glove bag, which was purged with N_2 for ~ 1 hour. The polymerization solution was finally transferred into vessels containing substrates modified with initiators, and polymerizations were carried out for different times. After polymerization, substrates were removed from the vessels, rinsed with methanol, sonicated (1 minute) in DMF, rinsed with THF followed by ethanol, and dried under a flow of N_2 .

For the polymerization of HEMA from porous alumina, substrates were first coated with gold, and the initiator was attached as a self-assembled monolayer as described above. Prior to gold coating, substrates were immersed in boiling methanol for 10 minutes and subsequently cleaned in a UV/ozone chamber for 10 minutes. Substrates were then sputter-coated (filtrate side only) with 5 nm of gold and again UV/ozone cleaned. Initiator anchoring was done, as described above, by immersion in an ethanolic solution of disulfide initiator (this immersion occurred in an air-tight vessel that was initially purged with N₂ gas). After monolayer formation, PHEMA was polymerized from the initiator surface as described above.

To derivatize PHEMA coatings, films were immersed in 7 mL of anhydrous DMF containing pentadecafluorooctanoyl chloride (0.08 M) and pyridine (0.1 M). After 15 minutes, films were removed from the solution, rinsed with DMF followed by ethanol, and dried with a flow of nitrogen. The fluorination was monitored by FTIR spectroscopy

of films on gold wafers and alumina membranes. PHEMA membranes were fluorinated after initial gas transport measurements.

3.2.4 Film Characterization on Gold Wafers

Ellipsometric thickness measurements were obtained using a rotating analyzer ellipsometer (model M-44; J.A. Woollam), assuming a film refractive index of 1.5. For each polymer film, thicknesses were measured at three different spots and averaged. At least three samples of each film were examined. External reflection FTIR spectroscopy was performed with a Nicolet Magna 560 FTIR using a Pike grazing angle (80°) accessory.

3.2.5 Film Characterization on Alumina Supports

Film growth was monitored by transmission FTIR spectroscopy (Mattson Instruments, Infinity Gold) and Field-Emission Scanning Electron Microscopy (FESEM, Hitachi S-4700II, acceleration voltage of 15 kV). Membranes were coated with 5 nm of gold for imaging purposes. In the case of cross-sectional images, membranes were freeze-fractured under liquid N₂ prior to sputter coating with gold.

3.2.6 Gas-Permeation Studies

Gas-permeation studies were performed using a permeation cell with a pressure relief valve, and permeate flux was measured as a function of inlet pressure (5-45 psig) using a soap-bubble flow meter (Figure 3.1). O₂, N₂, H₂, He, CH₄, and CO₂ were used for permeation studies, and measurements were performed for each gas separately in the above order. After examining all gases, O₂ permeability was remeasured to check the

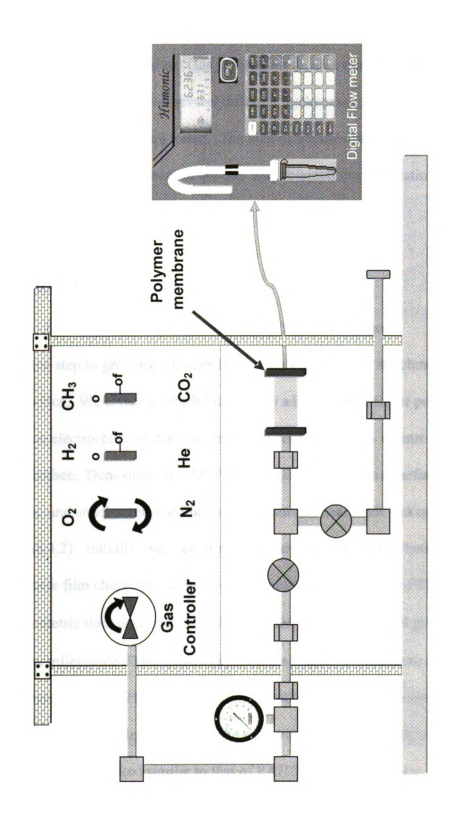


Figure 3.1: Apparatus for gas-permeation measurements.

stability of the membrane, and the O₂ flux changed by <10%. For each gas, the permeation cell was purged several times with the gas of interest over a 20-minute period to obtain a stable flux value. Gas permeation studies were done for each polymer (PEGDMA or PHEMA) at several different thicknesses, and for each thickness, three different membranes were tested. The area of the membrane exposed to gas was 2.0 cm². The selectivity of one gas over another was obtained from the ratio of the respective permeability coefficients at 45 psig.

3.3 Results and Discussion

3.3.1 Synthesis and Characterization of PEGDMA films

The first step in growing polymer films from a substrate is attachment of an initiator to the surface. We chose to attach initiators to adsorbed multilayer polyelectrolyte films because electrostatic adsorption provides a convenient way to introduce functional groups on a surface. Deposition of PAH/PSS/PAH films results in a surface rich in amine groups, and attachment of initiators to this surface via amide linkages occurs easily (Figure 3.2). Initially, we grew films on gold-coated Si wafers because this substrate facilitates film characterization by ellipsometry and reflectance FTIR spectroscopy. The ellipsometric thickness of PAH/PSS/PAH films on MPA-coated gold was 4.8 ± 0.4 nm, and the reflectance FTIR spectra (Spectrum a, Figure 3.3) of these films had strong sulfonate peaks at 1219 and 1177 cm⁻¹ as well as a number of peaks due to aromatic and -NH₃⁺ modes. After reaction of the film with the acid bromide initiator, the reflectance FTIR spectrum looked similar to that of PAH/PSS/PAH, but there was a small increase in the peak intensity in the amide region (1650-1560 cm⁻¹, Spectrum b, Figure 3.3),

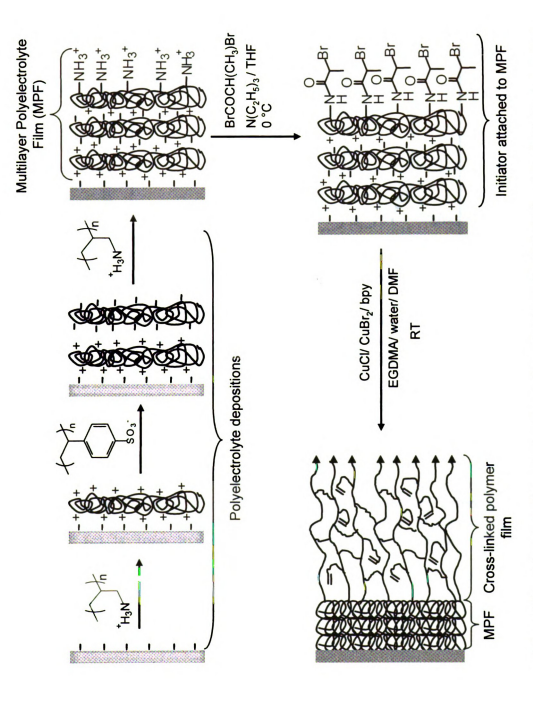


Figure 3.2: Schematic diagram showing polymerization of EGDMA from a polyelectrolyte surface modified with an initiator.

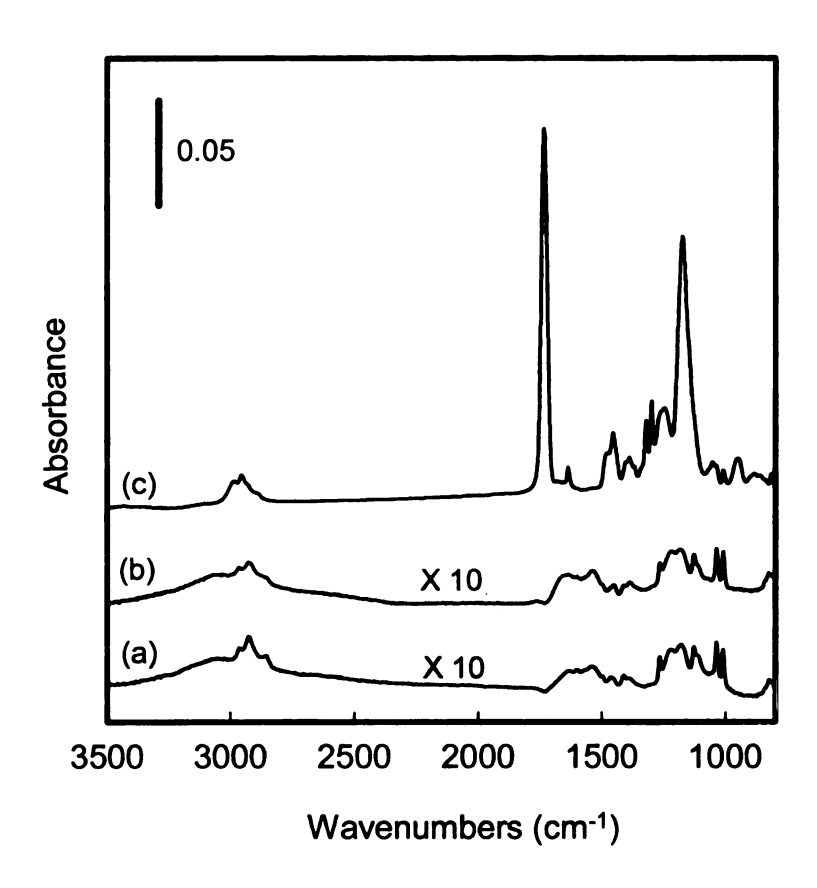


Figure 3.3: External reflection FTIR spectra of a PAH/PSS/PAH film on a MPA-modified Au surface before (a) and after reaction with an acid bromide initiator (b). Spectrum (c) is from a PEGDMA film grown for 20 hours from PAH/PSS/PAH modified with initiator.

indicating initiator attachment. Film thickness increased only slightly (<0.5 nm), as would be expected, upon initiator attachment.

Growth of PEGDMA films from the initiator-containing surfaces occurred upon exposure of the substrate to a DMF/H₂O solution containing monomer and Cu catalyst. Scheme 3.1 outlines the synthesis of cross-linked PEGDMA films from initiatormodified gold surfaces using ATRP. Cumulative film thickness increased to 20 ± 1.4 nm in 10 hours, 52 ± 1.1 nm in 20 hours and 73 ± 6.6 nm in 30 hours. Similar to previous studies, growth of PEGDMA was characterized by the appearance of a strong carbonyl peak at 1730 cm⁻¹ in the reflectance FTIR spectrum of the film (Spectrum c, Figure 3.2).³¹ A C=C stretching band (1637 cm⁻¹) from unpolymerized vinyl groups was also present in the spectrum. By taking the ratio of the IR absorbance of remaining (unpolymerized) vinyl groups to the absorbance of carbonyl groups and comparing this with the same ratio in the monomer (EGDMA) spectrum, we estimated that 25% of the total vinyl groups remain after polymerization. This suggests approximately 50% crosslinking in PEGDMA films. Previous studies done by our group showed that the C=C/C=O absorbance ratio is constant for different PEGDMA film thicknesses, indicating that the amount of cross-linking is independent of polymerization time ³¹

As a control experiment, we also attempted polymerization of EGDMA from PAH/PSS/PAH-coated wafers (no initiator was attached to this surface). Exposure of the PAH/PSS/PAH surface to EGDMA and Cu catalyst resulted in no detectable carbonyl peak in the reflectance FTIR spectrum of these films and no increase in ellipsometric thickness. This result provides further evidence that the derivatization of the amine

Scheme 3.1: Growth of cross-linked PEGDMA from an anchored initiator.

•

groups of PAH with 2-BPB was successful and that PEGDMA was chemically attached to the surface. When growing films on porous alumina, we deposited a PSS/PAH film rather than PAH/PSS/PAH because the surface of the alumina is positively charge below pH 8. 45.46 We limited the polyelectrolyte deposition to one bilayer to minimize any blocking effect from PSS/PAH. Top-view FESEM images show that pores are clearly open after depositing one bilayer of PSS/PAH (compare Figure 3.4a and Figure 3.4b). After subsequent polymerization of EGDMA from these surfaces, pores are completely covered with the polymer (Figure 3.4c and Figure 3.4d). Both Figure 3.4d and images of the permeate side of the membrane after polymerization (not shown) demonstrate that the interiors of the pores are open, indicating minimal deposition inside pores. Because of the high pore density in the alumina substrates, ellipsometric measurements were not possible on these surfaces, and thus PEGDMA thicknesses were estimated from the cross-sectional FESEM images. Thicknesses of films on porous alumina (Table 3.1) were similar (within ~25%) to those of films prepared on gold-coated Si.

3.3.2 Synthesis and Characterization of PHEMA films

To compare cross-linked PEGDMA with uncross-linked polymer films, we also synthesized PHEMA by polymerization from a surface.⁴⁷ In the case of HEMA polymerization, we chose methanol as a solvent instead of water because aqueous conditions yield very high film thicknesses that would not be conducive to high flux.¹⁹ However, PHEMA films grown from initiators attached to PAH/PSS/PAH on gold were only ~20 nm thick. To achieve larger thicknesses that should allow complete coverage of surface pores, we grew films from a self-assembled monolayer of initiator, (BrC(CH₃)₂COO(CH₂)₁₁S)₂, on gold.¹⁹ This monolayer likely has a higher density of

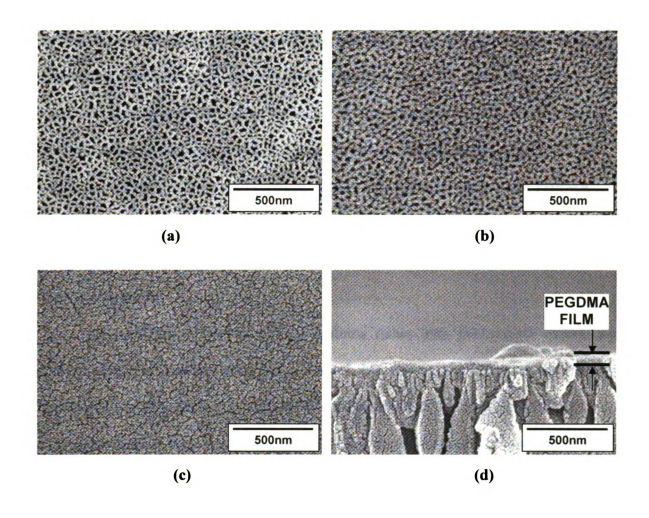


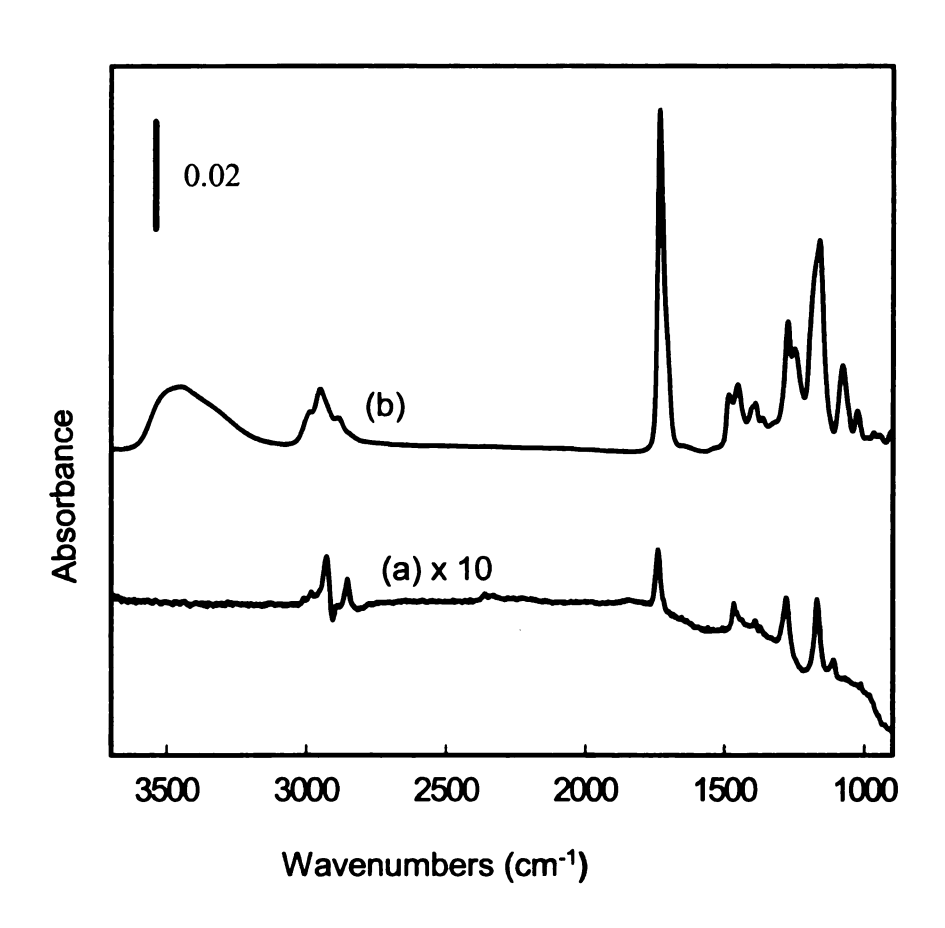
Figure 3.4: FESEM images of the filtrate side of porous alumina (0.02 μ m surface pore diameter) (a) before depositing polyelectrolytes (b) after depositing one bilayer of PSS/PAH, and (c) after growth of PEGDMA from the surface for 20 hours. Image (d) is a cross-section of the membrane shown in (c).

surface-initiating groups than the derivatized polyelectrolytes. After immersing a gold-coated substrate in disulfide initiator solution for 12 hours, the FTIR spectrum of the surface showed the appearance of a carbonyl peak at 1739 cm⁻¹ confirming the formation of an initiator monolayer (Figure 3.5). Polymerization of HEMA was carried out by immersing initiator-modified substrates in HEMA/methanol solutions containing the Cu catalyst system for different times. Scheme 3.2 outlines the synthetic pathway that we used to grow PHEMA from gold surfaces. Figure 3.6 shows the variation of PHEMA film thickness with polymerization time when growth occurs from the monolayer of initiators. Although film growth levels off after a few hours, films as thick as 100 nm can be easily produced.

To grow these films on porous alumina rather than gold-coated wafers, we sputter-coated the alumina with 5 nm of Au and then formed the self-assembled initiator layer on this surface. Similar to PEGDMA membranes, FESEM images of PHEMA films on porous alumina supports show that PHEMA effectively covers the surface without filling the pores. Thicknesses of films on porous alumina (determined by FESEM, Table 3.2) are similar (within ~30%) to those of films on gold-coated wafers (determined by ellipsometry, Figure 3.6).

3.3.3 Gas Permeation through Polymer Membranes

Flux through polymeric gas separation membranes, F, generally depends on transmembrane pressure drop and membrane thickness as shown in equation 3.1, where P is the permeability coefficient of the material, Δp is the pressure drop, and l is the membrane thickness.⁴⁸



Scheme 3.2: Growth of PHEMA brushes from a gold surface: (1) formation of a monolayer of initiator and (2) polymerization from the initiator-modified gold surface.

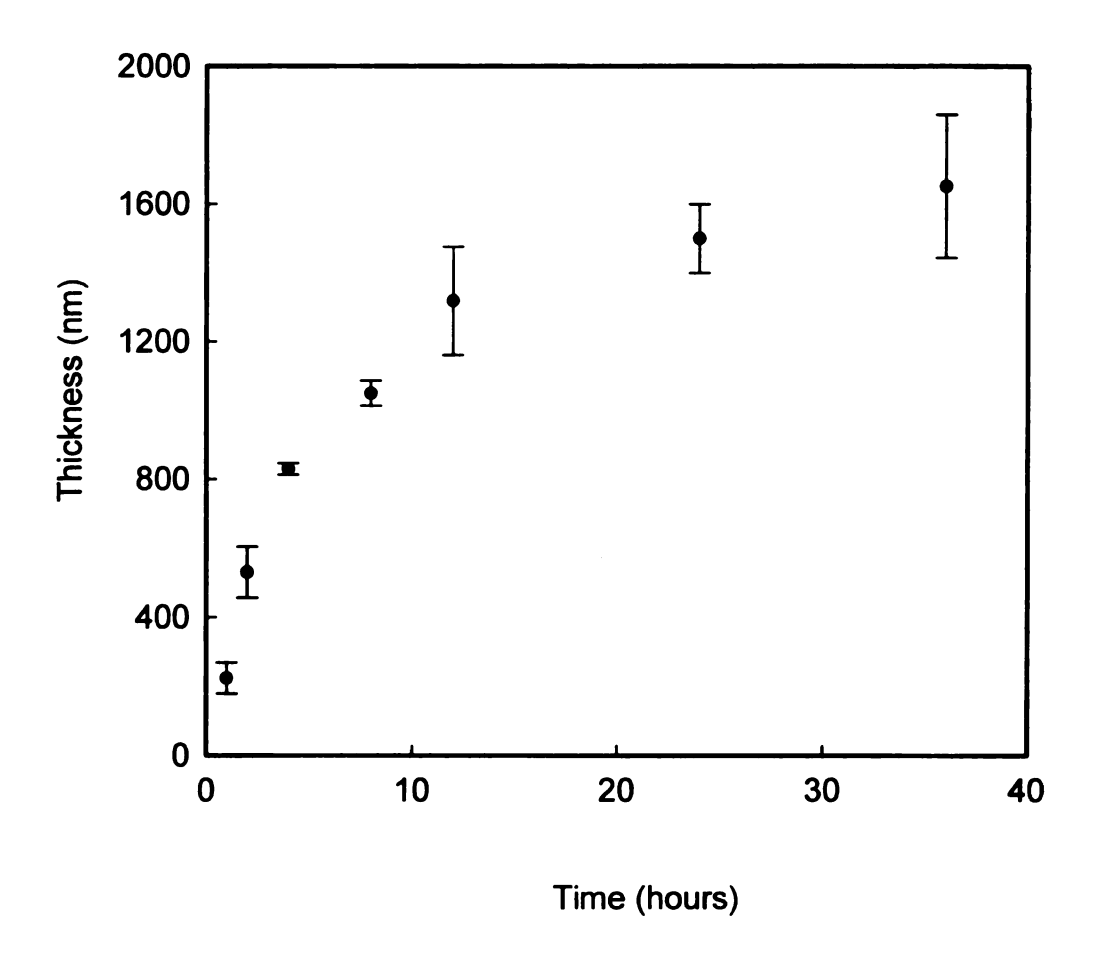


Figure 3.6: Ellipsometric thicknesses of PHEMA films as a function of polymerization time. Thickness values are the average of measurements on three different films, and the error bars represent standard deviations.

$$F = \frac{P \Delta p}{I}$$
 3.1

Theoretically, gas permeation through polymeric membranes is usually described by the solution-diffusion model. The gas dissolves in the high-pressure side of the membrane, diffuses through the membrane because of a concentration gradient, and desorbs at the low-pressure side. Hence, the permeability of a gaseous penetrant, P, can be written as a product of an average diffusivity, D, and an effective solubility coefficient, S, for the penetrant in the polymer matrix.⁴⁹

$$P = D \times S \tag{3.2}$$

The solubility coefficient depends on the condensability of the penetrant, polymer-penetrant interactions, and the free volume of the polymer matrix. Diffusivity provides a measure of the mobility of the penetrant in the polymer matrix and is determined by the packing of polymer chains and the size and shape of the penetrating gas. The ideal selectivity of a membrane, $\alpha_{A/B}$, is the ratio of the permeabilities of the two gases.

$$\alpha_{A/B} = \frac{P_A}{P_B} \tag{3.3}$$

By substituting equation (2) into equation (3),

$$\alpha_{A/B} = \frac{D_A}{D_B} \frac{S_A}{S_B}$$
 3.4

where D_A/D_B is the diffusivity selectivity and S_A/S_B is the solubility selectivity. Thus to improve the permselectivity of one gas over the other, one must increase either the diffusivity selectivity or the solubility selectivity or both.

3.3.4 Gas Permeation through Composite PEGDMA Membranes

Figure 3.7 shows gas fluxes through a PEGDMA membrane as a function of transmembrane pressure drop. Fluxes of different gases through the membrane increase in the approximate order N₂,CH₄,O₂<He,H₂<CO₂. Flux increases linearly with pressure drop for all gases except CO₂. The nonlinear increase in CO₂ flux with increasing pressure suggests a small amount of plasticization, which is surprising considering that pressures are less than 45 psig and the membrane is partially cross-linked. Table 3.1 summarizes the gas permeation data for several gases at three different PEGDMA film thicknesses. As the film thickness increases, selectivity initially increases and plateaus at a film thickness of ~50 nm. (Selectivity appears to decrease slightly for the 80 nm-thick film, but the small difference between selectivities of 50 and 80 nm-thick films is still within experimental error.) The lower selectivity of 30 nm-thick PEGDMA is likely due to areas where the film does not completely cover the substrate. Presumably, thicker films yield a more complete surface coverage.

Selectivity in these membranes is a function of both polymer and gas properties. Cross-linking reduces the polymer chain mobility and should enhance chain packing and the rigidity of the polymer. Tighter packing should favor the diffusion of smaller molecules. For example, CO₂, which is a linear molecule with a kinetic diameter of 3.3 Å, should diffuse faster than CH₄, which is a spherical molecule with a kinetic diameter of 3.8 Å. However, the possible plasticization noted above suggests that the PEGDMA

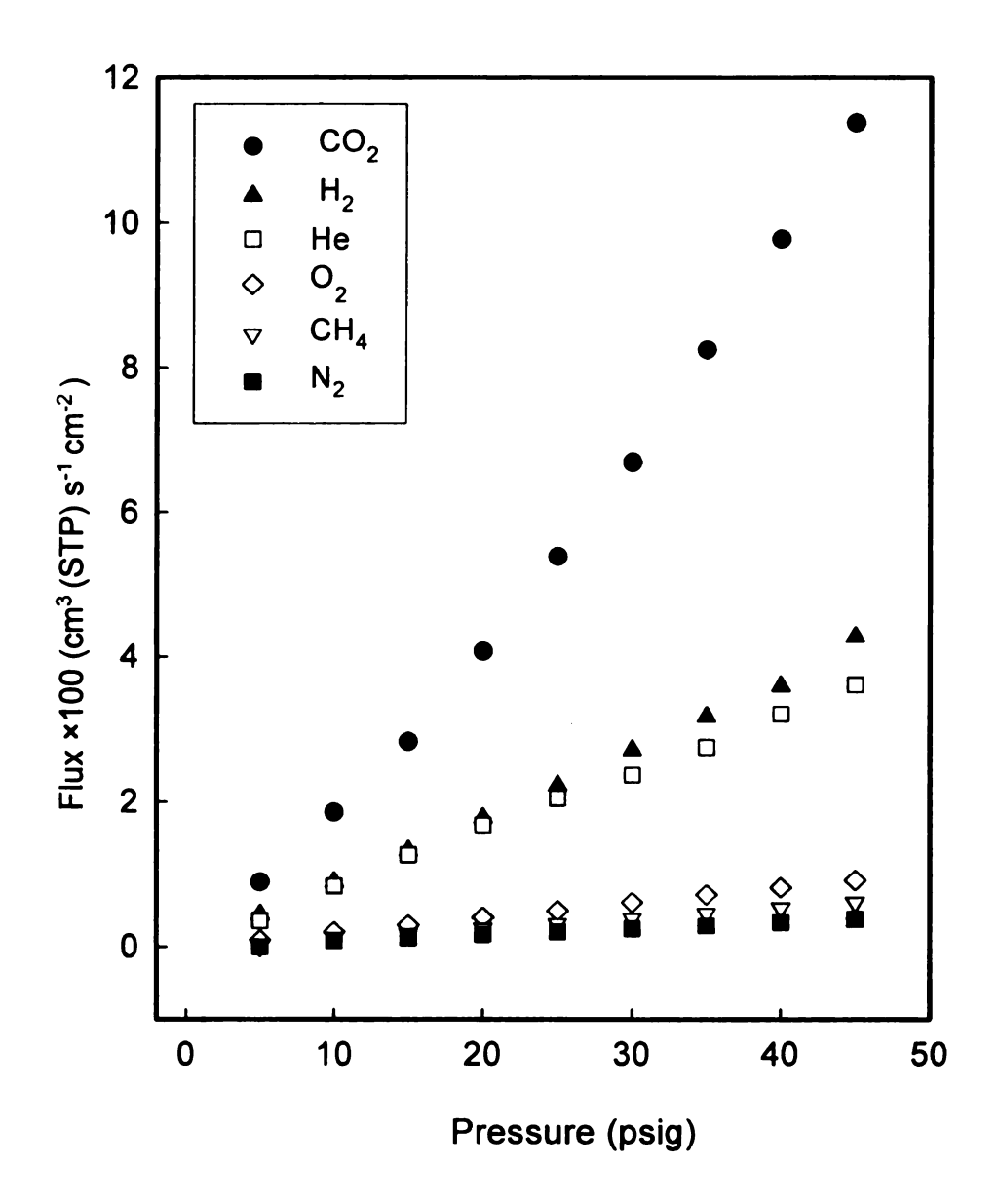


Figure 3.7: Fluxes of different gases through a PEGDMA membrane (50 nm thick) as a function of transmembrane pressure drop. The outlet pressure was 1 atm and the measurements were performed at room temperature. PEGDMA was deposited on porous alumina.

.

Table 3.1: Gas permeability coefficients, estimated film thicknesses, and ideal selectivities for PEGDMA membranes

Polymer- ization	Film	Calcula	ited Gas pe	Calculated Gas permeability Coefficients ^b (Barrers)	Coefficie	nts ^b (Barr	ers)		Selectivity ^c	
Time (hours)	(nm)	02	N_2	Не	H_2	CH4	CO ₂	O_2/N_2	CH ₄ CO ₂ O ₂ /N ₂ CO ₂ /CH ₄ CO ₂ /N ₂	CO ₂ /N ₂
12	30	1+4	4±1	14.3±3.5 18±4	18±4	5 ±2	22±7	1.2±0.2	5 ±2 22±7 1.2±0.2 4.5±0.7 6.3±0.7	6.3±0.7
20	20	2.0±0.1		0.9±0.2 8.2±0.2 9.8±0.3 1.3±0.1 24±4 2.2±0.4	9.8±0.3	1.3±0.1	24±4	2.2±0.4	18±2	56±6
30	08	1.5±0.03	1.0±0.2	.5±0.03 1.0±0.2 6.7±0.9 7.5±0.9 1.1±0.1 19±2 1.6±0.3	7.5±0.9	1.1±0.1	19±2	1.6±0.3	16±1	20±3

1 Barrer = 1×10^{-10} cm³ (STP) cm/ (cm² s cmHg)

^aThicknesses were estimated from FESEM images.

^bPermeability coefficients were calculated using equation 1. Listed values are the average of permeability coefficients for three different membranes. ^cSelectivities (at 45 psig) were calculated for three different membranes, and the average selectivity values are reported. Because of plasticization, CO₂/CH₄ and CO₂/N₂ selectivities are about 10 % higher at 45 psig than at pressures <25 psig. is not especially rigid. Solubility selectivity in PEGDMA is also possible due to interactions between polarizable CO₂ and the polar carbonyl groups of PEGDMA. Koros showed that CO₂/CH₄ selectivity increases with increasing concentration of carbonyl groups in a polymer due to the attraction between CO₂ and polar carbonyl groups.⁵⁰ Freeman and coworkers also demonstrated that the introduction of polar nitro groups into the backbone of polysulfone enhances CO₂/CH₄ selectivity due to interaction of the nitro groups with CO₂.⁵¹

Diffusivity and solubility selectivities should be much more effective in separating CO_2/CH_4 than O_2/N_2 .⁴⁸ The kinetic diameters of O_2 and N_2 differ by only 0.018 nm.⁴⁸ Accordingly, we didn't observe large O_2/N_2 selectivities. A recent study of polyimide membranes showed that cross-linking increases CO_2/CH_4 selectivity but has little effect on O_2/N_2 separation.¹⁰

Calculated permeability coefficients for PEGDMA (Table 3.1) are considerably higher than for poly(methyl methacrylate) (PMMA), which has a CO₂ permeability coefficient of about 0.6 Barrers. However, as might be expected, the CO₂/CH₄ selectivity of PMMA films is about 5-fold higher than that of PEGDMA. Poly(ethyl methacrylate) (PEMA), in contrast, has a CO₂ permeability coefficient of 7 Barrers and a CO₂/CH₄ selectivity of 20, and thus is similar in selectivity to PEGDMA, but slightly less permeable. These data suggest that the bulkier side groups in both PEMA and PEGDMA yield higher permeabilities and lower selectivities than PMMA. (All of these polymers should be glassy at room temperature.) Although PEGDMA is cross-linked, its bulky side chains still likely result in a higher free volume and, hence, higher permeability than that of either PMMA or PEMA. Studies done on various

methacrylates also showed that the free volume of the polymers depends on the side chain. 54-57

Hirayama and coworkers recently reported fabrication of partially cross-linked films from poly(ethylene oxide) (PEO) dimethacrylate. CO₂ permeabilities of these films are about 2-fold higher than those of PEGDMA, ⁴³ and CO₂/N₂ selectivity is 65. The high selectivity likely stems from interaction between CO₂ and PEO, and the high permeability probably results from the bulky PEO groups, which are amorphous. However, the PEO dimethacrylate films were 100-200 µm thick, and thus the PEGDMA membranes grown from a surface still allow 200-fold higher fluxes. In the future, growth of PEO dimethacrylate from a surface could result in very high CO₂ flux.

3.3.5 Gas Permeation through PHEMA Membranes

To compare cross-linked PEGDMA membranes with linear polymer films, we studied the gas-permeation properties of PHEMA that was grown from the surface of porous alumina. Figure 3.8 shows the fluxes of several gases through a PHEMA membrane as a function of transmembrane pressure. Gas permeation through these membranes is typical of Knudsen diffusion, as fluxes of the different gases are inversely proportional to the square root of molar mass. Unlike PEGDMA, PHEMA films show very little selectivity for CO₂ over CH₄. The observed CO₂/CH₄ selectivity was 0.7 and O₂/N₂ selectivity was only 0.9. Selectivities and calculated permeability coefficients for PHEMA at three different film thicknesses are given in Table 3.2. As mentioned above, PEMA has a CO₂/CH₄ selectivity of 20 with a CO₂ permeability coefficient of 7 Barrers at 35 °C. ⁵⁴ Both PHEMA and PEMA are glassy polymers with similar T_g values (T_g of PHEMA is 85 °C and T_g of PEMA is 65 °C. ⁵⁸), hence Tg shouldn't have a dramatic effect

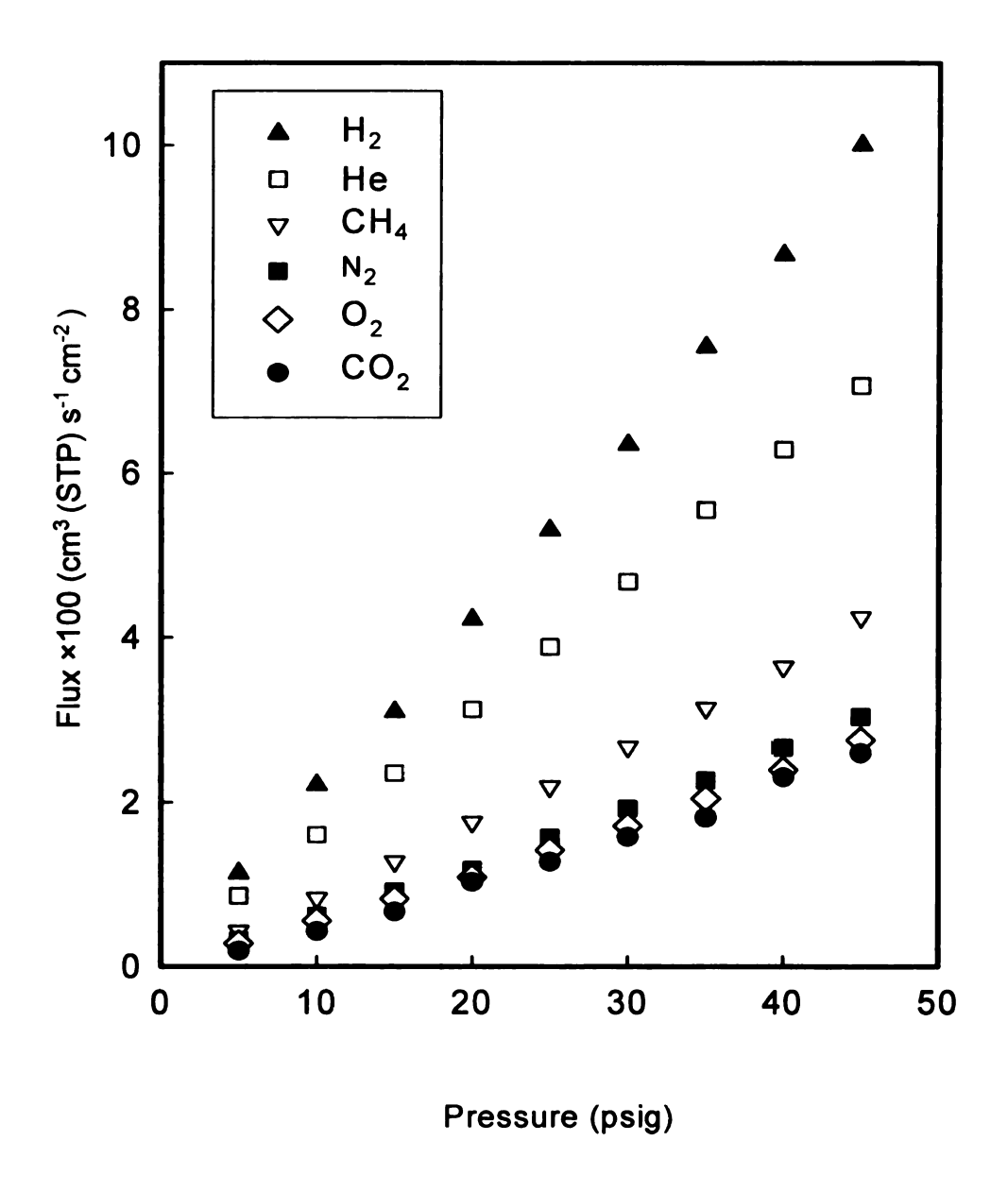


Figure 3.8: Fluxes of different gases through a PHEMA membrane (60 nm thick) as a function of transmembrane pressure drop. The outlet pressure was 1 atm and the measurements were performed at room temperature. PHEMA was deposited on porous alumina.

Table 3.2: Gas permeability coefficients, estimated film thicknesses and ideal selectivities for underivatized PHEMA membranes

Polymer -ization	Film		lculated Ga	as permea	bility Coe	Calculated Gas permeability Coefficients ^b (Barrers)	rrers)		Selectivity ^c	u
	(nm)	02	N_2	Не	H ₂	CH4	CO ₂	O ₂ /N ₂	O ₂ /N ₂ CO ₂ /CH ₄ CO ₂ /N ₂	CO ₂ /N ₂
1	18	8±1	9±2	20±3	29±5	12±2	8±1	6:0	9.0	6.0
2	35	7±1	7±1	16±3	23±5	10±2.0	7±1	6.0	9.0	6:0
4	09	7.2±0.3	7.9±0.3	15±3	23±4	10.6±0.3	7±1	6:0	0.7	6.0

^a Thicknesses were estimated from FESEM images.

^bPermeability coefficients were calculated from equation 1. Listed values are the average of permeability coefficients for three different membranes.

^c Selectivities (at 45 psig) were calculated for three different membranes and the average values are reported.

on permeability. The permeability of CO₂ obtained in our study is similar to the reported CO₂ permeability for PEMA, but the observed low selectivity of PHEMA compared with the selectivity reported for PEMA suggests that the hydroxyl groups in PHEMA dramatically alter polymer packing.

To improve the CO₂/CH₄ or O₂/N₂ selectivity of PHEMA membranes, we explored derivatization of PHEMA with fluorinated compounds. One attractive feature of PHEMA is that its hydroxyl groups can be easily derivatized with various acid chlorides or carbonyldiimidazole to introduce different functional groups. 19 We reacted PHEMA with pentadecafluorooctanoyl chloride in the presence of a base to obtain PHEMA with perfluorinated side chains (scheme 3.3). Disappearance of the alcohol peak (3500-3300 cm⁻¹) in the reflectance FTIR spectrum of PHEMA (Spectrum b, Figure 3.9) indicates conversion of the hydroxyl groups to fluorinated esters. The appearance of a fluorinated ester peak at 1800 cm⁻¹ and CF_x peaks at 1250 cm⁻¹ also confirm the esterification of PHEMA. Based on the density of HEMA and poly(1,1'dihydroperfluorooctyl methacrylate, we would expect to see a more than 100 % increase in thickness upon fluorination. Nevertheless, the ellipsometric thicknesses of PHEMA films increased only by ~ 70 % after reaction with pentadecafluorooctanoyl chloride, suggesting <100 percent derivatization of hydroxyl groups or very dense films. However, the disappearance of the alcohol peak in the IR spectrum of PHEMA points to virtually quantitative derivatization. In addition to examining PHEMA films on gold wafers, we also characterized the fluorinated films on alumina with transmission FTIR (Figure 3.10). Appearance of a carbonyl peak around 1800 cm⁻¹ suggests the incorporation of perfluorinated groups. The relatively small increase in film thickness

Scheme 3.3: Derivatization of PHEMA with perfluorooctanoyl chloride.

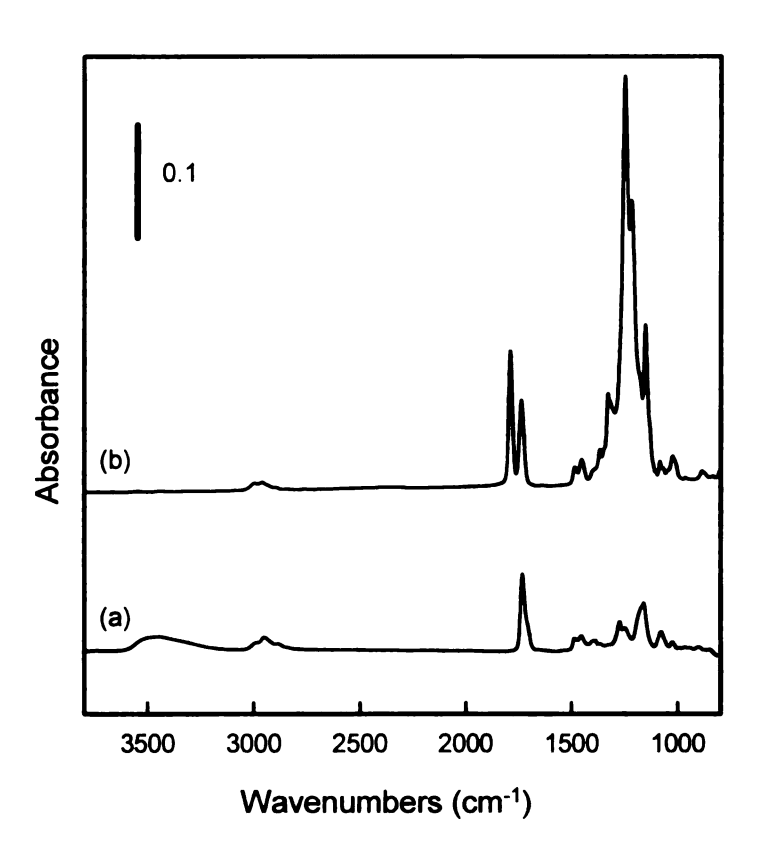


Figure 3.9: Reflectance FTIR spectra of a PHEMA film grown from (BrC(CH₃)₂COO(CH₂)₁₁S)₂ on gold (a) before and (b) after reaction with pentadecafluorooctanoyl chloride.

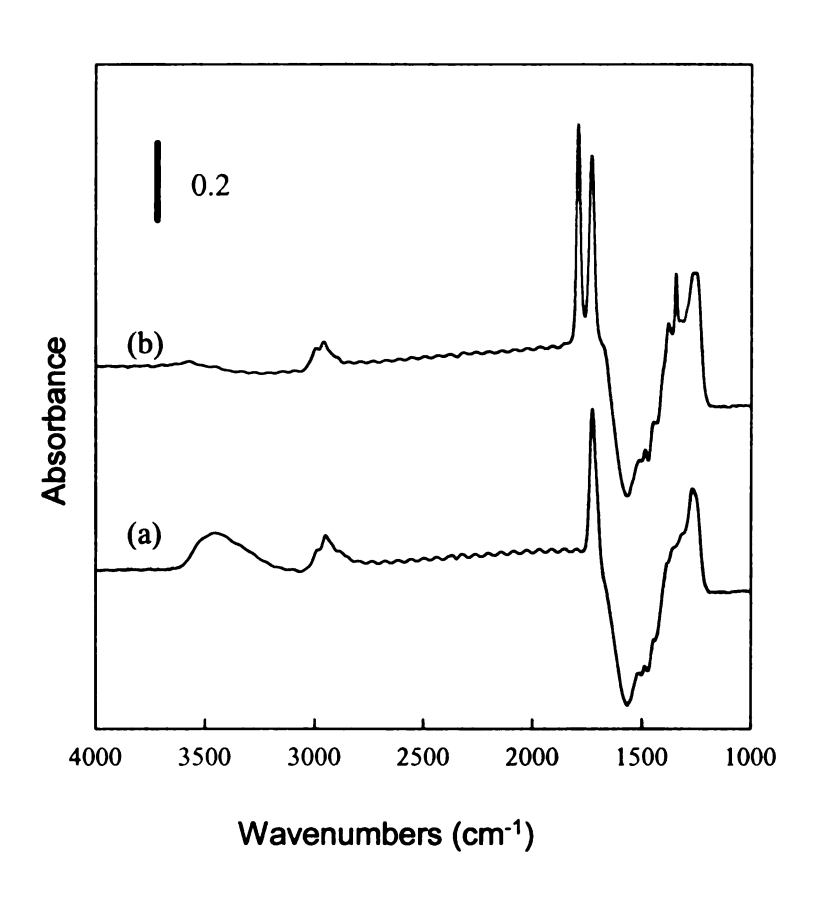


Figure 3.10: Transmission FTIR spectra of a PHEMA film grown from $(BrC(CH_3)_2COO(CH_2)_{11}S)_2$ on gold-coated porous alumina (a) before and (b) after reaction with pentadecafluorooctanoyl chloride.

after fluorination may indication a high film density (low free volume) after derivatization. This is consistent with the fact that fluorinated PHEMA is less permeable than poly(1,1'-dihydroperfluorooctyl methacrylate (vide infra), and the brush-like structure of these films might account for this high density.

Gas-permeation studies with PHEMA were repeated after fluorination, and Figure 3.11 shows the fluxes of several gases as a function of transmembrane pressure drop. After fluorination, the fluxes of various gases decrease in the order CO₂>He>H₂>O₂>N₂, CH₄ and are no longer dependent solely on the molar masses of the gases. Because fluorination enhances CO₂ flux relative to other gases, CO₂/CH₄ selectivity increases ~10-fold compared to non-fluorinated films. Similar to PEGDMA, fluorinated PHEMA also shows an increase in CO₂/CH₄ selectivity with increasing film thickness. The highest selectivity was obtained for a 100-nm thick fluorinated film (Table 3.3). At film thicknesses higher than 100 nm, flux values for some gases were lower than the detection limits of our flow meter.

The increase in CO₂/CH₄ selectivity and CO₂ permeability after fluorination probably occurs due to an increase in CO₂ solubility in the polymer matrix. Compared with the other gases we tested, CO₂ has a high polarizability and quadrupole moment⁴⁸ that should allow it to interact with the polar fluorinated side chains (the C-F dipole moment is 1.39 D⁵⁹). Thus CO₂ solubility is higher after fluorination compared to other gases hence we observe higher CO₂/CH₄ selectivity.

Arnold and coworkers reported the gas permeation properties of membranes prepared from poly(1,1'-dihydroperfluorooctyl acrylate) (PFOA) and poly(1,1'-dihydroperfluoro methacrylate) (PFOMA).⁶⁰ These membranes are similar to fluorinated

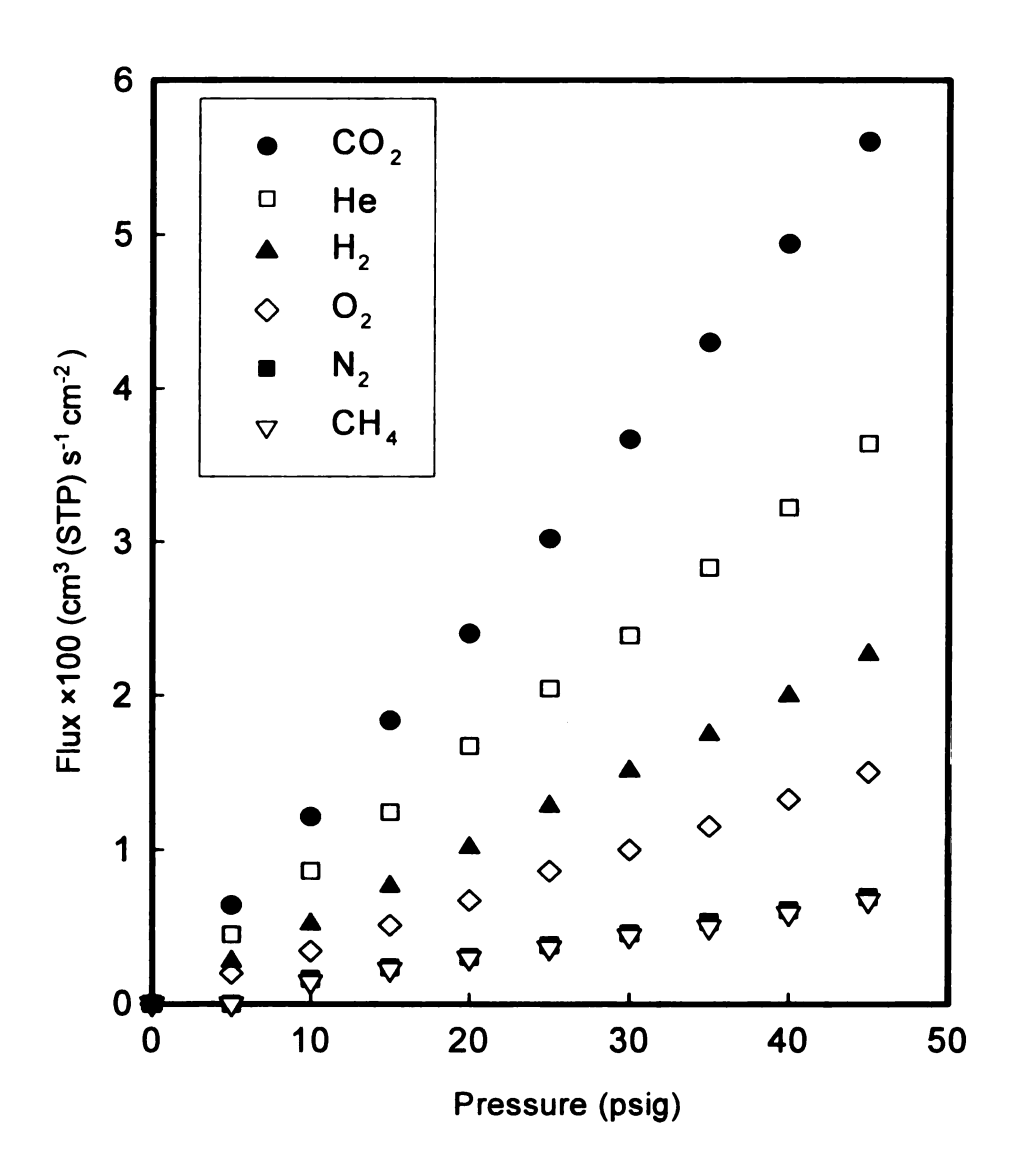


Figure 3.11: Fluxes of different gases through a fluorinated-PHEMA membrane (100 nm thick) as a function of transmembrane pressure drop. The outlet pressure was 1 atm and the measurements were performed at room temperature.

Table 3.3: Estimated film thicknesses, gas permeability coefficients and ideal selectivities for fluorinated PHEMA membranes

Film	Caj	culated Gas	permeabilit	ty Coeffici	Calculated Gas permeability Coefficients ^b (Barrers)	rs)		Selectivity ^c	
(nm) ^a	02	N_2	He	H_2	CH4	CO2	O_2/N_2	CO ₂ /CH ₄	CO ₂ /N ₂
30	8±1	5±1	19±2	17±3	7±2	25±3	1.6±0.1	4.0±0.9	4.9±0.9
09	8.4±0.9	4.5±0.2	21±3	16±2	5.0±0.7	31±6	1.8±0.1	6.0±0.7	6.7±1.1
100	7±1	3.6±0.3	18±4	12±2	3.3±0.6	28±4	1.9±0.4	8.6±0.6	7.8±0.9

^aThicknesses were estimated from FESEM images.

coefficients for three different membranes. Selectivities (at 45 psig) were calculated for three different membranes, and the average values are reported ^bPermeability coefficients were calculated using equation 1. Listed values are the average of permeability

PHEMA and have similar CO₂/CH₄ and O₂/N₂ selectivities. However, the permeability coefficients of CO₂ in PFOA and PFOMA are, respectively,18-fold and 5-fold higher than that of fluorinated-PHEMA.. The extra ester group in fluorinated PHEMA probably reduces the chain mobility and lowers the permeability, and as mentioned above, derivatized films may have a high density.. Other studies also showed that fluorinated side chains greatly enhance CO₂ permeability, and hence CO₂/CH₄ selectivity.^{61,62}

3.4 Conclusions

Surface ATRP provides a convenient way of synthesizing ultrathin, cross-linked films and linear polymer brushes on porous supports. FTIR and FESEM confirm film formation on these surfaces. Gas permeation studies with these films indicate that PEGDMA has a CO₂/CH₄ selectivity of ~20 and a CO₂ permeability coefficient of 20 Barrers. Unlike cross-linked PEGDMA, linear PHEMA films show only Knudsen-diffusion based selectivity. However, esterification of the hydroxyl groups of PHEMA with pentadecafluorooctanoyl chloride increases the CO₂/CH₄ selectivity to ~8 and the CO₂ permeability coefficient to ~20 Barrers. The derivatizability of PHEMA may make it a suitable candidate for specialty separations.

3.5 References and Notes

- (1) Ferjani, E.; Lajimi, R. H.; Deratani, A.; Roudesli, M. S. *Desalination* **2002**, *146*, 325-330.
- (2) Dutta, B. K.; Sikdar, S. K. Environ. Sci. & Tech. 1999, 33, 1709-1716.
- (3) Li, X.-G.; Huang, M.-R. J. Appl. Polym. Sci. 1997, 66, 2139-2147.
- (4) Kamada, K.; Kamo, J.; Motonaga, A.; Iwasaki, T.; Hosokawa, H. *Polym. J.* **1994**, *26*, 833-839.
- (5) Marek, M., Jr.; Brynda, E.; Houska, M.; Schauer, J.; Hynek, V.; Sipek, M. *Polymer* 1996, 37, 2577-2579.
- (6) Baker, R. W. Ind. Eng. Chem. Res. 2002, 41, 1393-1411.
- (7) Pinnau, I.; Freeman, B. D. In *Polymer Membranes for Gas and Vapor Separation*; Pinnau, I., Freeman, B. D., Eds.; American Chemical Society: Washington, DC, 2000; Vol. 744, pp 1-22.
- (8) Liu, C.; Martin, C. R. *Nature* **1991**, *352*, 50-52.
- (9) Petersen, R. J. J. Membr. Sci. 1993, 83, 81-150.
- (10) Staudt-Bickel, C.; Koros, W. J. J. Membr. Sci. 1999, 155, 145-154.
- (11) Hayakawa, Y.; Terasawa, N.; Hayashi, E.; Abe, T. J. Appl. Polym. Sci. 1996, 62, 951-954.
- Yanagishita, H.; Kitamoto, D.; Haraya, K.; Nakane, T.; Okada, T.; Matsuda, H.; Idemoto, Y.; Koura, N. J. Membr. Sci. 2001, 188, 165-172.
- (13) Pinnau, I.; Koros, W. J. *Ind. Eng. Chem. Res.* **1991**, *30*, 1837-1840.
- (14) Jordan, R.; Ulman, A. J. Am. Chem. Soc. 1998, 120, 243-247.
- (15) Jordan, R.; Ulman, A.; Kang, J. F.; Rafailovich, M. H.; Sokolov, J. J. Am. Chem. Soc. 1999, 121, 1016-1022.
- (16) Shah, R. R.; Merreceyes, D.; Husemann, M.; Rees, I.; Abbott, N. L.; Hawker, C. J.; Hedrick, J. L. *Macromolecules* **2000**, *33*, 597-605.
- (17) Huang, X.; Wirth, M. J. Macromolecules 1999, 32, 1694-1696.
- (18) Huang, X.; Doneski, L. J.; Wirth, M. J. Chemtech 1998, 28, 19-25.

- (19) Huang, W.; Kim, J.-B.; Bruening, M. L.; Baker, G. L. *Macromolecules* **2002**, *35*, 1175-1179.
- (20) Ejaz, M.; Yamamoto, S.; Ohno, K.; Tsujii, Y.; Fukuda, T. *Macromolecules* **1998**, 31, 5934-5936.
- (21) Zhao, B.; Brittain, W. J. J. Am. Chem. Soc. 1999, 121, 3557-3558.
- (22) Huang, W.; Skanth, G.; Baker, G. L.; Bruening, M. L. Langmuir 2001, 17, 1731-1736.
- (23) Zhao, B.; Brittain, W. J.; Zhou, W.; Cheng, S. Z. D. J. Am. Chem. Soc. 2000, 122, 2407-2408.
- (24) Prucker, O.; Rühe, J. *Macromolecules* **1998**, *31*, 602-613.
- (25) Husemann, M.; Mecerreyes, D.; Hawker, C. J.; Hedrick, J. L.; Shah, R.; Abbott, N. L. *Angew. Chem. Int. Ed.* **1999**, *38*, 647-649.
- (26) Jeon, N. L.; Choi, I. S.; Whitesides, G. M.; Kim, N. Y.; Laibinis, P. E.; Harada, Y.; Finnie, K. R.; Girolami, G. S.; Nuzzo, R. G. Appl. Phy. Lett. 1999, 75, 4201-4203.
- (27) Wang, J.-S.; Matyjaszewski, K. *Macromolecules* **1995**, *28*, 7901-7910.
- (28) Kato, M.; Kamigaito, M.; Sawamoto, M.; Higashimura, T. *Macromolecules* 1995, 28, 1721-1723.
- (29) Huang, X.; Wirth, M. J. Anal. Chem. 1997, 69, 4577-4580.
- (30) Matyjaszewski, K.; Miller, P. J.; Shukla, N.; Immaraporn, B.; Gelman, A.; Luokala, B. B.; Siclovan, T. M.; Kickelbick, G.; Vallant, T.; Hoffmann, H.; Pakula, T. *Macromolecules* 1999, 32, 8716-8724.
- (31) Huang, W.; Baker, G. L.; Bruening, M. L. Angew. Chem. Int. Ed. 2001, 40, 1510-1512.
- (32) Kim, J.-B.; Bruening, M. L.; Baker, G. L. J. Am. Chem. Soc. 2000, 122, 7616-7617.
- (33) Jones, D. M.; Huck, W. T. S. Adv. Mater. 2001, 13, 1256-1259.
- (34) Kita, H.; Inada, T.; Tanaka, K.; Okamoto, K. J. Membr. Sci. 1994, 87, 139-147.
- (35) Bos, A.; Pont, I. G. M.; Wessling, M.; Strathmann, H. J. Polym. Sci., Part B: Polym. Phys. 1998, 36, 1547-1556.

- (36) McCaig, M. S.; Paul, D. R. *Polymer* **1999**, *41*, 629-637.
- (37) Rezac, M. E.; Schoberl, B. J. Membr. Sci. 1999, 156, 211-222.
- (38) Bos, A.; Punt, I. G. M.; Wessling, M.; Strathmann, H. Sep. Purif. Tech. 1998, 14, 27-39.
- (39) Wright, C. T.; Paul, D. R. J. Membr. Sci. 1997, 129, 47-53.
- (40) Rezac, M. E.; Sorensen, E. T.; Beckham, H. W. J. Membr. Sci. 1997, 136, 249-259.
- (41) Liu, Y.; Wang, R.; Chung, T. S. J. Membr. Sci. 2001, 189, 231-239.
- (42) Hirayama, Y.; Tanihara, N.; Kusuki, Y.; Kase, Y.; Haraya, K.; Okamoto, K. i. *J. Membr. Sci.* **1999**, *163*, 373-381.
- (43) Hirayama, Y.; Kase, Y.; Tanihara, N.; Sumiyama, Y.; Kusuki, Y.; Haraya, K. J. Membr. Sci. 1999, 160, 87-99.
- (44) Stair, J. L.; Harris, J. J.; Bruening, M. L. Chem. Mater. 2001, 13, 2641-2648.
- (45) Parks, G. A. Chem. Rev. 1965, 65, 177-198.
- (46) Bluhm, E. A.; Bauer, E.; Chamberlin, R. M.; Abney, K. D.; Young, J. S.; Jarvinen, G. D. *Langmuir* 1999, 15, 8668-8672.
- (47) Actually, PHEMA is partially branched due to intermolecular transesterification and in some cases is lightly cross-linked.
- (48) Ghosal, K.; Freeman, B. D. Polym. Adv. Tech. 1994, 5, 673-697.
- (49) Stern, S. A. J. Membr. Sci. 1994, 94, 1-65.
- (50) Koros, W. J. J. Polym. Sci., Part B: Polym. Phys. 1985, 23, 1611-1628.
- (51) Ghosal, K.; Chern, R. T.; Freeman, B. D.; Savariar, R. J. Polym. Sci., Part B: Polym. Phys. 1995, 33, 657-666.
- (52) Hoover, J. M.; Smith, S. D.; DeSimone, J. M.; Ward, T. C.; McGrath, J. E. *Polymer Preprints* **1987**, *28*, 390-392.
- (53) Robeson, L. M. J. Membr. Sci. 1991, 62, 165-185.
- (54) Chiou, J. S.; Paul, D. R. J. Membr. Sci. 1989, 45, 167-189.

- (55) Raymond, P. C.; Paul, D. R. J. Polym. Sci., Part B: Polym. Phys. 1990, 28, 2079-2102.
- (56) Wright, C. T.; Paul, D. R. Polymer 1997, 38, 1871-1878.
- (57) Chiou, J. S.; Barlow, J. W.; Paul, D. R. J. Appl. Polym. Sci. 1985, 30, 1173-1186.
- (58) Andrews, R. J.; Grulke, E. A. In *Polymer handbook*; Brandrup, J., Immergut, E. H., Grulke, E. A., Eds.; John Wiley and Sons: New York, 1999; pp VI 193- VI 277.
- (59) Yampolskii, Y. P.; Alentiev, A. Y.; Shishatskii, S. M.; Shantarovich, V. P.; Freeman, B. D.; Bondar, V. I. *Polymer Preprints* **1998**, *39*, 884-885.
- (60) Arnold, M. E.; Nagai, K.; Freeman, B. D.; Spontak, R. J.; Betts, D. E.; DeSimone, J. M.; Pinnau, I. *Macromolecules* **2001**, *34*, 5611-5619.
- (61) Nagale, M.; Kim, B. Y.; Bruening, M. L. J. Am. Chem. Soc. 2000, 2000, 11670-11678.
- (62) Xiao, K. P.; Harris, J. J.; Park, A.; Martin, C. M.; Pradeep, V.; Bruening, M. L. *Langmuir* **2001**, *17*, 8236-8241.

CHAPTER 4

Ion Transport through Grafted Poly(2-hydroxyethyl methacrylate) Membranes and their Derivatives

4.1 Introduction

Chapter 3 demonstrated the fabrication of ultrathin skins on porous supports using surface-initiated atom transfer radical polymerization. This chapter investigates the ion permeability of poly(2-hydroxyethyl methacrylate) (PHEMA) membranes that were also prepared by ATRP from a surface. Although such membranes did not prove highly selective in gas separations, they do allow selective transport of monovalent ions.

Derivatization of PHEMA with a cross-linking agent, succinyl chloride, results in Cl⁻/SO₄²⁻ selectivities as high as 300.

Such selectivities may be important in nanofiltration (NF), which has become an important area of research in membrane-based separations. This technique is widely used in applications such as water softening and purification, removal of heavy metals from water streams, waste-water reclamation, and separation of organic solutes. NF is sometimes preferable to reverse osmosis because it occurs at lower pressures and hence, has lower energy costs. The separation characteristics in NF fall between reverse osmosis and ultrafiltration, and separation is based on sieving and electrostatic effects. Typical NF membranes are synthesized from polymers such as polysufones, polyamides, modified aromatic polyamides, and derivatives of polyvinyl alcohols.

In 1965, Baddour and coworkers demonstrated that hydrogels made from PHEMA are capable of desalinating brackish or sea water.^{6,7} They showed that membranes synthesized by copolymerization of HEMA and ethylene glycol

dimethacrylate have NaCl rejections up to 87.6%.^{6,7} Haldon and Lee examined the permeability of PHEMA membranes that were prepared by copolymerization with different cross-linkers (ethylene glycol dimethacrylate, trimethylolpropane trimethacrylate (TPT) or pentaerythritol tetramethacrylate) and showed that the waterpermeability of the membrane depends on the cross-linking density.⁸ A similar study by Jadwin and coworkers found that water permeability through cross-linked PHEMA membranes decreases from 6×10⁻⁶ m³-m/m²-day to 6×10⁻⁹ m³-m/m²-day, and salt rejection increases from 78% to 94% as the amount of cross-linking with TPT increases from 0 to 11 mole percent.⁷ However, such membranes were prepared by solution casting followed by photoirradiation, and thus, the thicknesses of these materials were relatively high (100-500 μm). This, of course, results in unacceptably low fluxes.

The main objective of this work was to determine whether ultrathin, PHEMA skins prepared by ATRP from a surface can successfully separate different ions. Iontransport studies with composite PHEMA membranes showed moderate selectivities (CI⁻/SO₄²-selectivity of 15, K⁺/Mg²⁺ selectivity of 47 and CI⁻/Fe(CN)₆³⁻ selectivity of 164), but CI⁻ fluxes in diffusion dialysis were quite low (15% of that through the bare alumina support). (Higher selectivities were obtained with even thicker films, but flux was even lower.) The relatively low fluxes occurred in spite of the fact that film thickness was less than 100 nm, suggesting that films are relatively dense. One advantage of PHEMA is that it can be easily tailored for specific applications through derivatization of its hydroxyl groups.⁹ In chapter 3, I showed that derivatization of PHEMA with pentadecafluorooctanoyl chloride enhanced gas-transport selectivities. This chapter shows that reaction of PHEMA with succinyl chloride dramatically increases ion-

transport selectivities, while still allowing reasonable flux values with 28 nm-thick films (Cl⁻ flux was 50% of that through bare alumina).

4.2 Experimental

4.2.1 Chemicals and Solutions

Poly(allylamine hydrochloride) (PAH) (M_w = 70,000), sodium poly(styrenesulfonate) (PSS) ($M_w = 70,000$), 3-mercaptopropionic acid (MPA), pyridine, dimethylformamide (DMF, anhydrous, 99.8%), tetrahydrofuran (THF, anhydrous, inhibitor free, 99.8%), ethyl acetate, ethanol, 2-bromopropionylbromide (2-BPB), CuCl (99.999%), CuBr (99.999%), CuBr₂ (99%), 2,2'-bipyridine (bpy, 99%), 1,1'carbonyldiimidazole (CDI, 98%), 2-hydroxymethyl-18-crown-6 (90%) and succinyl chloride (90%) were used as received from Aldrich. MnCl₂ (Acros) and NaBr (Spectrum) were also used as received. Triethylamine (Spectrum, 98%) was vacuum distilled over CaH₂. 2-Hydroxyethyl methacrylate (HEMA, Aldrich, 98%, inhibited with 300 ppm hydroquinone monomethyl ether (MEHQ)) was purified by passing it through a column of activated basic alumina (Spectrum). Deionized water (Milli-Q, 18.2 M Ω cm) was used for preparation of solutions and rinsing. AnodiscTM porous alumina membranes (Fisher) with 0.02 µm-diameter surface pores were used as supports for membrane formation. Gold-coated slides (200 nm of sputtered Au on 20 nm Cr on a Si (100) wafer) were used as substrates for ellipsometry and Fourier transform infrared (FTIR) external reflection spectroscopy.

4.2.2 Polymerization of HEMA from Gold-coated wafers and Porous Alumina

For polymerization of HEMA from gold wafers, 2-BPB was immobilized on a multilayer polyelectolyte film (PAH/PSS/PAH) using the procedure described in Chapter 3. In the case of porous alumina, the initiator was attached to a PSS/PAH bilayer. Polymerization of HEMA occurred by immersion of the initiator-coated substrates in an aqueous solution containing HEMA and a Cu catalyst system. 9 To prepare the catalyst solution, 42 mL of HEMA and deionized water (1:1, v:v) were first degassed in a threenecked flask by three freeze-pump-thaw cycles. Then, 55 mg (0.55 mmol) of CuCl, 36 mg (0.16 mmol) of CuBr₂, and 244 mg (1.56 mmol) of bpy were quickly added to the HEMA/water solution under a flow of nitrogen. The mixture was immediately subjected to another two freeze-pump-thaw cycles and subsequently stirred until a homogeneous dark brown solution formed. The sealed vessel containing the polymerization solution was then transferred to a glove bag, which was purged with N₂ gas for ~1 hour. The polymerization solution was finally transferred into vessels containing substrates modified with initiators, and polymerizations were carried out for different times. After polymerization, substrates were removed from the vessels, rinsed with deionized water, sonicated (1 minute) in DMF, rinsed with THF followed by ethanol, and dried under a flow of N_2 .

4.2.3 Derivatization of PHEMA with Crown ethers

To couple crown-ethers to PHEMA, a film-coated substrate was immersed into a 0.2 M solution of CDI in DMF for 12 h and subsequently rinsed with DMF. CDI-functionalized PHEMA substrates were then immersed in a 10-mL DMF solution containing 2-hydroxymethyl-18-crown-6 (0.1 M) and triethylamine (0.1 M). The

reaction was carried out at 70 °C for 4.5 days, after which the substrate was rinsed with DMF, followed by ethanol and dried with a flow of nitrogen. Derivatization was performed after ion-permeability studies with the underivatized PHEMA membrane.

4.2.4 Chemical Cross-linking of PHEMA

PHEMA-coated substrates were immersed in 10 mL of DMF containing succinyl chloride (0.1 M) and pyridine (0.1 M). After 10 minutes, substrates were removed from the reaction solution, rinsed with DMF, and dried with N₂. Derivatization was performed after ion-permeability studies.

4.2.5 Film Characterization

Ellipsometric measurements were obtained with a multiwavelength, rotating analyzer ellipsometer (model M-44; J.A. Woollam) using WVASE32 software at an incident angle of 75°. The refractive index of the films at all wavelengths was assumed to be 1.5. For each substrate, thicknesses were measured at three different spots and averaged. Reflectance FTIR spectroscopy was performed using a Nicolet Magna-IR 560 spectrometer containing a PIKE grazing angle (80°) attachment. The spectra were collected with 256 scans using a MCT detector.

4.2.6 Ion-Transport Studies with PHEMA Membranes

Diffusion-dialysis studies with PHEMA membranes were performed using two glass half cells (Figure 2.2) as described in Chapter 2 (section 2.2). The permeate cell contained deionized water (90 mL), and the feed cell contained 0.1 M salt solutions (90 mL) of KCl, K₂SO₄, K₃Fe(CN)₆ and MgCl₂. After dialysis with each salt, the entire apparatus was rinsed well with deionized water and subsequently filled with water for 30

minutes to remove any adsorbed ions. Salts were examined in the same order as given above, and after MgCl₂ dialysis, a second KCl dialysis was performed to check the integrity of the membrane. (The difference between KCl fluxes in the first and second dialyses was <10%). Conductivity (Orion model 115) of the receiving side was recorded at every 5 minutes for a period of 45 minutes, and conductivity values were converted to concentration using a calibration curve of conductivity vs. concentration for each salt. Fluxes were calculated from the slopes of concentration vs. time plots using equation 2.1. Selectivity of monovalent over divalent ions was calculated from the ratio of respective flux values (equation 2.2).

For chemically cross-linked PHEMA membranes, I also examined dialysis with solutions containing 1000 ppm Cl⁻ and 1000 ppm SO₄²⁻ or 500 ppm Cl⁻ and 2500 ppm SO₄²⁻ (solutions were prepared with KCl and K₂SO₄.). Dialysis was carried out for 90 min, and 2 mL samples were withdrawn from both sides at 10-min intervals. These samples were analyzed with an ion chromatograph (Dionex 600) using an AS14A anion column and an 8 mM Na₂CO₃/1 mM NaHCO₃ eluent. Normalized fluxes were calculated from the respective slopes of normalized concentration vs time plots, and the anion-selectivities were determined from the ratio of normalized fluxes. Normalization was performed by dividing by the source-phase concentration.

4.3 Results and Discussion

4.3.1 Synthesis and Characterization of PHEMA Membranes

Initiator anchoring and polymerization were initially performed on gold-coated wafers to facilitate film characterization. First, 2-BPB was covalently attached to the

polyelectrolytes through amide linkages. As previously discussed (section 3.3.1), we did not observe a prominent change in the reflectance FTIR spectrum of polyelectrolytes after initiator anchoring, but there was a small absorbance increase in the amide region (1650-1560), confirming initiator attachment. Polymerization was carried out by immersing the initiator-modified substrates in HEMA/water solutions containing CuCl/CuBr₂/bpy. Unlike gas-permeability studies, the HEMA polymerization was carried out in water, rather than methanol, because aqueous polymerization is a more controlled process that yields a relatively linear relationship between film thickness and polymerization time. Several previous studies showed that aqueous conditions also accelerate ATRP of hydrophilic monomers. 9-11 The appearance of a strong carbonyl peak at 1730 cm⁻¹ in the reflectance FTIR spectrum of films after polymerization indicated formation of PHEMA on the surface.

4.3.2 Ion-Transport Studies with Composite PHEMA Membranes

Figure 4.1 shows results of diffusion dialysis through a composite membrane containing a 28 nm-thick PHEMA skin. The linear relationship between receiving-phase concentration and time shows that flux is constant and confirms that ion concentrations in the receiving phase were negligible compared to those in the source phase. Table 4.1 gives the cumulative thicknesses of PHEMA films, ion-transport selectivities and ion fluxes through PHEMA membranes. As the PHEMA film thickness increases, selectivity increases, presumably because the film more completely covers the substrate.

Since PHEMA is neutral, the observed selectivities among ions are probably due to differences in hydration energies and hydrated radii. Both hydration energy and

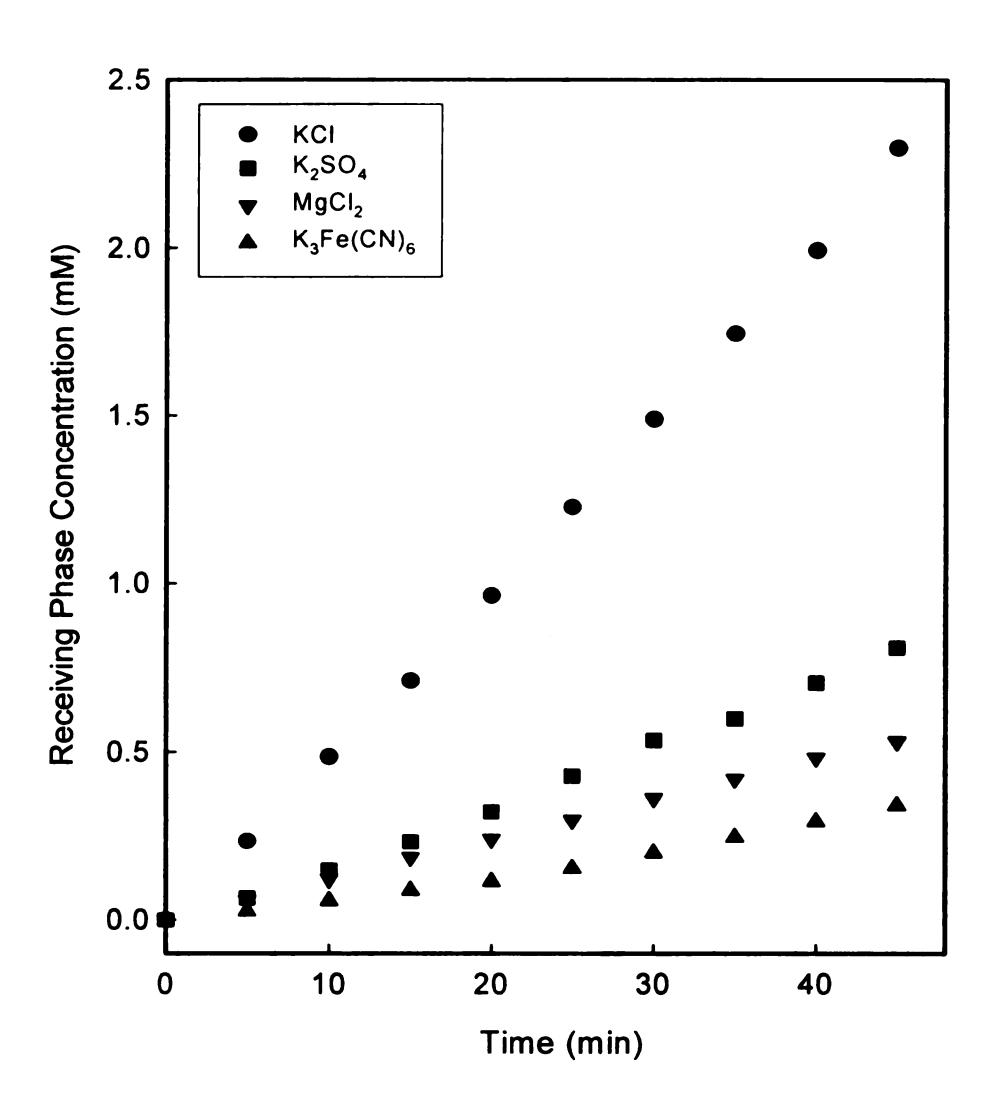


Figure 4.1: Plot of receiving phase concentration as a function of time in diffusion dialysis when the source phase (0.1 M salt) was separated from the receiving phase (initially deionized water) by a porous alumina substrate capped with 28 nm of PHEMA.

Table 4.1: Film thicknesses, fluxes and selectivities for composite PHEMA membranes (porous alumina support).

Polymerization	Film		Flux ^b (mo	Flux ^b (moles/cm ² s)×10 ⁹			Selectivity ^c	
Time (min)	(nm)	CI.	SO ₄ ²-	Fe(CN) ₆ ³⁻	${ m Mg}^{2+}$	CI/SO ₄ ²-	CI'Fe(CN) ₈ ³⁻ K ⁺ /Mg ^{2+d}	K ⁺ /Mg ^{2+d}
09	28	45 ± 4	14±3	5±1	7.2±0.9	3.0±0.6	9±3	6±1
130	64	8±1	0.4±0.1	0.05±0.01	0.21±0.08	15±4	164±11	47±15
180	91	4.8±0.4	900:0=90:00	4.8±0.4 0.06±0.006 0.005±0.001 0.04±0.003	0.04±0.003	76±10	950±170	125±20

measurements, which varied by less than 10%. Thicknesses include the polyelectrolyte/initiator film, which was 4.8 nm thick. ^bFlux values were calculated from the slopes of concentration in receiving phase vs. time plots. Errors represent standard ^a Thicknesses were determined by ellipsometry of PHEMA films on gold wafers. Values represent the average of two deviations of at least three measurements.

Ratio of respective of flux values. Calculated as the average of selectivity values for each membrane and not from average flux

^dFlux of potassium ion was the same as the reported Cl⁻ flux as that experiment was performed with KCl.

hydrated radii decrease in the order $Mg^{2^+} > SO_4^{2^-} > Cl^- > K^+$ (See Table 4.2). Since hydration energy and hydrated radius are higher for Mg^{2^+} than $SO_4^{2^-}$, one would expect to observe higher selectivity values for K^+/Mg^{2^+} than for $Cl^-/SO_4^{2^-}$. This was indeed the case for all three PHEMA thicknesses. The $Cl^-/Fe(CN)_6^{3^-}$ selectivity is higher than monovalent/divalent selectivities probably because of the large hydration radius and hydration energy of $Fe(CN)_6^{3^-}$.

Although we were successful in obtaining reasonable selectivities with PHEMA membranes, Cl⁻ flux values were relatively low for thicker films. For 28 nm-thick PHEMA films, Cl- flux was 80% of that through bare alumina (Cl⁻ flux through bare alumina was 5.2×10⁻⁸ moles/cm²s¹), but flux decreased dramatically with increasing PHEMA thickness (Table 4.1). We thought that cross-linking of thin PHEMA membranes might allow both high flux and high selectivity. Cross-linking should reduce swelling and may allow thin films to fully cover a substrate.

4.3.3 Chemically Cross-linked PHEMA Membranes and their Ion-Transport Properties

We cross-linked PHEMA by derivatizing films with a di-acid chloride that would react with hydroxyl groups in adjacent PHEMA chains. Scheme 4.1 outlines the reaction of grafted PHEMA layer with succinyl chloride. Reflectance FTIR spectra of PHEMA films after derivatization showed the disappearance of the hydroxyl peak and a ~2-fold increase in the intensity of ester carbonyl peak, suggesting quantitative conversion of hydroxyl groups to esters (Spectrum b, Figure 4.2). However, the appearance of a small shoulder at 1819 cm⁻¹ suggested the presence of unreacted acid

Table 4.2: Hydrated radii and hydration energies of various ions. 12

Ion	Hydrated Radius (pm)	Hydration Energy (kJ/mol)
K ⁺	212	330
Cl.	224	365
SO ₄ ²⁻	278	1035
Mg ²⁺	299	1945
Fe(CN) ₆ ³⁻	396	

Scheme 4.1: Cross-linking of PHEMA by reaction with succinyl chloride.

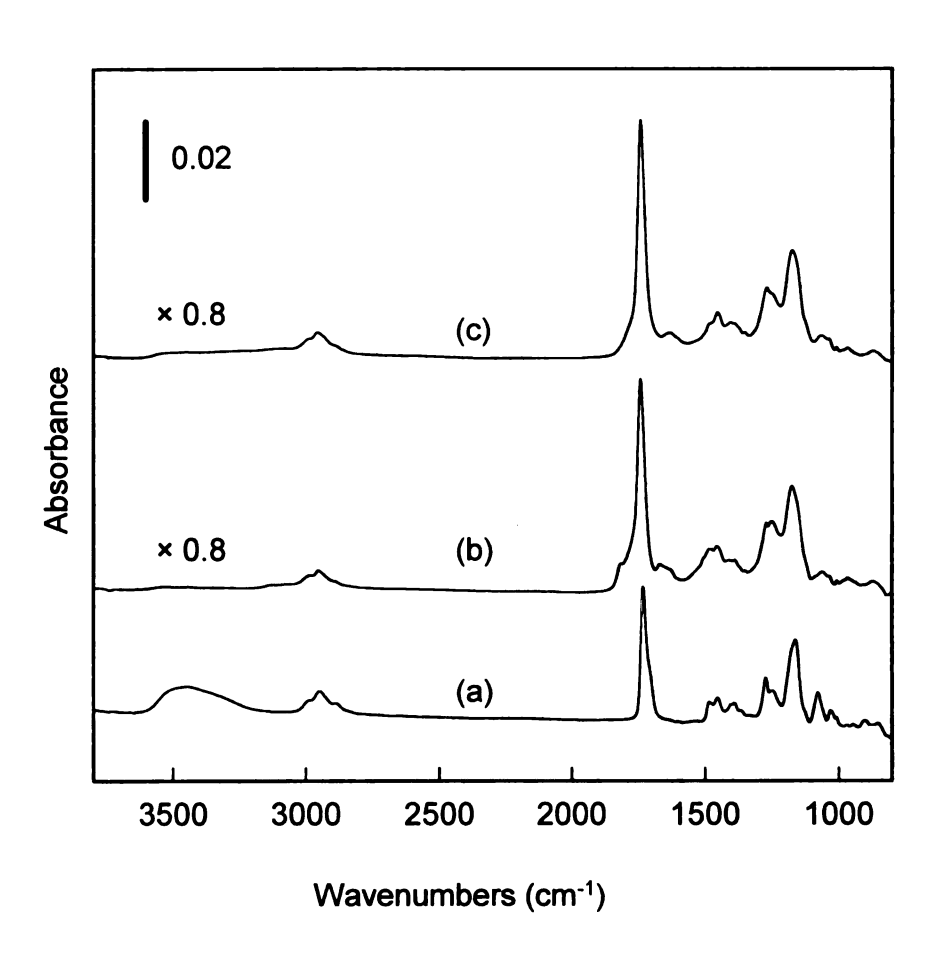


Figure 4.2: Reflectance FTIR spectra of a 28-nm thick grafted PHEMA film on a gold-coated wafer before (a) and after reaction with succinyl chloride (b) and subsequent exposure to water (c).

chlorides, implying less than 100% cross-linking. Disappearance of the 1819 cm⁻¹ peak upon exposure to water confirmed that this peak is probablydue to unreacted acid chloride (spectrum c, Figure 4.2). Nevertheless, the small size of the acid chloride peak suggests that cross-linking is >50%.

Figure 4.3 shows results of diffusion dialysis through a composite membrane containing a 35 nm-thick cross-linked PHEMA skin. (The PHEMA film was ~28 nmthick prior to cross-linking, so these results can be compared to those in Figure 4.1.) Table 4.3 summarizes the fluxes and selectivities of chemically cross-linked PHEMA membranes. For the 35 nm-thick film (initially 28 nm of PHEMA), reaction with succinyl chloride increased Cl⁻/SO₄²⁻ selectivity by a factor of 100 and Cl⁻/Fe(CN)₆³⁻ selectivity by a factor of 90. The large increase in monovalent/multivalent anion selectivities suggests that in addition to cross-linking, which reduces membrane swelling and increases size-based selectivity, we also introduced fixed negative charges into the PHEMA film. As reflectance FTIR spectra indicate, these negative charges probably result from hydrolysis of unreacted acid chlorides. When the membrane is negatively charged, Donnan potentials cause substantial exclusion of multiply charged anions such as SO₄² and Fe(CN)₆³ and hence, higher monovalent/ multivalent anion selectivities. In contrast to anion transport, K⁺/Mg²⁺ selectivity increases only 4-fold after cross-linking. Negative charges in the membrane should reduce monovalent/divalent cation selectivity, and thus we see only a small increase in K⁺/Mg²⁺ selectivity after cross-linking. The 4fold increase in selectivity is likely due to a reduction in film swelling. Consistent with decreased film swelling, large increases in anion-transport selectivities with thin PHEMA



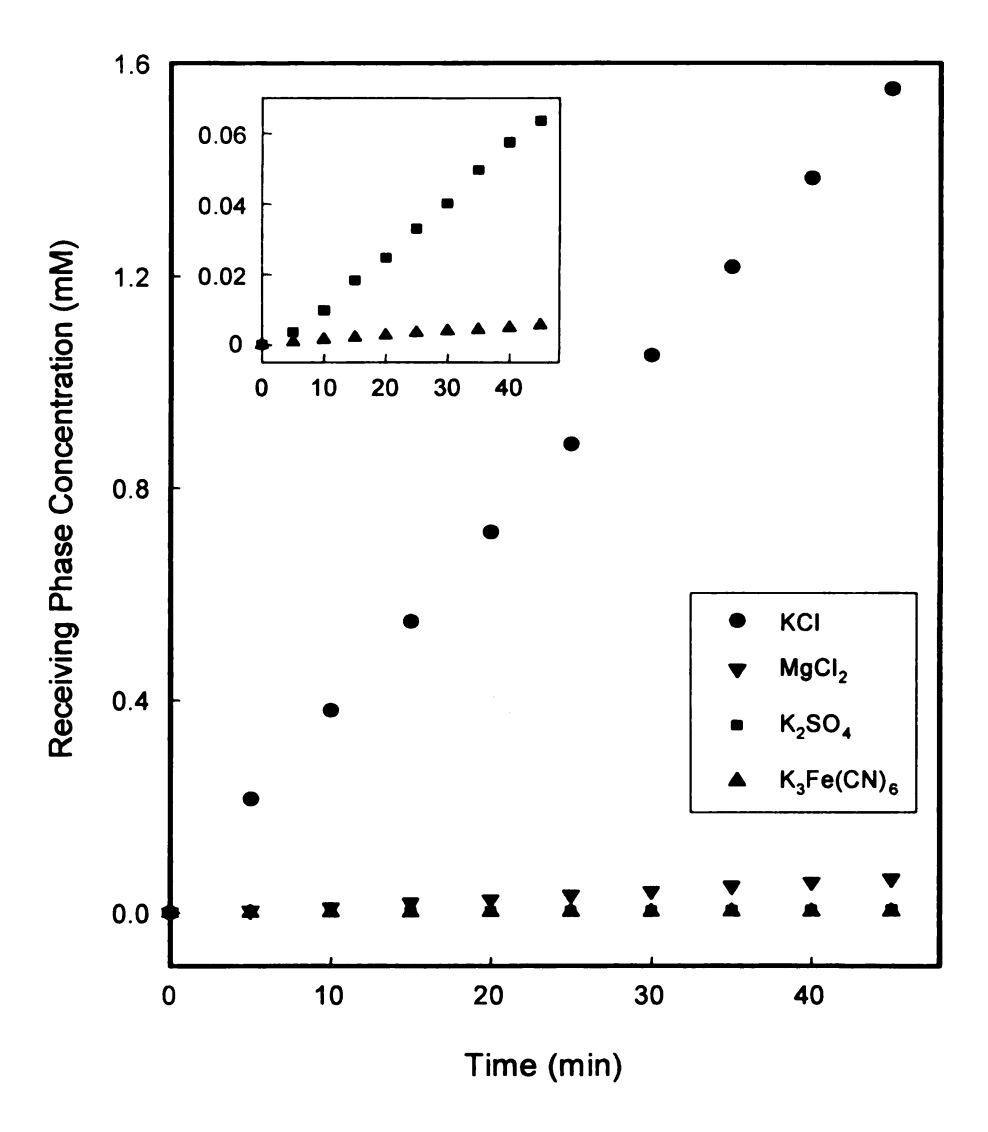


Figure 4.3: Plot of receiving phase concentration as a function of time in diffusion dialysis when the source phase (0.1 M salt) was separated from the receiving phase (initially deionized water) by a composite membrane of 35 nm cross-linked PHEMA film. The inset expands the concentration scale for SO_4^{2-} and $Fe(CN)_6^{3-}$. PHEMA was cross-linked by succinyl chloride.

Table 4.3: Film thicknesses, fluxes and selectivities for cross-linked PHEMA membranes in diffusion dialysis with single-salt solutions.

Selectivity ^c	K ⁺ /Mg ²⁺	2	22
	CI'/Fe(CN) ₆ ³⁻	89	807
	CI'/SO ₄ ²-	23	300
Flux ^b (moles/cm ² s) ×10 ⁹	${ m Mg}^{2+}$	16	1.2
	Fe(CN) ₆ ³⁻ Mg ²⁺	0.54	0.03
	SO ₄ ²⁻	1.6	0.08
	CI.	37	25
Film Thickness ^a (nm)		21	35

^a Thicknesses are estimated from measured ellipsometric thicknesses of corresponding films on gold wafers as described in experimental section. Cumulative film thicknesses are reported.

^bFlux values were calculated from the slopes of concentration of receiving phase vs. time plot as described in the experimental

Ratio of flux values.

films are accompanied by a 40% decrease in Cl⁻ flux (See Tables 4.1 and 4.2). However, flux is still about 50% of that through bare alumina.

The ion-transport studies described above were performed with source-phase solutions that contained single salts. Actual ion separations occur from mixed salts, however, so we briefly examined ion-transport with both KCl and K₂SO₄ in the source phase. Table 4.4 contains preliminary selectivities and flux values obtained with cross-linked PHEMA membranes. The Cl'/SO₄²⁻ selectivity obtained with solutions of mixed salts is a factor of 1.6 to 4.5 higher (depending on the ratio of Cl' to SO₄²⁻) than the selectivity obtained from single-salt experiments. The increase in selectivity with mixed solutions is presumably due the fact that the diffusion potential is lower in mixed KCl/K₂SO₄ solutions than it is when only K₂SO₄ is present. In K₂SO₄ solutions, diffusion of K⁺ is faster than diffusion of SO₄²⁻, so a diffusion potential develops to resist current flow. The diffusion potential decreases K⁺ transport and increases SO₄²⁻ transport. When KCl is present, a smaller diffusion potential develops because Cl' has a higher mobility than SO₄²⁻. The no-current condition can be reached with a smaller potential that increases Cl' flux much more than SO₄²⁻ flux.

4.3.4 Crown Ether-Derivatized PHEMA Membranes and their Ion-Transport Properties

We hoped to improve the selectivity of PHEMA membranes by derivatization with a complexing agent that can selectively bind a particular ion. Selective hopping of ions between crown-ether binding sites could facilitate the transport of one ion over another. Crown ethers are well known for both selective binding and fast release of alkali metal

Table 4.4: Film thicknesses, normalized fluxes and selectivities for cross-linked PHEMA membranes in diffusion dialysis with mixed salt solutions.

Film Thickness ^a (nm)	Normalized Flux ^d ×10 ⁹		Selectivity ^e
	Cl ⁻	SO ₄ ² -	Cl ⁻ /SO ₄ ²⁻
21 ^b	450	4	106
35°	440	0.9	490

^aThicknesses are estimated from measured ellipsometric thicknesses of corresponding films on gold wafers as described in experimental section. Thicknesses after derivatization are reported.

^bDiffusion dialysis was done using a 1000 ppm Cl⁻ and 1000 ppm SO₄²⁻. ^cDiffusion dialysis was done using 500 ppm Cl⁻ and 2500 ppm SO₄²⁻.

^dNormalized fluxes are reported.

^eRatio of noramalized fluxes.

cations.¹³ We derivatized PHEMA with 2-hydroxymethyl-18-crown-6 because the size of the crown ether cavity matches with the ionic radius of K⁺.^{14,15}

In the derivatization of PHEMA, films were first reacted with CDI for 12 hours (Step 1, Scheme 4.2). After coupling of PHEMA with CDI, the reflectance FTIR spectrum of the film showed complete disappearance of the hydroxyl peak (3500 cm⁻¹-3300cm⁻¹) and the appearance of a strong carbonyl peak at 1771 cm⁻¹ due to the imidazole carboxylic acid intermediate, suggesting quantitative reaction (Spectrum b. Figure 4.4). Since imidazole groups can be displaced with nucleophiles such as amines and alcohols, CDI-derivatized PHEMA is attractive for the immobilization of a variety of functional groups. In this case imidazole-derivatized PHEMA films were reacted with 2hydroxymethyl-18-crown-6 to introduce crown ether functionalities into the film (Step 2, Scheme 4.2). Since the reaction was very slow, the solution was heated to 70 °C for 4.5 days. Disappearance of the carbonyl peak at 1771 cm⁻¹ and the appearance of peaks at 1265 cm⁻¹ and 1155 cm⁻¹ (C-O-C stretches of the crown ether) in the reflectance FTIR spectrum of derivatized films confirmed the reaction with the crown ether (spectrum c, Figure 4.3). Additionally, the ellipsometric thickness increased by 55 %, indicating incorporation of crown ether moieties.

However, diffusion dialysis yielded a K^+ flux (2.3 x 10^{-10} molescm⁻²s⁻¹) through crown ether derivatized membranes that was smaller than Na⁺ flux (2.9 x 10^{-10} molescm⁻²s⁻¹). The lack of K^+/Na^+ selectivity could be due to crown ether moieties that are not in the right conformation for K^+ ion binding, or perhaps hopping between binding sites is slower than diffusion. A better way of performing this derivatization would be to use a K^+ -salt of the crown ether and subsequently remove the K^+ ions after derivatization.

Scheme 4.2: Functionalization of PHEMA with 2-hydroxy methyl 18-crown-6.

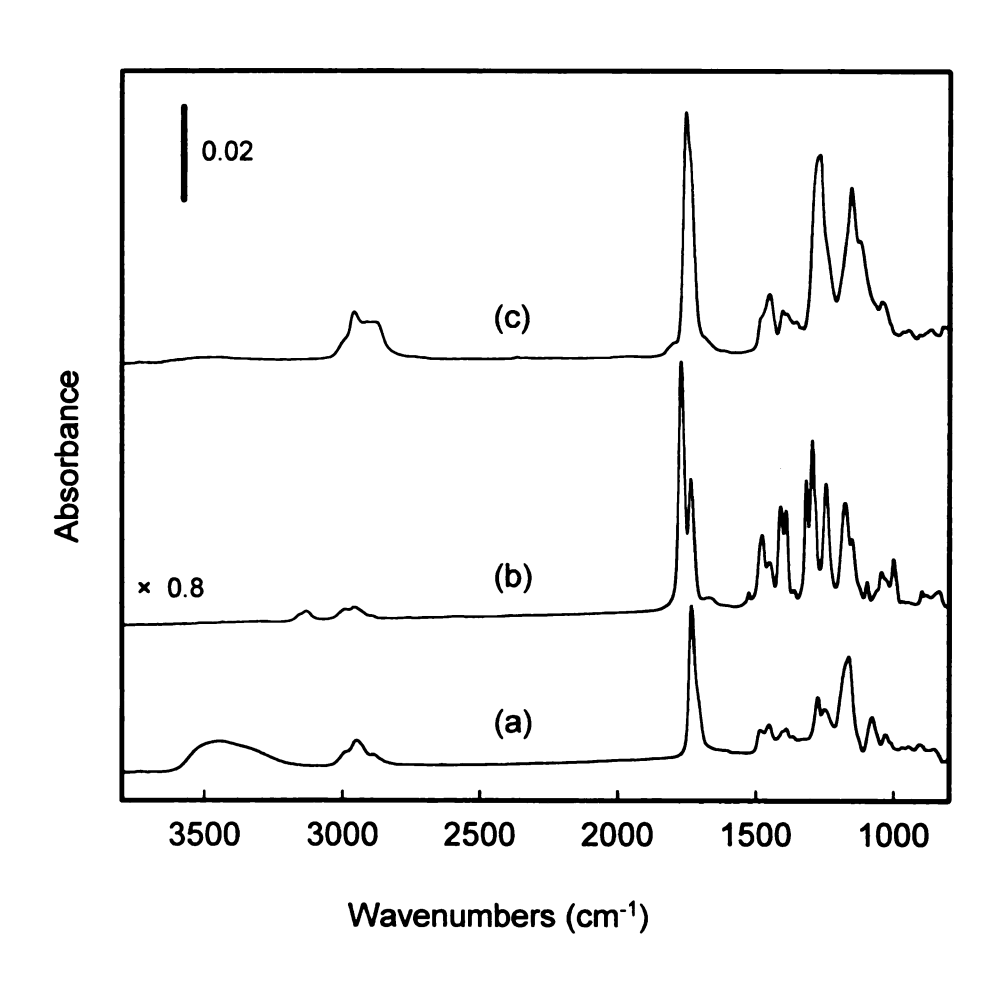


Figure 4.4: Reflectance FTIR spectra of (a) a grafted PHEMA layer (28 nm) (b) CDI-derivatized PHEMA and (c) CDI-derivatized PHEMA after reaction with 2-hydroxymethyl-18-crown-6 (43 nm).

4.4 Conclusions

Surface-initiated ATRP is an attractive and versatile method of forming ultrathin polymer skins on porous supports. Ion-permeability studies with composite PHEMA membranes showed moderate selectivities for monovalent over divalent and trivalent ions. However, reaction with succinyl chloride enhanced Cl⁻/SO₄²⁻ and Cl⁻/Fe(CN)₆³⁻ selectivities by 2 orders of magnitude, presumably due to the introduction of crosslinking and negative charges into the membrane. Using mixed-salt solutions, even better selectivities were obtained because of a reduction in diffusion potentials.

4.5 References

- (1) Xu, X.; Spencer, G. Desalination 1997, 113, 85-93.
- (2) Wang, X.-L.; Zhang, C.; Ouyang, P. J. Membr. Sci. 2002, 204, 271-281.
- (3) Bowen, W. R.; Mohammad, A. W.; Hilal, N. J. Membr. Sci. 1997, 126, 91-105.
- (4) Bowen, W. R.; Mukhtar, H. J. Membr. Sci. 1996, 112, 263-274.
- (5) Haraya, K.; Li, S.; Mizoguchi, K. Springer Series in Materials Science 1999, 35, 95-124.
- (6) Baddour, R. F.; Graves, D. J.; Vieth, W. R. J. Colloid Sci. 1965, 20, 1057-1069.
- (7) Jadwin, T. A.; Hoffman, A. S.; Vieth, W. R. J. Appl. Polym. Sci. 1970, 14, 1339-1359.
- (8) Halden, R. A.; Lee, B. E. Br. Polym. J. 1972, 4, 491-501.
- (9) Huang, W.; Kim, J.-B.; Bruening, M. L.; Baker, G. L. *Macromolecules* **2002**, *35*, 1175-1179.
- (10) Wang, X. S.; Lascelles, S. F.; Jackson, R. A.; Armes, S. P. Chem. Commun. 1999, 1817-1818.
- (11) Robinson, K. L.; Khan, M. A.; de Banez, M. V.; Wang, X. S.; Armes, S. P. *Macromolecules* **2001**, *34*, 3155-3158.
- (12) Marcus, Y. Biophys. Chem. 1994, 51, 111-127.
- (13) Noble, R. D. J. Chem. Soc. Faraday Trans. 1991, 87, 2089-2092.
- (14) Thunhorst, K. L.; Noble, R. D.; Bowman, C. N. J. Membr. Sci. 1999, 156, 293-302.
- (15) Reusch, C. F.; Cussler, E. L. AIChE Journal 1973, 19, 736-741.

CHAPTER 5

Conclusions and Future Work

5.1 Conclusions

The work reported in this dissertation demonstrated the versatility of multilayer polyelectrolyte deposition and surface-initiated atom transfer radical polymerization (ATRP) in the formation of defect-free, ultrathin membrane skins. These skins are quite selective in both ion and gas separations. Chapter 2 described a method of introducing fixed negative charges into the bulk of multilayer polyelectrolyte membranes (MPMs) to enhance anion-transport selectivities. This method relies on complexation of Cu²⁺ by the -COO groups of poly(acrylic acid) (PAA) during the deposition of PAA/ poly(allylamine hydrochloride) (PAH) films on porous alumina supports. Subsequent removal of Cu²⁺ and deprotonation results in ion-exchange sites in the bulk of the membrane skin. Diffusion dialysis studies with Cu²⁺-templated PAA/PAH membranes showed a 4-fold increase in Cl⁻/SO₄²⁻ selectivity compared to pure PAA/PAH membranes deposited under similar conditions. Post deposition cross-linking of these membranes further increased Cl /SO₄² selectivity to values as high as 600. These remarkable selectivities are presumably due to increased fixed negative charge density in the bulk of the membrane, which increases the Donnan potential to give greater exclusion of divalent than monovalent anions. However, modeling of ion-transport data suggested that selectivity is due to both Donnan exclusion and diffusivity differences among ions.

The second method I utilized in thin film formation was room-temperature, surface-initiated ATRP. Chapter 3 showed the versatility of this technique in the synthesis of cross-linked polymer films from a modified porous alumina support.

Cross-linked poly(ethylene glycol dimethacrylate) (PEGDMA) membranes exhibited a CO₂/CH₄ selectivity of 20. In comparison non cross-linked poly(2-hydroxyethyl methacrylate) (PHEMA) grown form a modified porous alumina support showed minimal gas-transport selectivities. However, derivatization of the hydroxyl groups of PHEMA with fluorinated acid chloride yielded moderate gas-transport selectivity. Polymer growth was monitored by scanning electron microscopy (SEM) and transmission FTIR spectroscopy. Both top-down and cross-sectional SEM images showed that these polymer films effectively cover the surface pores of the alumina support.

Chapter 4 discussed the promise of PHEMA membranes in ion separations. PHEMA by itself showed moderate ion-transport selectivities. However, crosslinking PHEMA via reaction with succinyl chloride increased Cl⁻/SO₄²⁻ and Cl⁻/Fe(CN)₆³⁻ selectivity by 100-fold. This large increase in anion-selectivities is probably due to reduced film swelling and introduction of negative charge by hydrolysis of unreacted acid chlorides.

Overall, these studies demonstrate novel methods for the formation of ultrathin membranes. Although new procedures for film deposition may not be practical on a large scale, they should allow development of membrane for specific small-scale (i.e., analytical) separations. Work with both multilayer polyelectrolyte and grafted polymer films shows that the minimal thickness of these systems allows

high flux. Additionally, the wide variety of functional groups that can be included in these membranes allows tailoring of transport properties.

5.2 Suggestions for Future Work

My success in growth of a cross-linked film from a porous substrate should now allow investigation of new types of membrane systems such as imprinted polymers. Cross-linked polymers are attractive materials for separations because of their low free volume (which will reduce film swelling) and ability to withstand drastic separation conditions. An interesting area of research will be the examination of PEGDMA membranes in ion separations. However, ion-transport through PEGDMA itself is quite low, and thus, incorporation of non cross-linkable monomers into PEGDMA films will likely be necessary to achieve a desirable flux. Introduction of charged functionalities into these films could be achieved by co-polymerizing ethylene glycol dimethacrylate (EGDMA) with *t*-butyl methacrylate and subsequently hydrolyzing *t*-butyl groups to -COOH groups. Deprotonation of these -COOH groups will yield ion-exchange sites in the membrane. Such membranes have the potential to be extremely selective in anion separations.

In chapter 4, I showed the potential of derivatized poly(2-hydroxyethyl methacrylate) (PHEMA) films in anion separations. Similarly PHEMA could be derivatized for cation separation by reaction with a di-amine (e.g. ethylene diamine). This derivatization could be easily performed by first coupling PHEMA with 1,1'-carbonyldiimidazole (CDI) and then reacting CDI-derivatized PHEMA with the diamine. Similar to reaction of PHEMA with succinyl chloride, derivatization with a

diamine should result in cross-linking along with residual free amine groups that can give fixed positive charge to the membrane. It will also be interesting to test PHEMA and its derivatives in neutral-molecule separations. This will provide valuable information in understanding the separation mechanism in these systems. As previous studies demonstrated² that thick PHEMA membranes can be used in nanofiltration, it will definitely be interesting to test ultrathin PHEMA and cross-linked PHEMA (HEMA copolymerized with EGDMA) films in nanofiltration.

Another very interesting and challenging area of research will be the synthesis of ultrathin, imprinted polymer membranes. In imprinting, a template, a monomer and a cross-linker are polymerized together, and the subsequent release of the template results in a polymer that contains cavities that are selective for the template.

3-5 Imprinted polymers could be prepared by copolymerizing EGDMA (cross-linker) with HEMA that was hydrogen bonded with a template molecule. For templates, we could use any molecule of interest (possibly a high molecular weight species) that can interact with HEMA through hydrogen bonding. Removal of the template should leave behind recognition sites in the membrane through which transport could take place. These imprinted membranes may be useful in selective separation of the template molecule.

In summary, the development of new techniques for forming ultrathin membrane skins has the potential to yield a wide variety of separation membranes ranging from imprinted to ion-exchange systems.

5.3 References

- (1) Huang, W.; Kim, J.-B.; Bruening, M. L.; Baker, G. L. *Macromolecules* **2002**, 35, 1175-1179.
- (2) Jadwin, T. A.; Hoffman, A. S.; Vieth, W. R. J. Appl. Polym. Sci. 1970, 14, 1339-1359.
- (3) Shea, K. J. Trends Polym. Sci. 1994, 2, 166-173.
- (4) Wulff, G. Angew. Chem. Int. Ed. 1995, 34, 1812-1832.
- (5) Kriz, D.; Ramstrom, O.; Mosbach, K. Anal. Chem. 1997, 69, 345A-349A.

MICHIGAN STATE UNIVERSITY I